Doctoral Dissertation

Cooperative behaviors in optically pumped lasing from thiophene/phenylene co-oligomer single crystals

(チオフェン/フェニレン) コオリゴマー単結晶の
光励起レーザー作用における協同的な振る舞い

Takumi Matsuo

Graduate school of Materials Science
Nara Institute of Science and Technology

March 17th, 2021

Supervisor: Professor Hisao Yanagi

Table of Contents

Abstract

Organic materials are promising candidates as laser media owing to their wavelength tunabilities and processabilities. After optically pumped lasing has been widely demonstrated for a variety of organic materials since several decades ago, electrically driven lasing in organic light emitting field effect transistors (OLEFETs) has been achieved in 2019 for the first time using single crystals of 5,5″-bis(biphenylyl)-2,2′:5’,2″-terthiophene (BP3T), which is one of thiophene/phenylene co-oligomers (TPCOs). Although the origin of lasing or amplified light emissions from TPCO and other organic single crystals have been conventionally recognized as stimulated emission (SE) processes, unique lasing or light emitting behaviors indicating cooperative behaviors have been recently reported for single crystals of TPCOs. In this study, structure dependences for lasing or amplified light emission characteristics were investigated for BP3T and its end-substituted derivatives. Among them, those detail characteristics were investigated especially for single crystals of BP3T in terms of polaritonic lasing and superfluorescence (SF).

In Chapter 1, fundamental structures and characteristics of organic lasers were described at first. Then, optically pumped lasing with unique lasing behaviors suggesting cooperative light amplification processes were described. After that, representative cooperative behaviors such as polaritonic emissions, superradiance (SR) and SF, were explained. Finally, aim of this study was stated.

In Chapter 2, syntheses of methoxy- and cyano-substituted BP3T (BP3T-OMe and BP3T-CN, respectively) were described. Their identified crystal structures were orthorhombic and

triclinic forms for BP3T-OMe and BP3T-CN, respectively, while that of unsubstituted BP3T has been identified as a monoclinic form in a previously published report. Orientations of π-electronic transition dipole moments with respect to the basal plane in thin platelet single crystals of BP3T-OMe and BP3T-CN were significantly different from that of BP3T owing to the changes in interaction between substituents, resulting in the possibility to control the lasing performances and characteristics by chemical modifications for TPCO series.

In Chapter 3, optically pumped lasing from single crystals of BP3T, BP3T-OMe and BP3T-CN were described. To achieve lasing in Fabry-Pérot (F-P) oscillating conditions for BP3T single crystals, improved crystal growth in solution phase was proposed to provide large and well-shaped single crystals, then, following optically pumped lasing was achieved. Optically pumped lasing from single crystals of BP3T-OMe and BP3T-CN was also achieved. Group refractive index (n_g) values estimated in lasing spectra of all three BP3T derivatives were enough large for efficient light confinement in those single-crystal cavities, strongly suggesting their superiority as active lasing media.

In Chapter 4, excitation area dependences for threshold of amplified light emissions from BP3T single crystals suggested superfluorescent behaviors in the 0-2 band while the SE process usually in the 0-1 band. The values of threshold of amplified light emissions in 0-1 was constant while these in 0-2 band was gradually decreased with increasing excitation beam area. Time-resolved PL profiles measured at room temperature showed pulse shaped delayed emissions with respect to excitation pulse.

The values of delay time were several tens picoseconds (ps) while these originating from SE process have been only a few ps, which indicated the existence of cooperative process in

amplified light emissions from BP3T single crystals. The delay time was maximized above threshold, and gradually decreased with increasing excitation density, which might suggest the transition from cooperative emitting behaviors to SE process. Moreover, the maximum delay time observed in 0-2 band was larger than that observed in 0-1 band, which suggest the fact that amplified light emissions in 0-2 band was more cooperative in comparison to 0-1 band, and this suggestion was consistent with the results of excitation area dependence for threshold of light amplification. Furthermore, larger delay time was observed from larger size of BP3T crystal, which suggested that the pulse shaped delayed emissions were originated from cooperative behaviors.

Furthermore, exciton-polariton (EP) characteristics were investigated for BP3T single crystals by estimating energy vs. wavenumber (*E*-*k*) dispersion plots obtained from optically pumped lasing spectra. The obtained *E*-*k* plots were well-attributed to EPs or vibrationally-dressed exciton-polaritons (VDEPs).

In Chapter 5, summary and future prospect of this research were described. To enhance the EP formation, Au-coating onto BP3T crystals was proposed to increase the reflectivity of single-crystal cavity. Moreover, investigation of excited state dynamics by pump-probe technique was described. As an engineering prospect, the possibility to demonstrate electrically pumped polariton lasers using single-crystal cavities was also discussed.

Chapter 1

General introduction

1.1 Research backgrounds

Among various optical platforms, photons with coherence have ideal characteristics for optical communication or observation systems owing to the monochromaticity, high intensity, high directionality and high polarizability. In general, coherent light emissions are obtained by constructing laser systems, which have been obtained from a variety of materials. Among them, organic materials are advantageous as lasing media in comparison to inorganic counterparts because of the possibilities to demonstrate lasing with high processabilities and efficient gain systems categorized in four- energy level systems. Although the origin of lasing is regarded as stimulated emission (SE) processes in general, indications or realizations of unique lasing behaviors such as superradiant or polaritonic emissions have been reported recently. Especially, owing to highly stable excitons described as Frenkel excitons and large oscillator strength for organic materials, polaritonic emissions have been widely demonstrated in microcavity structures using organic active media even at room temperature. These phenomena have potentials to obtain coherent emissions efficiently in comparison to that originating from SE processes, however, their excited state dynamics have not been well-clarified, and the guidelines to construct efficient device structures have not been well-established. Furthermore, in spite of low reflectivity for cavity photons, exciton polariton (EP) formation has been reported for organic single crystals even without introducing external cavity structures. Among

various aggregating conditions for organic materials, single crystal states can be regarded as ideal platforms to cause coherent emissions efficiently owing to their highly ordered and densely packed π-electronic transition dipole moments.

In this Chapter, amplified light emissions, lasing and laser-like behaviors in organic materials are described as fundamental background at first, then, the optoelectronic characteristics and unique lasing behaviors of thiophene/phenylene co-oligomers (TPCOs) which are the target materials in this dissertation are introduced. After that, polaritonic emissions, superradiance (SR) and superfluorescence (SF) are described as representative cooperative light emitting behaviors. Finally, aim of this study is stated.

1.2 Organic lasers

1.2.1 Mechanism of lasing from organic materials

Fundamental optical transition processes are categorized in 3 processes as shown in Figure 1.1 (a-c). Absorption is a transition process from ground-state (GS) to excited-state (ES) accomplished by the absorption of photon (Figure 1.1(a)). Figure 1.1 (b) shows the scheme of spontaneous emission, which is a light emission process caused by the electron energy relaxation through emitting a photon. The last one is stimulated emission (SE) process, which is accomplished by the formation of population inversion (Figure 1.1 (c)). The light emission causes the resonant photo-emission at population inversion state and each photon acquire coherence through in-phase emission.

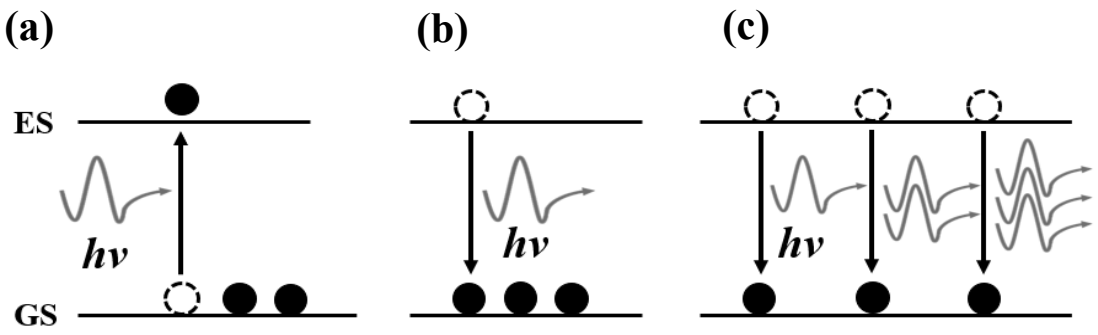

Figure 1.1. Schematic depictions of (a) (stimulated) absorption, (b) spontaneous emission and (c) stimulated emission (SE).

For organic semiconducting materials with π-electronic systems, the highest occupied molecular orbitals (HOMO) and lowest unoccupied molecular orbitals (LUMO) are essential to determine their optoelectronic characteristics. in the case of SE processes in organic materials, optical transitions are generally considered between singlet ground state (S_0) and singlet excited state (S_1). Each electronic energy level possesses quantized vibronic energy levels. As shown in Figure 1.2, optical excitation is normally depicted as the transition from level I to level II. After that, the excited state non-radiatively relaxes from level II to level III at very fast rate (within a few ps). The light emission is caused by the relaxation from level III to level IV. Finally, the population in level IV non-radiatively relax to level I at fast rate (within a few ps). Owing to the fast vibronic relaxation, the population inversion is easily formed between level III and level IV, resulting in efficient gains in the four energy level systems for organic π-conjugated materials.

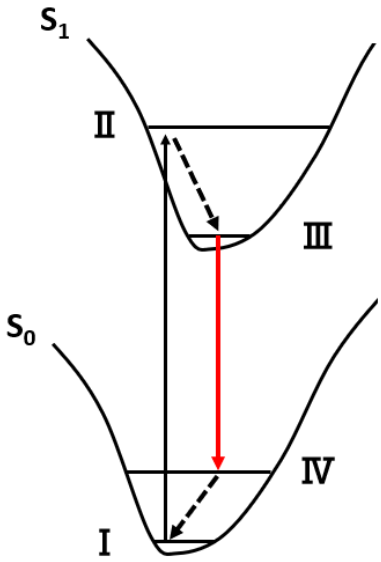

Figure 1.2. Schematic depiction of energy diagram for organic materials. The energy levels of I ~IV are electronic and vibrational ground state, electronic and vibrational excited state, electronic excited and vibrational ground state, and electronic ground and vibrationally excited state, respectively.

After the optical excitation process, the HOMO and LUMO orbitals in each molecule have one hole and one electron, respectively. The coulomb interaction between the hole and electron results in the formation of a quasi-particle, called exciton. Excitons in organic materials are generally described as the Frenkel exciton model, of which Bohr radius is smaller than a crystal unit cell, while that of inorganic materials are described as Mott-Wannier excitons, which are described as widely delocalized quasi-particles. Owing to high exciton binding energy for the Frenkel excitons, the excitons in organic materials are highly stable even at room temperatures, leading to stable SE processes. The emission wavelengths are variously changed by controlling the energy gap values between HOMO and LUMO. As well-known, with increasing the degree

of π-conjugation, the gap energy values become smaller, resulting in emissions in longer wavelengths.

The light emissions originating from the SE processes are called amplified spontaneous emissions (ASE), which is one of laser like emissions and it can occur even without any cavity structures. The term “LASER” is an acronym of the word “Light Amplification by Stimulated Emissions of Radiation”. As this term expresses, the origin of emissions of laser is generally considered as SE. Although lots of reports have been distributed to claim lasing, the exact criteria are sometimes confused. To govern the criteria for claiming lasing, one report was published in 2009.[1] According to the literature, the demands to claim lasing is as follows. i) Showing clear threshold for both or either light emission intensity and band width in excitation density dependences. ii) Clear cavity structures for the formation of narrower emission band width. In this dissertation, the word “laser” or “lasing” are used when the emission characteristics show both i) and ii) described above. If only the condition of i) is satisfied, the emissions are called such as “amplified light emission” or “light amplification behaviors”.

1.2.2 Structures of organic lasers

In this section, various types of organic lasers are described. The components of lasers can be categorized in i) excitation sources, ii) active media and iii) cavity structures. From the standpoint of i), it’s still challenging to demonstrate electrically-pumped lasing, however, optically-pumped one has been widely demonstrated using organic active media. As shown in Figure1.3 (a, b), electrically-pumped lasing has been reported recently for both organic light emitting diodes (OLEDs)[2] and organic light emitting field effect transistors (OLEFETs)[3] ,

after the achievement of electrically-pumped ASE.[4,5]

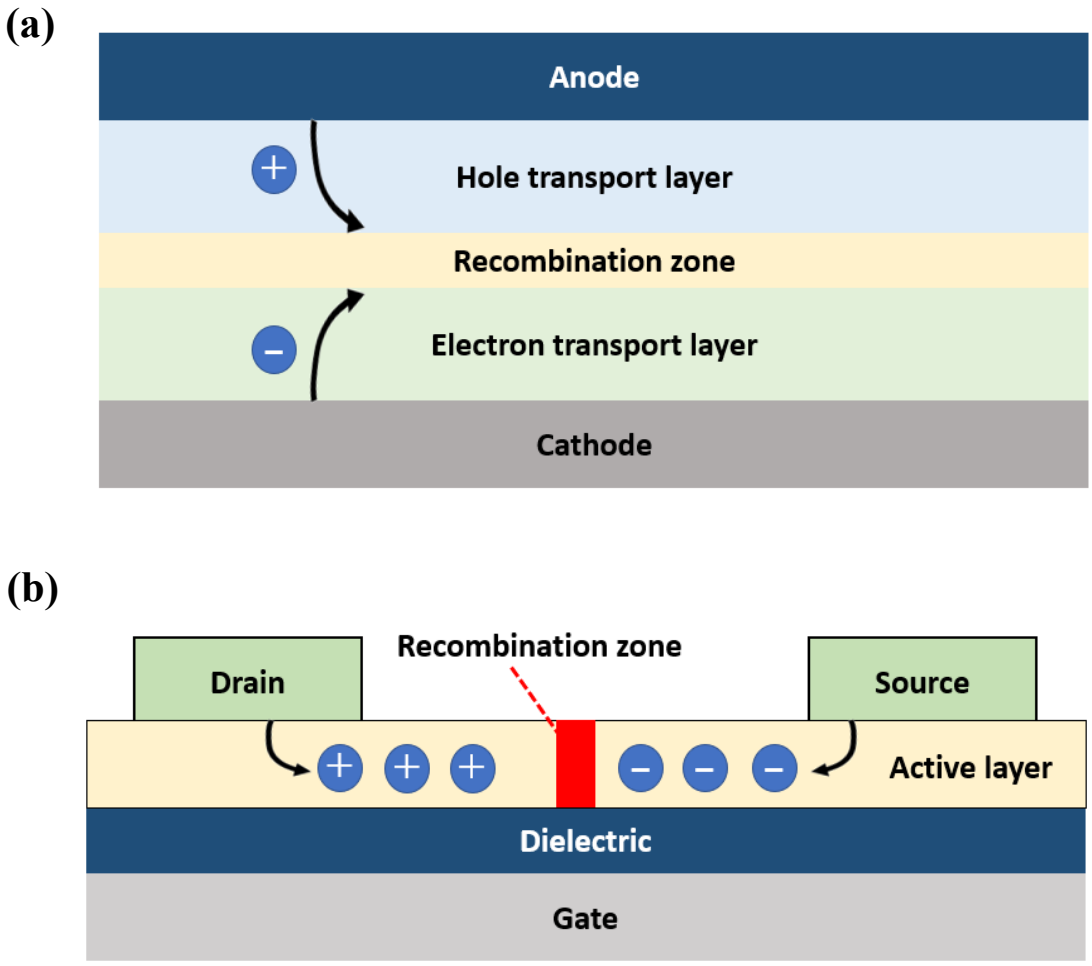

Figure 1.3. Structures of electrically-pumped organic lasers; (a) OLED type and (b) OLEFET type.

With respect to the standpoint of ii), the active media of organic compounds are roughly categorized in polymers or oligomers/co-oligomers. In general, polymeric state of organic π-conjugated materials are advantageous to fabricate active media via solution processes because of their flexibilities while oligomer one is advantageous to form highly ordered active media,

leading to the construction of efficient gain systems and waveguiding functions. For organic materials, optically-pumped lasing has been achieved for the first time using dye molecules dispersed in solution phases.[7] After that, ASE and lasing have been demonstrated in solid state materials such as polymer thin films, dye dispersed films and monolithic organic single crystals.[8] Solid state materials are advantageous as lasing media because of their robustness while dye molecules in solution can be easily deactivated. In Figure 1.4, the representative molecular backbones of π-conjugated co-oligomers for laser active media are depicted where backbones of (a) oligothiophenes, (b) oligophenylenes, (c) thiophene/phenylene co-oligomers and (d) distyrylbenzenes, respectively. Although the target materials in this dissertation are TPCOs, lasing or amplified light emissions from other types of oligomers shown in Figure 1.4, have been demonstrated. [9,10,11]

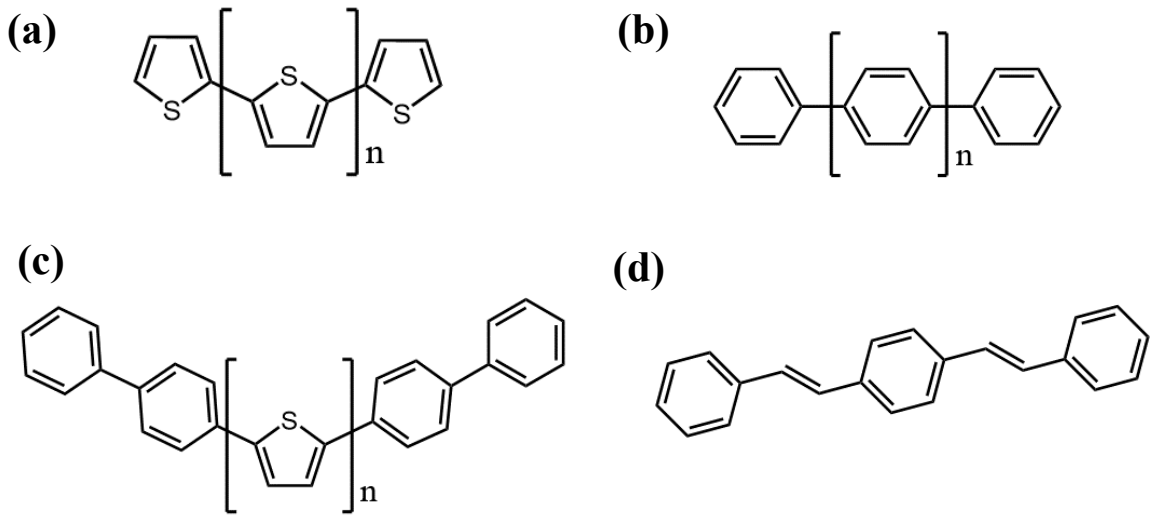

Figure 1.4. Typical molecular backbones of co-oligomers for active media of organic lasers (a) oligothiophenes, (b)oligophenylenes, (c) thiophene/phenylene co-oligomers and (d) distyrylbenzenes, where n is a natural number to have several hundreds of molecular weights.

With respect to the standpoint of iii), organic lasers have been demonstrated using a variety

of cavity structures. As mentioned in the previous section, cavity structures must be prepared to claim lasing, however, well-shaped organic single crystals can lase even without introducing external cavity structures due to the self-cavity effect, and those types of cavities can be called single crystal self-cavities. Although two dimensional thin platelet single crystals are widely utilized as single crystal self-cavities, one- or zero-dimensional single crystal cavities have also been fabricated, and lasing or amplified light emissions from those structures have been observed.[12-16] Single crystal cavities with lower dimensions are more advantageous to pursue the realization of low threshold lasers owing to their decreased mode volumes.[17]

As shown in Figure1.5 (a, b) oscillating conditions in single crystal self-cavities are categorized in Fabry-Pérot (F-P) modes and whispering gallery modes (WGM).[16] The former conditions can be achieved using a pair of parallel crystal edges while the latter one occurs by the traveling of photon waves along single crystal circumferences.

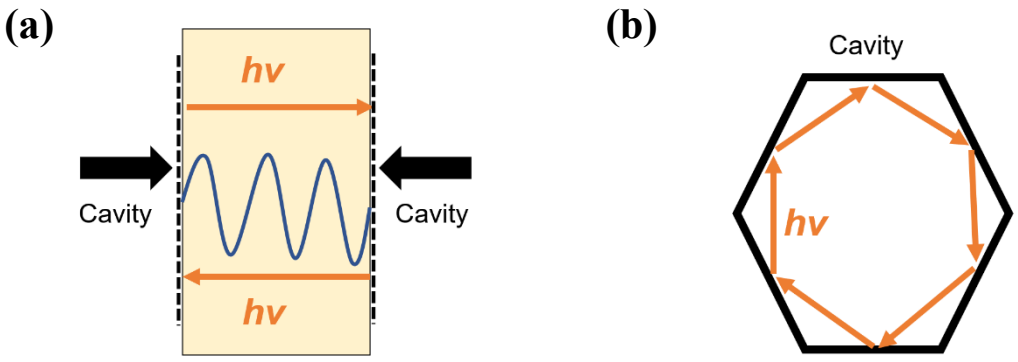

Figure 1.5. Schematic drawings of lasing in (a) F-P oscillation and (b) WGM oscillation for organic single crystal cavities.

Representative organic solid-state lasers with external cavity structures are vertical cavity

surface emitting lasers (VCSELs)[18] and distributed feedback (DFB) lasers[19,20]. The former one can lase in wide area, and highly monochromatic lasing can be achieved when the thickness of organic layers and external mirrors are rigorously controlled in the scales of emission wavelengths. Lasing from the latter structures can also be monochromatic owing to the construction of a diffraction grating with hierarchically controlled groove intervals. However, these structures are disadvantageous to construct organic active media because of the difficulty of accurate thickness control of active media or accurate estimations of refractive index values. Although single crystals of organic compounds are advantageous to construct efficient gain systems in comparison to amorphous or polycrystalline one, the determination of their refractive index values are complicated because of the existence of birefringence. Recently, T. Yamao *et al.*, have developed the method to construct DFB lasers with well-determined refractive index values for organic single crystal active media.[19,20]

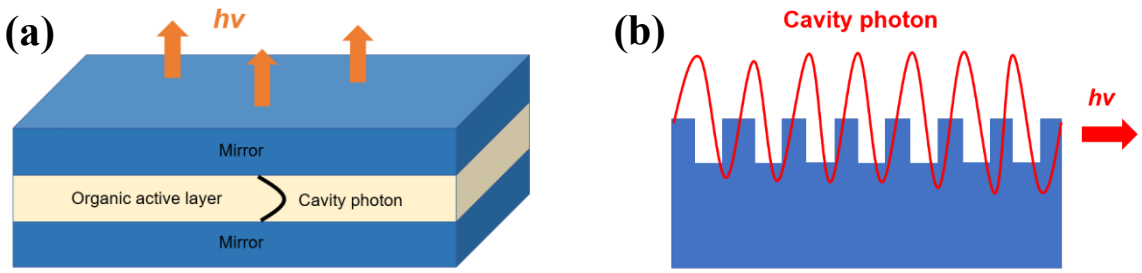

Figure 1.6. Schematic depictions of lasing from (a) VCSEL and (b) DFB structures.

Not only the lasing or amplified light emissions originating from the SE process, other unique gain systems have been constructed or proposed. For example, efficient gain systems based on excited state intramolecular proton transfer (ESIPT)[21] and Förster resonance energy transfer (FRET)[22] have been demonstrated. Especially, one of gain systems using FRET, utilizing triplet excited states have been established, which leads to the possibilities to realize highly

efficient electrically-pumped lasing. Formation of triplet excited states are normally energy loss to achieve lasing because amplified light emissions from the states have hardly been observed.

1.2.3 Engineering potential of organic lasers

So far, organic materials have been already industrially utilized as laser media owing to their superior characteristics described in the previous section. Organic dye lasers are representative examples, which are operated in dispersed solution conditions. Owing to easy chemical modification of organic dye molecules, highly tunable laser emission has been achieved, however, those dispersed solution systems cost too much to operate and the dye molecules are easily being deactivated. To overcome these problems, solid state organic materials are suitable as alternatives.

Furthermore, owing to the solution processabilities for some organic materials, organic laser media can be constructed even on flexible substrates, resulting in the fabrication of flexible laser devices.[9]

Apart from the potentials as illumination sources, organic lasers are applicable for sensing. Lasing wavelength are sensitively changed depending on the refractive indices of surrounding media, which are variably changed by the existence of molecules or gases in the vicinity of organic active media.[9]

1.3 Thiophene/phenylene co-oligomers (TPCOs)

1.3.1 Molecular and crystal structures of TPCOs and their optoelectronic characteristics

TPCOs are composed of linearly chained phenylene and thiophene units. Various TPCO molecules have been synthesized so far, [23-29] and their crystal structures have been revealed[30-34]. Similar to the cases of other types of organic semiconducting compounds, TPCOs have been synthesized via coupling reactions named Negishi-coupling or Suzuki-coupling, which are well-known and frequently utilized reactions to produce carbon-carbon bonding. Almost all of TPCOs as laser media being investigated nowadays have been synthesized from two decades ago.

Conditions for fabrication of solid-state organic materials are categorized in vapor or solution phases. To grow TPCO single crystals as laser media, both conditions have been utilized. The representative crystal growth method in former conditions is called physical vapor transport (PVT) method, which is a sublimation process under inert gas flowing conditions.[33] On the other hand, crystal growth under the latter conditions utilizes temperature gradient in TPCO dispersed solutions.[34]

Since π-electronic dipole moments in TPCO molecules are almost parallel to molecular long axes, the orientation of transition dipole moments can be easily determined by estimation of that of molecular long axes. Figure 1.7 shows the crystal structures of TPCO compounds with fluorescence or transmittance microscope images and molecular structures. The double-headed arrows express the directions of transition dipole moments. Crystal structures are variously changed depending on the molecular structures owing to the differences of intermolecular

interactions. As shown in Figure 1.7 (a), the transition dipole moments are inclined to the crystal bottom planes (*ab*-plane) in the case of P6T,[8] however, those of BP1T are almost perpendicular to the crystal bottom planes (*ab*-plane),[30] which indicates uniaxial molecular orientation for biphenyl capped TPCO molecules. Not only the case of BP1T, other biphenyl end-capped TPCOs abbreviated as BP_nT series (n = 1 ~ 4, and structures are depicted in Figure 1.4 (c)) have uniaxial orientation of their molecular long axis, leading to the perpendicularly oriented transition dipole moments to the crystal bottom planes.[32] Not only the differences of molecular backbones, substituents are also critical to crystal structures. Although almost all of TPCOs including BP1T crystallize in the monoclinic form, methoxy-substituted BP1T (BP1T-OMe) and cyano-substituted BP1T (BP1T-CN) crystallize in orthorhombic and triclinic forms, respectively.[31,33] The origins of these different crystal structures have been attributed to the interactions between substituents. For BP1T-OMe, hydrogen bonding leads to different molecular packing from that of unsubstituted BP1T, while electrostatic interactions between cyano-substituents contribute to form the slipped molecular packing in the case of BP1T-CN.

Owing to the differences of molecular and crystal structures, the orientation of π-electronic transition dipole moments is variously changed, leading to the drastic differences in light emitting properties especially for lasing from single crystal states. For example in the cases of BP1T and its end-substituted derivatives described in Figure 1.7 (b, c), owing to the perpendicular molecular orientation to the crystal basal planes for BP1T and BP1T-OMe, light emissions from their single crystals propagate along crystal basal planes, and light emissions occur from crystal edges.[35,36] Moreover, their emissions are highly polarized in transverse magnetic (TM) modes. Not only for the above example, almost all of crystals of biphenyl end-

capped TPCOs show those edge emissive characteristics. On the other hand, light emissions from single crystals of cyano-substituted TPCOs appear from their platelet surface owing to their inclined molecular orientation to the crystal basal planes.[33] These surface emissive characteristics are suitable for active media in VCSELs.

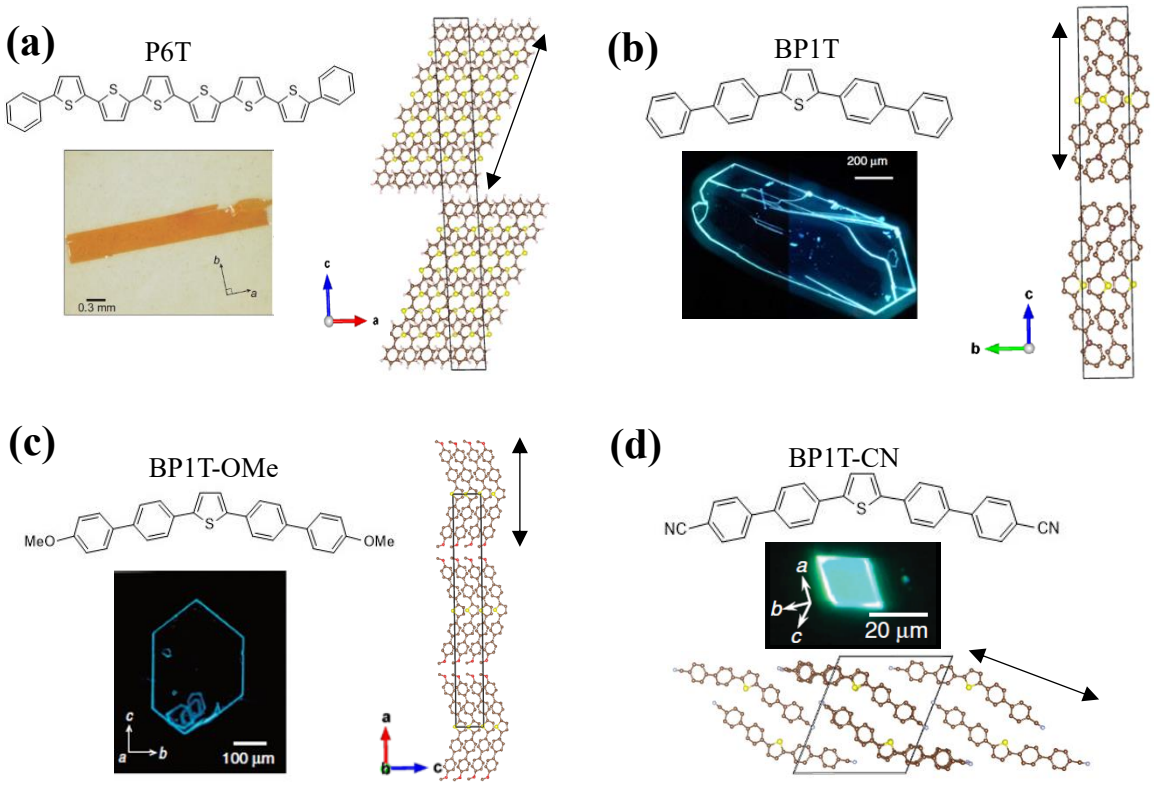

Figure 1.7. Molecular and crystal structures of TPCOs. (a) P6T, (b) BP1T, (c) BP1T-OMe and (d) BP1T-CN with each fluorescence or transmittance microscope image of single crystals. The double-headed arrows express the directions of π-electronic transition dipole moments. (*a*) Reproduced with a permission.[8] Copyright 2005, Wiley-VCH. (b) Reproduced with a permission.[35] copyright 2010, The Japan Society of Applied Physics. (c) Reproduced with a permission.[36] copyright 2011, The Japan Society of Applied Physics. (d) Reproduced with a permission.[33] Copyright 2014, Wiley-VCH.

π-electronic transition dipole moments for almost all of TPCOs have parallel orientations each other in the crystal unit cells, which structures are called H-aggregates. In these aggregating conditions, the absorption and light emissions assigned as the 0-0 transitions (electronic transitions without excitation of vibronic modes) are inhibited due to the anti-parallel coupling of dipole moments, while their vibronic replica are clearly found in absorption or PL spectra. In the case of crystal structures of BP_nT series (n = 1,2,3,4) of TPCOs, the molecules align with zig-zag orientation each other in the *ab*-plane, which is called herringbone structure, while the face-to-face stacking of π-electronic molecules is called π-stack type orientation. The carrier transport characteristics in the former orientation are isotropic while the latter ones are anisotropic.

Although oligothiophenes which are one of promising organic semiconducting compounds show high carrier mobilities, TPCO molecules have shown both high carrier mobility and high fluorescence quantum yields. Of these, one of TPCO compounds, 5,5″-bis(4-biphenylyl)-2,2′:5,2″-terthiophene (BP3T) has shown 80% of quantum efficiency,[13] 1.64 cm^2/Vs of hole mobility and 0.17 cm^2/Vs of electron mobility in single crystal state,[4] showing remarkably superior characteristics in both carrier transport and light emissions.

1.3.2 Optically pumped lasing from TPCO single crystals

Owing to the densely and uniaxially packed molecular orientations in single crystals, TPCO single crystals are advantageous to achieve optically pumped lasing owing to their self-cavity effects. As shown in Figure 1.8 (a), a well-shaped TPCO single crystal has a pair of parallel edges, which is expectable to serve as a F-P cavity. Under optical pulse excitation, the integrated intensity of photoluminescence (PL) is nonlinearly increased (Figure 1.8 (b)), and longitudinal multi-modes appear above a threshold as shown in Figure 1.8 (c), which indicates the oscillation of emitted light in a cavity. Thin platelet single crystals of biphenyl capped TPCOs are suitable for active media of organic lasers, because the perpendicular orientation of π-electronic transition moments to the crystal bottom planes are ideal to interact with electric field of cavity photons. So far, optically pumped lasing by the self-cavity effects from TPCO single crystals has been observed for one- or two-dimensional TPCO single crystals.[8-15, 17, 33, 34, 36-43] Moreover, lasing from VCSEL structures have also been observed using cyano-substituted TPCOs as active media.[44-49] Not only the ideal orientation of π-electronic transition moments, TPCO single crystals possess high refractive indices, which gives ideal conditions to confine cavity photons efficiently.[50-53]

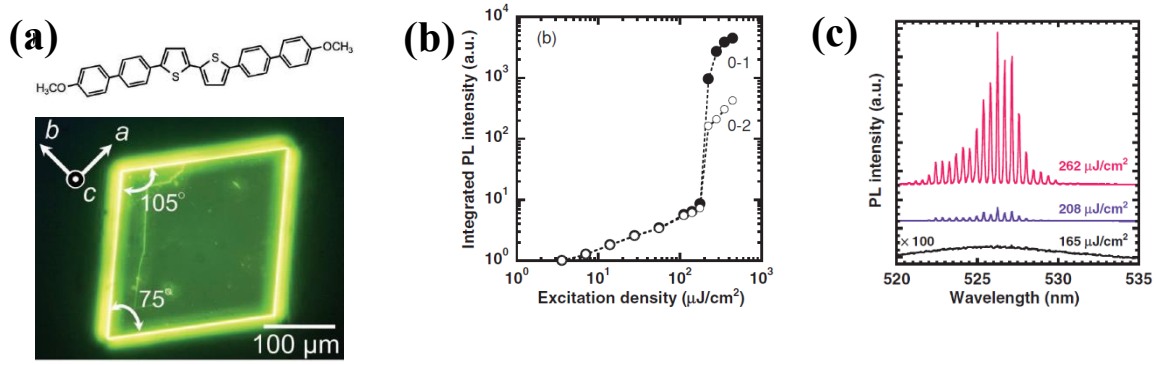

Figure 1.8. (a) Molecular structure of BP2T-OMe and a fluorescence microscope image of its single crystal showing a pair of parallel crystal edges for F-P oscillation. (b) Excitation density dependences of integrated photoluminescence (PL) intensity showing clear thresholds. (c) Excitation density dependence of PL spectra showing longitudinal multi-mode lasing at 262 μJ/cm^2 (above threshold), which is an evidence of oscillation in F-P modes. Reproduced with a permission.[34] Copyright 2012, Wiley-VCH.

To evaluate the waveguiding functions in TPCO single crystals, optical gain values have been estimated using variable stripe length (VSL) or pump-probe technique.[33,54,55] According to the literatures, [33,54,55] high optical gain values (ca. 50 ~ 120 cm^{-1}) have been reported above the threshold of amplified light emissions.

1.3.3 Unique lasing and amplified light emission characteristics in TPCO single crystals.

Although the origin of optically-pumped lasing or amplified light emissions from organic single crystals has been conventionally attributed to the SE process, however, that from TPCO crystals sometimes cannot be described as the SE process, but is attributable to cooperative behaviors such as superfluorescence or polaritonic emissions.[56] Those behaviors are described

as following i) ~ iv), and the detail description of cooperative processes are shown in the next section.

ⅰ) Unusually split lasing spectra with longitudinal multi-mode in a specific vibronic transition band have been observed in F-P oscillating conditions, which cannot be attributed to random lasing because of the existence of clear oscillation modes with constant mode intervals in lasing spectra.[36] Figures 1.9 (a), (b), (c) show the excitation density dependence for PL spectra, the excitation density dependence of integrated PL intensity and enlarged lasing spectra at excitation density of 3.20 mJ/cm^2, respectively. As shown in Figure1.9 (a), the split spectra are gradually converged into one PL band from splitting conditions with increasing excitation density. Figure 1.9 (c) shows split lasing band below threshold. Because of this band splitting below the threshold, these phenomena have been named prethreshold lasing. The origin of prethreshold lasing is possibly attributable to polaritonic behaviors.

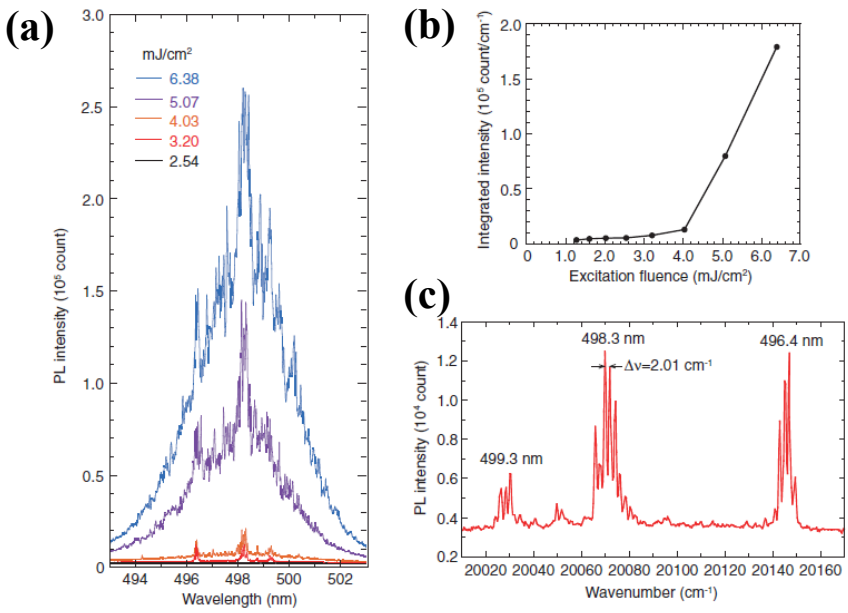

Figure 1.9. (a) Excitation density dependence of optically pumped PL spectra obtained from a single crystal of BP1T-OMe and (b) that of integrated PL intensity. (c) Lasing spectrum at excitation density of 3.20 μJ/cm² showing unusually split lasing spectrum with longitudinal multi-modes. Reproduced with a permission.[36] copyright 2011, The Japan Society of Applied Physics.

ii) Pulse-shaped emissions accompanied with time delay from several tens to several hundred picoseconds with respect to the excitation pulse origin have been observed in time resolved PL measurements.[36,57,58] Figures 1.10 (a) and (b) show time-resolved PL profiles obtained from a BP1T-OMe single crystal at each excitation density for the 0-2 and 0-1 vibronic progressions, respectively. In the former profiles, the time decays become pulse shapes with delay time above the threshold, and the delay time is gradually decreased with increasing excitation density. The maximum delay time above the threshold is *ca.* 300ps while the delay time in the SE process above the threshold is only a few ps. On the other hand, the profiles in the 0-1 emission lines have not shown such long delay times, indicating the fact that the pulse-shaped delayed emissions are wavelength selective behaviors. The unusually long delay time has been

interpreted as build-up time of a macroscopically correlated emitters, which resembles that of polaritonic behaviors in a microcavity structure with inorganic or organic semiconductors as active media.

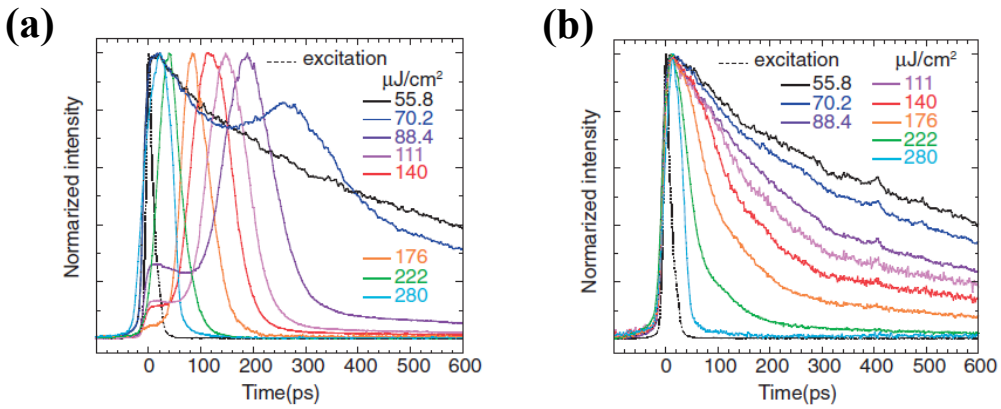

Figure 1.10. Time-resolved PL profiles at each excitation density for (a) 0-2 and (b) 0-1 emission bands observed from a BP1T-OMe single crystal, showing wavelength selective pulse-shaped emissions at 0-2 emission bands. As for (a), maximum delay time is shown at lower excitation density, and the delay time is gradually decreased with increasing excitation density, which can be attributed to the transitions from polaritonic behavior to SE process. For (b), the shorter delay time can be attributed to SE process. Reproduced with a permission.[36] copyright 2011, The Japan Society of Applied Physics.

iii) Excitation beam area dependences for the threshold of gain-narrowed amplification have been observed, which strongly suggest the contribution of superfluorescent phenomena in amplified light emissions. For the case of the measurement using a BP3T single crystal at 12K shown in Figure 1.11 (a), the optical excitation beam area is varied by changing the length (L) of stripe shaped excitation beam without changing excitation beam width.[59] In the case of SE processes, the excitation density threshold of light amplification or gain-narrowing is

independent of the excitation area. Figure 1.11 (b) shows excitation density dependences of full width at half maximum (FWHM) in the 0-1 emission line at each *L*, and (c) for the 0-2 line. As explained above, the 0-1 line shows SE like behaviors and 0-2 line shows superfluorescent behaviors. Furthermore, these excitation area dependences have been observed even at room temperature for one of furan-chained oligomers, 2-([1,1′-biphenyl]-4-yl)-5-(5-([1,1′-biphenyl]-4-yl)thiophene-2-yl)furan (BPFT), recently.[60]

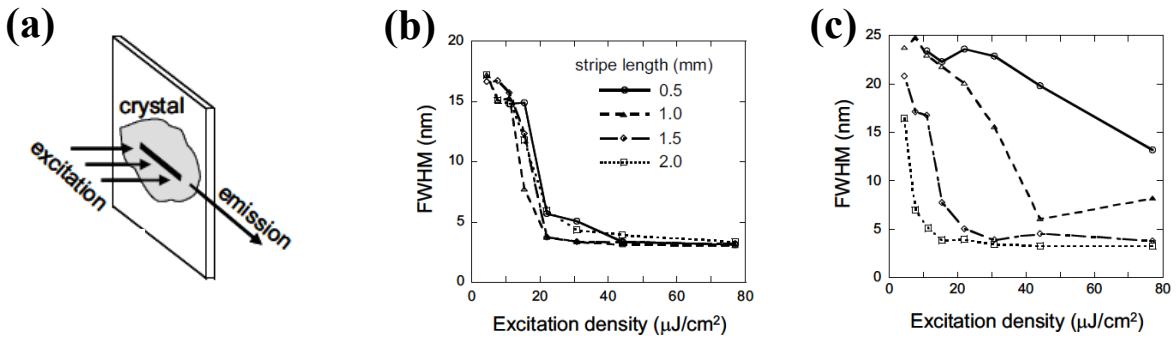

Figure 1.11 (a) Schematic depiction for measurement of excitation beam length dependence of excitation gain-narrowing threshold. Excitation area is varied by changing excitation beam length (L) without changing excitation beam width. (b) Excitation density dependences of band width at each L for 0-1 line and (c) for 0-2 line. For 0-2 line, threshold of gain-narrowing is gradually decreased with increasing L, while such dependence is not seen in 0-1 line. Reproduced with a permission.[59] copyright 2009, The Japan Society of Applied Physics.

iv) Mirrorless lasing based on stimulated resonance Raman scattering (SRRS) has been observed for TPCO single crystals, which strongly suggests the formation of cooperatively coupled molecular vibrations.[61-63] Figure 1.12 (a) shows SRRS spectra observed for a BP3T

single crystal around vibronic transition of 0-1 and 0-2 emission lines (around 575 nm and 625 nm, respectively).[63] With increasing excitation wavelength, the emission wavelength accordingly increases keeping a constant energy interval between excitation and emission wavelengths. Although SRRS has been observed under resonant excitation, that from BP3T single crystals can be observed under off-resonant excitation condition (Figure 1.12 (b)), which origin is attributed to the contribution of molecular vibration at optical excitation. Not only for TPCO single crystals, SRRS has been observed for dye doped polymers, single crystals of anthracene and DSB derivatives.[64-66] The light emissions based on SRRS are substantially narrow compared to that of ASE, and their emission wavelengths are highly tunable by changing the optical excitation wavelength. Moreover, SRRS can be observed even at room temperature.

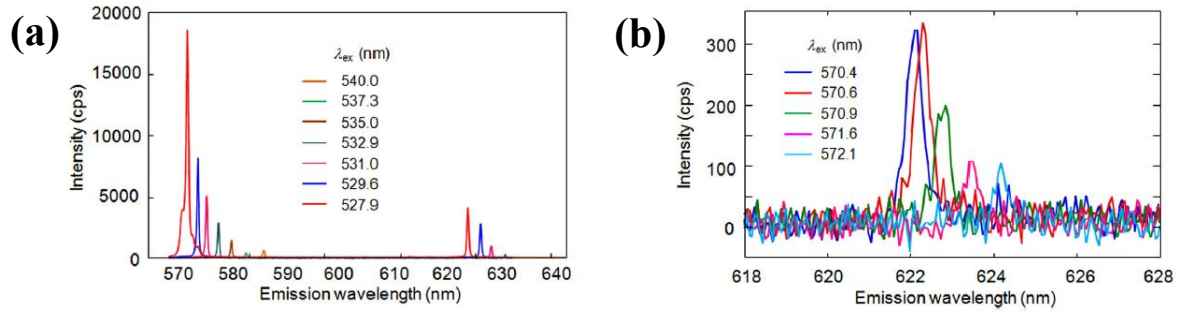

Figure 1.12 (a) SRRS spectra at each excitation wavelengths observed around the wavelength of vibronic transitions in 0-1 and 0-2 lines. (b) SRRS spectra around 0-2 emission line under off-resonant excitation. Reproduced with a permission.[61] Copyright 2013, American Institute of Physics.

As another unique lasing behavior, the effect of cavity quantum electro-dynamics (QED) can appear in amplified light emitting characteristics.[39,67] By this effect, light amplification threshold can be decreased with decreasing cavity length, while conventional lasing shows opposite dependences.

1.4 Cooperative behaviors in coherent light emissions

Conventional photon lasing process derives from the SE processes can be categorized in "collective behaviors", in which case each exciton emits a photon individually. In other cases, coherent light emissions sometimes can be described as "cooperative behaviors". In that case, the aggregate of excitons behaves as one macroscopic emitter, instead of behaving as individual one. Since the excitons of organic molecules are described as Frenkel excitons, the origins of amplified light emissions or lasing from organic materials generally regarded as conventional photon lasing, however, cooperative behaviors have been indicated as described in the previous section. In this section, cooperative behaviors are described in more detail.

1.4.1 Superradiance (SR) and superfluorescence (SF)

Superradiance (SR) is one of cooperative coherent light emitting behaviors, in which excited state coherence is formed by the interaction between individual emitters and vacuum field. On the other hand, coherence among emitters in superfluorescence (SF) is acquired via interaction with photon field. As described in Figure 1.13 (a), SF is coherent photon burst with delay time relative to optical pulse excitation originating from the formation of macroscopically correlated emitters. The pulse-shaped delayed emissions in SF are theoretically follow the relationships

shown below,

$$\tau_D \propto \frac{\log(N)}{N} \tag{1.1}$$

$$\tau_{SF} \propto \frac{\tau_{sp}}{N} \tag{1.2}$$

$$I_{SF} \propto N^2 \tag{1.3}$$

where N, τ_D,τ_{sp}, τ_{SF}, I_{SF} are the number of individual emitters after excitation by optical pulse, delay time from optical excitation, lifetime of spontaneous emission as individual emitters, lifetime of SF and peak intensity in time profiles, respectively. SF behaviors have been observed under optical pulse excitation, and the number N can be replaced with the number of excitation fluence (μJ/cm^2). As shown in Figure 1.13 (b), the values of τ_D and τ_{SF} decrease with increasing the number of N, which resembles the behaviors observed for TPCO single crystals.[36,57,58] Characteristics in time profiles are dependent on N in the case of SF, while those of SE process is independent. SR was first suggested in 1954 by R. H. Dicke.[68] Afterwards, SF has been observed for gas phase materials.[69,70] Then, SR and SF have been reported for solid state materials.[71-83] Although coherence among excited species is easily diminished by thermal perturbation at high temperature, SR has been observed even at room temperature recently.[83] For organic materials, SR and SF have been suggested in light emissions from π-conjugated polymers, single crystals of *J*- or *H*-aggregated compounds. Furthermore, SF has been suggested for organic single crystals as described in the previous section. Although SF is coherent photon burst, cavity structures is not necessary to be prepared.

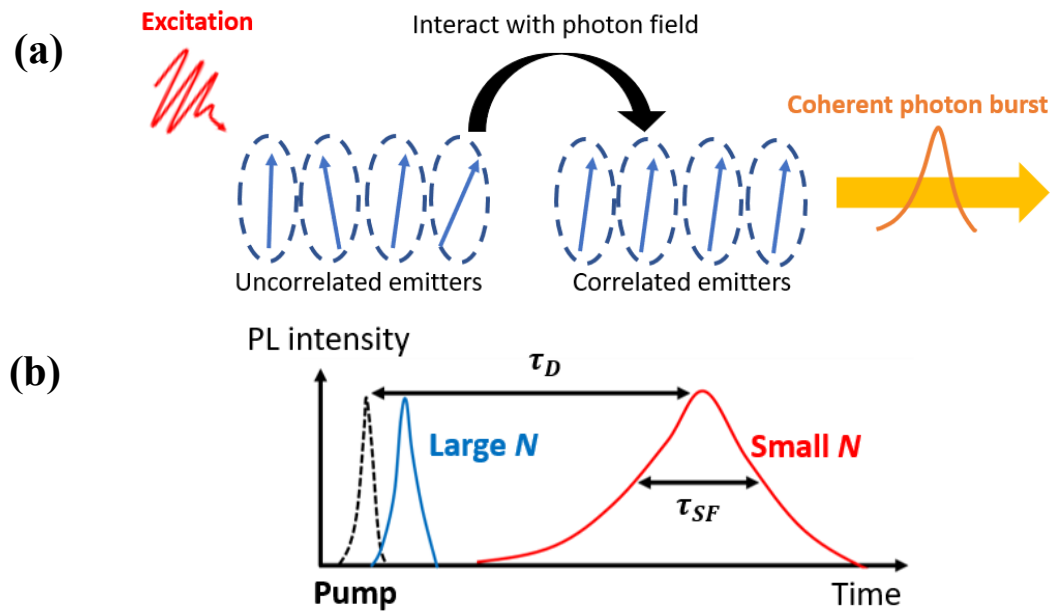

Figure 1. 13 (a) Schematic depiction for mechanism of SF. The blue arrows and circles drawn by dashed lines represent the directions of dipole moments and each unit of emitters. (b) Time profiles of PL intensity in the case of larger number of N and smaller number of N.

1.4.2 Exciton-polaritons (EPs)

Exciton-polaritons (EPs) are quasi-particles which are formed by the strong coupling between excitons and cavity photons. Same as the cases of SF, coherence among EPs is acquired by interaction between excitons and coherent photon field. Although the degree of interaction between excitons and photons are roughly categorized in week coupling regime and strong coupling one, SF is categorized in the former while EP formation is the latter. In the EP formation, photons interact many times with excitons until radiating from cavity structures, and both excitons and photons cannot be regarded as each particle. The time profiles of light emissions from EPs have shown several tens picosecond of delay time, which resemble the pulse-shaped delayed emissions observed for TPCO single crystals.[84] Moreover, these delay time has been observed also for organic microcavity structures.[45]

The structures for constructing EPs are microcavity structures or waveguiding structures. For EP formations using organic materials, the former structures have been mainly utilized.

1.4.3 Polaritonic behaviors in organic microcavity structures

EP formation and polariton lasing have been demonstrated for organic materials in microcavity structures.[44-48,85-92] To confirm the EP formation in microcavity structures, angle resolved optical measurements have been performed in emissions, reflectance or transmittance spectroscopies (Figure 1.14(a)). EP formations have been confirmed by observation of anti-crossing behaviors in transition energy vs angle plots. While excitons do not show angle dependence in transition energy, polariton branches composed of upper polariton branch (UPB) and lower polariton branch (LPB) show angle dependences in energy dispersions. (Figure 1.14(b))

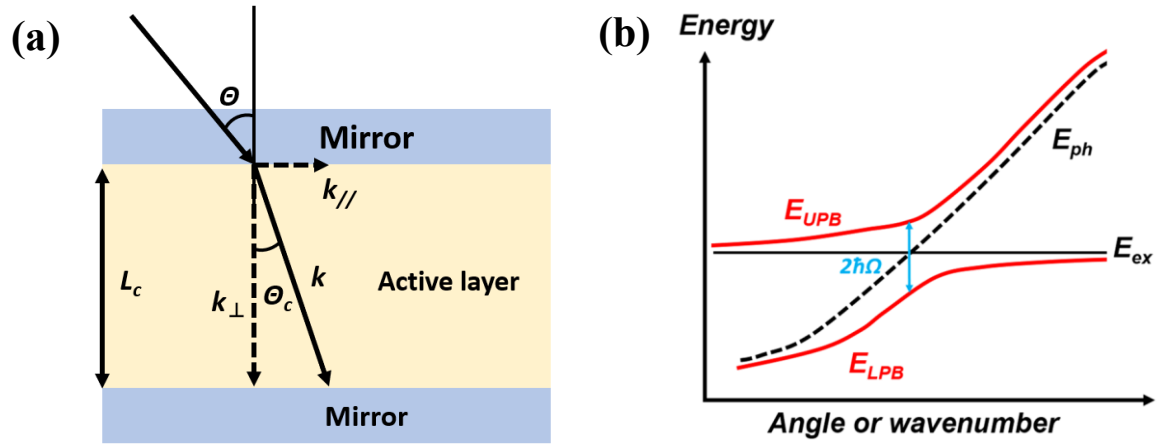

Figure 1.14 (a) Schematic depiction of angle dependent optical measurement to confirm the existence of EPs, and (b) dispersion curves of lower polariton branch (LPB) and upper polariton branch (LPB) as a result of strong coupling between excitons and cavity photons.

The EP formation in organic materials has been demonstrated for the first time in 1998 by D. G. Lidzey *et al.* using one of porphyrin dye molecules as an active medium in a microcavity structure.[85] Although excitons of organic materials are Fermions, EPs are described as Bosonic particles. Owing to the Bosonic characteristics, EPs can exhibit the phenomena named Bose-Einstein condensation (BEC), which is one of phase transition phenomena. In BEC, a large number of EPs can occupy the most stable energy level, which can be regarded as a macroscopically correlated emitters similar to superfluorescence. Coherent photon burst results from BEC are called polariton lasing, which has been observed from the most stable energy level (0 degree (k = 0) in Figure 1.14 (b)) in LPB. In organic materials, EPs can be stably formed owing to their high exciton binding energy resulting in demonstration of polariton lasing even at room temperature. Polariton lasing has been demonstrated in 2010 for the first time using an anthracene single crystal as an active medium, and then it has been demonstrated

for several organic materials.[86,87] To construct low threshold laser devices based on polariton lasing, excited state dynamics have been investigated using time resolved optical measurements such as pump-probe technique.[88-90] Not only under optical pumping, EP formation has been confirmed under electrical pumping.[91-93]

1.4.4 EPs in single crystal cavity

The EP formations has been reported also for single crystal cavity even without introducing external cavity structures. K. Takazawa *et al.* have reported EP waveguiding in sub-milimeter length for organic materials, and the EP formations have also been reported for other single crystals of organic materials.[94-97] However, lasing from EPs *i.e.* polariton lasing in these structures has not been achieved. To the best of our knowledge, all reports of EP formations in organic single crystal cavity have been reported for one-dimensional cavity structures. In these literatures, efficient EP propagation is reported. To confirm the EP formation, wavenumber dependences of energy dispersion have been investigated similar to the cases of microcavity structures.

1.4.5 Contribution of molecular vibrations in cooperative behaviors

Different from most of the cases in inorganic materials, intra- or intermolecular vibrations should be considered in electronic transitions because of their coupling with electronic transitions. In SR or SF, generally, molecular vibronic or phonon modes are considered to dissipate coherence among excited state molecules, however, SF has been suggested in the energy levels of vibronic transitions.[59,60] In those cases, vibronic modes should also be

coherent among excited state molecules.

For EP formation, vibrationally-assisted polariton relaxation processes (Figure 1.15) are reported for microcavity structures.[98] Due to the scattering by molecular vibrations from exciton reservoir to LPB, polariton population is accumulated at certain energy levels in LPB.[98] According to the theoretical calculations and time resolved optical experiments, the time scale of relaxation from exciton reservoir to LPB has been estimated around several ps to several hundred of ps.[99-102] Moreover, molecular vibrations can contribute to form unique EP states termed vibrationally-dressed exciton polaritons (VDEPs), which are EPs dressed with molecular vibrations.[103,104]

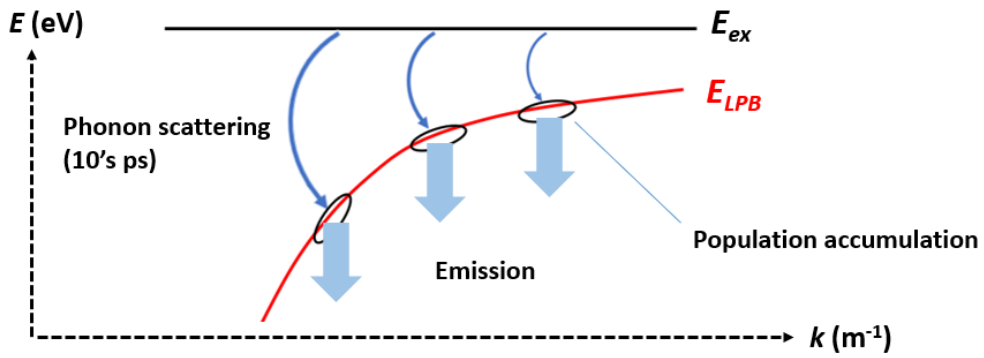

Figure 1.15 A schematic depiction of polaritonic emissions as a result of population accumulation at certain energy levels in LPB caused by vibrationally assisted relaxation from energy levels of exciton reservoir to LPB.

1.5 Aim of this study

From viewpoints of research backgrounds mentioned above, in this dissertation, optically pumped lasing characteristics in TPCO single crystals were further investigated in terms of cooperative behaviors.

In this research, single crystals of BP3T were adapted as main target among a variety of TPCO series since the compound has shown superior optoelectronic characteristics such as high quantum yield and ambipolar carrier transport characteristics, resulting in the possibilities to construct efficient laser devices based on cooperative phenomena.

To discuss the effect of substituents at molecular terminal ends for lasing characteristics, BP3T derivatives were newly synthesized, and lasing characteristics were compared among those BP3T derivatives including BP3T. Lasing characteristics including cooperative ones can be variously modulated by modification of molecular structures owing to the modulation of crystal structures.

For investigation of lasing characteristics in single crystals of BP3T derivatives under optical pumping conditions, improved crystal growth method was proposed in this dissertation. Although F-P lasing has been reported for single crystals of TPCOs under optical pumping conditions, it's still difficult to fabricate well-shaped single crystals with high reproducibility, resulting in the difficulties in investigation of lasing characteristics and fabrication of organic laser devices.

As described in this Chapter, pulse shaped delayed emissions observed in TPCO single crystals are indicative of cooperative phenomena, however, further investigation is necessary to claim cooperative behaviors. To claim cooperative phenomena in optically pumped lasing

or amplified light emissions for TPCO single crystals, the cooperative phenomena were investigated in more detail in terms of both SF and polaritonic behaviors. Especially, lasing characteristics were investigated by energy vs wavenumber plots for the first time to claim polaritonic behaviors for optically pumped lasing in organic single crystals.

References:

[1] I. D. W. Samuel, E. B. Namdas and G. A. Turnbull, *Nat. Photonics*, **2009**, 3, 546.

[2] S. Sandanayaka, T. Matsushima, F. Bencheikh, S. Terakawa, W. J. Potscavage Jr, C. Qin, T. Fujihara, K. Goushi, J. Ribierre and C. Adachi, *Appl. Phys. Express*, **2019**, 12, 061010.

[3] T. Kanagasekaran, H. Shimotani, K. Kasai, S. Onuki, R. D. Kavthe, R. Kumashiro and K. Tanigaki, arXiv:1903.08869, **2019**.

[4] S. Z. Bisri, T. Takenobu, Y. Yomogida, H. Shimotani, T. Yamao, S. Hotta and Y. Iwasa, *Adv. Funct. Mater.*, **2009**, 19, 1728.

[5] S. Z. Bisri, K. Sawabe, M. Imakawa, K. Maruyama, T. Yamao, S. Hotta, Y. Iwasa and T. Takenobu, *Sci Rep.*, **2012**, 2, 985.

[6] R. Ding, M. H. An, J. Feng, and H. B. Sun, *Laser Photonics Rev.*, **2019**, 13, 1900009.

[7] F. P. Schäfer, W. Schmidt and J. Volze, *Appl. Phys. Lett.*, **1966**, 9, 306.

[8] M. Ichikawa, R. Hibino, M. Inoue, T. Haritani, S. Hotta, K. Araki, T. Koyama and Y. Taniguchi, *Adv. Mater.*, **2005**, 17, 2073.

[9] J. C. Kuehne and M. C. Gather, *Chem. Rev.*, **2016**, 116, 12823.

[10] J. Gierschner, S. Varghese and S. Y. Park, *Adv. Opt. Mater.*, **2016**, 4, 348.

[11] H. H. Fang, J. Yang, J. Feng, T. Yamao, S. Hotta and H. B. Sun, *Laser Photonics Rev.*,

2014, 8, 687.

[12] M. T. Hill, M. C. Gather, *Nat. Photon.*, **2014**, 8 904.

[13] S. Kanazawa, M. Ichikawa, T. Koyama, Y. Taniguchi, *Chem. Phys. Chem.*, **2006**, 7, 1881.

[14] K. Torii, T. Higuchi, K. Mizuno, K. Bando, K. Yamashita, F. Sasaki and H. Yanagi, *Chem. Nano. Mat.*, **2017**, 3, 625.

[15] H. Mizuno, I. Ohnishi, H. Yanagi, F. Sasaki and S. Hotta, *Adv. Mater.*, **2012**, 24, 2408.

[16] H. Yanagi, M. Kondo, N. Matsuoka, M. Nagawa, and Y. Taniguchi, *Chem. Mater.*, **2001**, 13, 4800.

[17] H. Mizuno, Y. Mekata, F. Sasaki and H. Yanagi, *Jpn. J. Appl. Phys.*, **2020**, 59, SGGG02.

[18] D. Ballarini and S. D. Liberato, *Nanophotonics*, **2019**, 8, 641.

[19] T. Yamao, S. Higashihara, S. Yamashita, H. Sano, Y. Inada, K. Yamashita, S. Ura, and S. Hotta, *J. Appl. Phys.*, **2018**, 123, 235501.

[20] Y. Inada, Y. Kawata, T. Kawai, S. Hotta and T. Yamao, *J. Appl. Phys.*, **2020**, 127, 053102.

[21] S. Park, O.-H. Kwon, S. Kim, S. Park, M.-G. Choi, M. Cha, S. Y. Park and D.-J. Chang, *J. Am. Chem. Soc.*, **2005**, 127, 10070.

[22] Y. Jiang, P. Lv, J.-Q. Pan, Y. Li, H. Lin, X.-W. Zhang, J. Wang, Y.-Y. Liu, Q. Wei, G.-C. Xing, W.-Y. Lai and W. Huang, *Adv. Funct. Mater.*, **2019**, 29, 1806719.

[23] S. Hotta, S. A. Lee and T. Tamaki, *J. Heterocycl. Chem.*, **2000**, 37, 25.

[24] S. Hotta, H. Kimura, S. A. Lee and T. Tamaki, *J. Heterocycl. Chem.*, **2000**, 37, 281.

[25] S. Hotta, *J. Heterocycl. Chem.*, **2000**, 38, 923.

[26] S. Hotta and T. Katagiri, *J. Heterocyclic Chem.*, **2003**, 40, 845.

[27] T. Katagiri S. Ota T. Ohira T. Yamao and S. Hotta, *J. Heterocyclic Chem.*, **2007**, 44, 853.

[28] R. Hirase, M. Ishihara, T. Katagiri, Y. Tanaka, H. Yanagi and S. Hotta, *Org. Electron.*, **2014**, 15, 1481.

[29] Y. Inada, M. Koda, Y. Urabe, T. Katagiri, T. Yamao, Y. Yoshida and S. Hotta, *Sci. Rep.*, **2019**, 9, 9739.

[30] S. Hotta and M. Goto, *Adv. Mater.*, **2002**, 14, 498.

[31] S. Hotta, M. Goto and R. Azumi, *Chem. Lett.*, **2007**, 36, 270.

[32] S. Hotta, M. Goto, R. Azumi, M. Inoue, M. Ichikawa and Y. Taniguchi, *Chem. Mater.*, **2004**, 16, 237.

[33] H. Mizuno, T. Maeda, H. Yanagi, H. Katsuki, M. Aresti, F. Quochi, M. Saba, A. Mura, G. Bongiovanni, F. Sasamiki and S. Hotta, *Adv. Opt. Mater.*, **2014**, 2, 529.

[34] H. Mizuno, U. Haku, Y. Marutani, A. Ishizumi, H. Yanagi, F. Sasaki and S. Hotta, *Adv. Mater.*, **2012**, 24, 5744.

[35] N. Matsuoka, T. Hiramatsu, H. Yanagi, F. Sasaki and S. Hotta, *Jpn. J. Appl. Phys.*, **2010**, 49, 01AD05.

[36] H. Yanagi, Y. Marutani, F. Sasaki, Y. Makino, T. Yamao and S. Hotta, *Appl. Phys. Express*, **2011**, 4, 062601.

[37] Y. Ono, F. Sasaki and H. Yanagi, *Mol. Cryst. Lliq.Cryst.*, **2016**, 629, 229.

[38] S. Fujiwara, K. Bando, Y. Masumoto, F. Sasaki, S. Kobayashi, S. Haraichi and S. Hotta, *Appl. Phys. Lett.*, **2007**, 91, 021104.

[39] Y. Ido, Y. Masumoto, F. Sasaki, M. Mori, S. Haraichi and S. Hotta, *Appl. Phys. Lett.*, **2010**, 3, 012702.

[40] T. Yamao, K. Yamamoto, Y. Taniguchi, T. Miki and S. Hotta, *J. Appl. Phys.*, **2008**, 103, 093115.

[41] T. Yamao, K. Yamamoto, T. Inoue, Y. Okuda, Y. Taniguchi and S. Hotta, *Jpn. J. Appl. Phys.*, **2009**, 48, 04C174.

[42] H. Mizuno, H. Yanagi, F. Sasaki and S. Hotta, *Phys. Status Solidi A*, **2012**, 209, 2437.

[43] M. Ichikawa, K. Nakamura, M. Inoue, H. Mishima, T. Haritani, R. Hibino, T. Koyama and Y. Taniguchi, *Appl. Phys. Lett.*, **2005**, 87, 221113.

[44] K. Yamashita, T. Nakahara, T. Hayakawa, Y. Sakurai, T. Yamao, H. Yanagi and S. Hotta, *Appl. Phys. Lett.*, **2014**, 104, 253301.

[45] Y. Tanaka, K. Goto, K. Yamashita, T. Yamao, S. Hotta, F. Sasaki and H. Yanagi, *Appl. Phys. Lett.*, **2015**, 107, 163303.

[46] K. Goto, K. Yamashita, H. Yanagi, T. Yamao and S. Hotta, *Appl. Phys. Lett.*, **2016**, 109, 061101.

[47] R. Hatano, K. Goto, K. Yamashita, F. Sasaki and H. Yanagi, *Jpn. J. Appl. Phys.*, **2017**, 56, 04CL02.

[48] K. Yamashita, U. Huynh, J. Richter, L. Eyre, F. Deschler, A. Rao, K. Goto, T. Nishimura, T. Yamao, S. Hotta, H. Yanagi, M. Nakayama, R. H. Friend, *ACS Photonics*, **2018**, 5, 2182.

[49] T. Nishimura, K. Yamashita, S. Takahashi, T. Yamao, S. Hotta, H. Yanagi and M. Nakayama, *Opt. lett.*, **2018**, 43, 1047.

[50] W. Takahashi, K. Maruyama, J. Li, M. Imakawa and T. Takenobu, *Jpn. J. Appl. Phys.*, **2014**, 53, 02BB02.

[51] Y. Sakurai, W. Hayashi, T. Yamao and S. Hotta, *Jpn. J. Appl. Phys.*, **2014**, 53, 02BB01.

[52] T. Yamao, Y. Okuda, Y. Makino and S. Hotta, *J. Appl. Phys.*, **2011**, 110, 053113.

[53] T. Yamao, N. Sakamoto, S. Hotta, H. Mizuno and H. Yanagi, *Jpn. J. Appl. Phys.*, **2012**, 51, 11PD03.

[54] K. Bando, T. Nakamura, Y. Masumoto, F. Sasaki, S. Kobayashi and S. Hotta, *J. Appl. Phys.*, **2006**, 99, 013518.

[55] T. Yamao, K. Yamamoto and S. Hotta, *J. Nanosci. Nanotechnol.*, **2009**, 9, 2582.

[56] H. Yanagi, F. Sasaki and K. Yamashita, *Adv. Opt. Mater.*, **2019**, 7, 1900136.

[57] F. Sasaki, S. Kobayashi, S. Haraichi, H. Yanagi, S. Hotta, M. Ichikawa and Y. Taniguchi, *Jpn. J. Appl. Phys.*, **2006**, 45, L1206.

[58] N. Matsuoka, T. Hiramatsu, H. Yanagi, F. Sasaki and S. Hotta, *Jpn. J. Appl. Phys.*, **2010**, 49, 052401.

[59] T. Hiramatsu, N. Matsuoka, H. Yanagi, F. Sasaki and S. Hotta, *Phys. Status solidi C*, **2009**, 6, 338.

[60] H. Shang, H. Shimotani, S. Ikeda, T. Kanagasekaran, K. Oniwa, T. Jin, N. Asao, Y. Yamamoto, H. Tamura, K. Abe, M. Kannno, M. Toshizawa and K. Tanigaki, *J. Phys. Chem. C*, **2017**, 121, 2364.

[61] H. Yanagi, Y. Marutani, N. Matsuoka, T. Hiramatsu, A. Ishizumi, F. Sasaki and S. Hotta, *Appl. Phys. Lett.*, **2013**, 103, 243301.

[62] H. Yanagi, A. Yoshiki, S. Hotta, and S. Kobayashi, *Appl. Phys. Lett.*, **2003**, 83, 1941.

[63] H. Yanagi, A. Yoshiki, S. Hotta and S. Kobayashi, *J. Appl. Phys.*, **2004**, 96, 4240.

[64] I. Sakata, S. Fujimoto and H. Yanagi, *Appl. Phys. Lett.*, **2006**, 88, 191104.

[65] S. Varghese, S.-J. Yoon, E. M. Calzado, S. Casado, P. G. Boj, M. A. D´ıaz-Garc´ıa, R. Resel, R. Fischer, B. Mili´an-Medina, R. Wannemacher, S. Y. Park and J. Gierschner, *Adv. Mater.*, **2012**, 24, 6473.

[66] A. A. Maksimov and I. I. Tartakovskii, *Phys. Status Solidi B*, **1981**, 107, 55.

[67] H. Yanagi, K. Tamura and F. Sasaki, *AIP adv.*, **2016**, 6, 085319.

[68] R. H. Dicke, *Phys. Rev.*, **1954**, 93, 99.

[69] R. Florian, L. O. Schwan and D. Schmid, *Phys. Rev. A*, **1984**, 29, 2709.

[70] M. S. Malcuit, J. J. Maki, D. J. Simkin and R. W. Boyd, *Phys. Rev. Lett.*, **1987**, 59, 1189.

[71] S. V. Frolov, W. Gellermann, M. Ozaki, K. Yoshino and Z. V. Vardeny, *Phys. Rev. Lett.*, **1997**, 78, 729.

[72] S. V. Frolov, W. Gellermann, M. Ozaki, K. Yoshino and Z. V. Vardeny, *Phys. Rev. Lett.*, **1997**, 78, 729.

[73] S. V. Frolov, Z. V. Vardeny and K. Yoshino, *Phys. Rev. B*, **1998**, 57, 9141.

[74] J. J. Maki, M. S. Malcuit, M. G. Raymer and R. W. Boyd, *Phys. Rev. A*, **1989**, 40, 5135.

[75] C. Zhou, Y. Zhong, H. Dong, W. Zheng, J. Tan, Q. Jie, A. Pan, L. Zhang and W. Xie, *Nat. Commun.*, **2020**, 11, 1.

[76] S. Yokoyama, T. Nakahara, A. Otomo and S. Mashiko, *Colloids and Surfaces A: Physicochem. Eng. Aspects*, **2002**, 198, 433.

[77] G. M. Akselrod, E. R. Young, K. W. Stone, A. Palatnik, V. Bulovi´c and Y. R. Tischler, *Phys. Rev. B*, **2014**, 90, 035209.

[78] G. Rainò, M. A. Becker, M. I. Bodnarchuk, R. F. Mahrt, M. V. Kovalenko and T. Stöferle, *Nature*, **2018**, 563, 671.

[79] S. Özçelik and D. L. Akins, *J. Phys. Chem. B*, **1999**, 103, 8926.

[80] H. Fidder, J. Knoester, and D. A. Wiersma, *Chem. Phys. Lett.*, **1990**, 171, 529.

[81] F. Meinardi, M. Cerminara, A. Sassella, R. Bonifacio and R. Tubino, *Phys. Rev. Lett.*, **2003**, 91, 247401.

[82] A. Angerer, K. Streltsov, T. Astner, S. Putz, H. Sumiya, S. Onoda, J. Isoya, W. J. Munro, K. Nemoto, J. Schmiedmayer and J. Majer, *Nat. Phys.*, **2018**, 14, 1168.

[83] C. Bradac, M. T. Johnsson, M. Breugel, B. Q. Baragiola, R. Martin, M. L. Juan, G. K. Brennen and T. Volz, *Nat. Commun.*, **2017**, 8, 1.

[84] H. Deng, H. Haug and Y. Yamamoto, *Rev. Mod. Phys.*, **2010**, 82, 1489.

[85] D. G. Lidzey, D. D. C. Bradley, M. S. Skolnick, T. Virgili, S. Walker and D. M. Whittaker, *Nature*, **1998**, 395, 53.

[86] S. K. Cohen and S. R. Forrest, *Nat. Photonics.*, **2010**, 4, 371.

[87] J. D. Plumhof, T. Stöferle, L. Mai, U. Scherf and R. F. Mahrt, *Nat. Mater.*, **2014**, 13, 247.

[88] T. Virgili, D. Coles, A. M. Adawi, C. Clark, P. Michetti, S. K. Rajendran, D. Brida, D. Polli, G. Cerullo and D. G. Lidzey, *Phys. Rev. B*, **2011**, 83, 245309.

[89] K. S. Daskalakis, S. A. Maier, R. Murray and S. K. Cohen, *Nat. Mater.*, **2014**, 13, 271.

[90] M. Ramezani, A. Halpin, S. Wang, M. Berghuis and J. G. Rivas, *Nano Lett.*, **2019**, 19, 8590.

[91] A. Graf1, M. Held, Y. Zakharko, L. Tropf, M. C. Gather and J. Zaumseil, *Nat. Mater.*, **2017**, 16, 911.

[92] M. Held, A. Graf, Y. Zakharko, P. Chao, L. Tropf, M. C. Gather and J. Zaumseil, *Adv. Opt. Mater.*, **2018**, 6, 1700962.

[93] S. Dokiya, H. Mizuno, H. Mizuno, H. Katsuki, K. Yamashita, F. Sasaki and H. Yanagi, *Appl. Phys. Express*, **2019**, 12, 111002.

[94] K. Takazawa, J. Inoue, K. Mitsuishi and T. Takamasu, *Phys. Rev. Lett.*, **2010**, 105, 067401.

[95] K. Takazawa, K. Mitsuishi and J. Inoue, *Appl. Phys. Lett.*, **2011**, 99, 253302.

[96] C. Zhang, C. L. Zou, Y. Yan, R. Hao, F. W. Sun, Z. F. Han, Y. S. Zhao and J. Yao, *J. Am. Chem. Soc.*, **2011**, 133, 7276.

[97] Q. Liao, Z. Xu, X. Zhong, W. Dang, Q. Shi, C. Zhang, Y. Weng, Z. Lid and H. Fu, *J. Mater. Chem. C*, **2014**, 2, 2773.

[98] D. M. Coles, P. Michetti, C. Clark, W. C. Tsoi, A. M. Adawi, J. S. Kim and D. G. Lidzey, *Adv. Funct. Mater.*, **2011**, 21, 3691.

[99] M. Litinskaya, P. Reineker and V. Agranovich, *J. Lumin.*, **2006**, 119, 277.

[100] M. Litinskaya, P. Reineker and V. Agranovich, *J. Lumin.*, **2004**, 110, 364.

[101] P. Michetti and G. C. La Rocca, *Phys. Rev. B*, **2008**, 77, 195301.

[102] T. Virgili, D. Coles, A. M. Adawi, C. Clark, P. Michetti, S. K. Rajendran, D. Brida, D. Polli, G. Cerullo and D. G. Lidzey, *Phys. Rev. B*, **2011**, 83, 245309.

[103] S. Hou, Y. Qu, X. Liu and S. R. Forrest, *Phys. Rev. B*, **2019**, 100, 045410.

[104] F. C. Spano, *J. Chem. Phys.*, **2020**, 152, 204113.

Chapter 2

Synthesis of methoxy- and cyano-substituted thiophene/phenylene co-oligomers

---

2.1 Introduction

As described in Chapter 1, single crystals of BP3T are promising candidates to achieve electrically pumped lasing, and have shown unique amplified light emitting behaviors. For further pursuit of superior lasing performances and investigation of structure dependences of light amplification behaviors, BP3T derivatives with methoxy- and cyano-groups at the para-positions of molecular terminals were synthesized. Although a variety of TPCO compounds have been synthesized so far,[1-6] the effect of substituents for amplified light emitting characteristics has not been well-described. Lasing and amplified light emitting characteristics can be drastically varied by changing molecular and/or crystal structures, according to literatures.[7-9]

In general, lasing easily occur when the π-electronic transition dipole moments and electric field of cavity photons interact efficiently both in the cases of SE and cooperative processes. Not only the realization of various molecular orientation by introducing substituents, electronic characteristics can also be changed, toward realization of a variety of electrically driven lasing devices. From this point view, here methoxy- and cyano-substituted BP3Ts, 5,5''-bis(4'-methoxy-[1,1'-biphenyl]-4-yl)-2,2':5',2''-terthiophene (BP3T-OMe) and 4',4'''-([2,2':5',2''-terthiophene]-5,5''-diyl)-bis(([1,1'-biphenyl]-4-carbonitrile)) (BP3T-CN), characterized as p-

type and n-type organic semiconductors, respectively, were synthesized and their crystal structures and lasing properties were investigated.

2.2 Experimental Section

Synthesis

According to literatures, TPCO molecules have been synthesized via Negishi- or Suzuki-coupling reaction, same as the cases of various π-conjugated organic light emissive compounds.[4] To the best of our knowledge, BP3T-OMe has been synthesized via coupling reactions, so far.[6] Here we synthesized both BP3T-OMe and BP3T-CN via Negishi coupling reaction as shown in scheme 1.

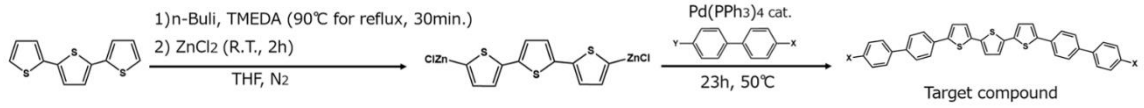

Scheme 1 Synthesis protocol of BP3T-OMe and BP3T-CN where X=OCH_3, Y=Br for BP3T-OMe, and X=CN, Y=I for BP3T-CN.

Synthesis of BP3T-OMe:

4-Bromo-4'-hydroxybiphenyl (5.004 g, 20.09 mmol), potassium carbonate (13.873 g, 100.38 mmol) and anhydrous acetone (50 mL) were put into a two-neck flask. To this solution, iodomethane (1.6 mL) was added and then heated for 24 hours under reflux. Then, the solution was gathered in a beaker and water was added until all of the solid was dissolved. Next, the solution was put into a separation funnel, and extracted 3 times using 100 - 300 mL dichloromethane. Then, the dichloromethane phase was gathered in a 1 neck flask, and

magnesium sulfate was added to remove residual water. After filtrating this solution, all of the solvent was removed, and the remaining solid was recrystallized 3 times using acetone as highly soluble solvent and n-hexane as poor soluble solvent, yielding 4-Bromo-4'-methoxybiphenyl (4.21 g, 16.0 mmol, 80 %).

2,2':5',2''-Terthiophene (681 mg, 2.74 mmol) was mixed with anhydrous tetrahydrofuran (10 mL) and *N,N,N′,N′*-tetramethylethylenediamine (1.00 mL, 6.68 mmol). To this solution, 4 mL of 1.6 M *n*-butyllithium in cyclohexane was added dropwise at 0℃ and the reaction mixture was refluxed for 30 minutes and successively cooled down to -10℃. Anhydrous zinc chloride (1.233 g, 9.045 mmol) dispersed in anhydrous tetrahydrofuran (15 mL) was added and the reaction solution was kept at 25℃ for 2 hours. Tetrakis(triphenylphosphine)-palladium(0) (106.5 mg, 0.09220 mmol) was immediately added and subsequently 4-bromo-4'-methoxybiphenyl (1.743 g, 6.624 mmol) dispersed in anhydrous tetrahydrofuran (5 mL) was added. The reaction mixture was warmed to 50℃ and kept for 23 hours to yield a precipitate. The precipitate was washed with 50 mL tetrahydrofuran, 50 mL water, 10 mL 10% hydrochloric acid, 50 mL water, 50 mL acetone and 250mL hot 1,2,4-trichlorobenzene, yielding 377 mg (0.615 mmol, 22 %).

Synthesis of BP3T-CN:

4-biphenylcarbonitrile (5.0037 g, 27.919 mmol) was mixed with acetic acid (13.7 mL) and water (2.8 mL) and 98% sulfuric acid (0.42 mL) in a one-neck flask. Iodine (3.646 g, 14.37 mmol) and periodic acid (1.405 g, 6.164 mmol) were added. After that, the mixture was heated to 90℃ for 24 hours. During this heating, the solution color changed from colorless to red and

a precipitate formed. The precipitate was washed by water and methanol alternately 3 times, and dissolved in chloroform (100 mL). This solution was washed with a saturated aqueous sodium chloride solution and dried over anhydrous magnesium sulfate. After evaporating chloroform, the remaining solid was dissolved in hot ethyl acetate (50 mL). Methanol (25 mL) was added and cooled down to 5℃ for crystallization. The precipitates were isolated by filtration and dried to give yellow crystals of 5.199 g (17.04 mmol, 61%) of 4'-iodo-biphenyl-4-carbonitrile, which was identified by ^{1}H NMR (solvent: deuteriochloroform) and showed the same chemical shift and proton integral values as reported in the literature.[4]

Using this obtained compound, BP3T-CN was synthesized according to the reaction scheme 1. 2,2':5',2''-Terthiophene (671 mg, 2.701 mmol) was mixed with anhydrous tetrahydrofuran (10 mL) and *N,N,N′,N′*-tetramethylethylenediamine (1.00 mL, 6.68 mmol). To this solution, 4 mL of 1.6 M n-butyllithium in cyclohexane was added dropwise at 0℃ and the reaction mixture was heated under reflux for 30 minutes and successively cooled down to -10℃. Anhydrous zinc chloride (1.335 g, 9.793 mmol) dispersed in anhydrous tetrahydrofuran (15 mL) was added and the reaction solution was kept at 25℃ for 2 hours. Tetrakis(triphenylphosphine)-palladium(0) (0.105 g, 0.0909 mmol) was immediately added and subsequently 4'-iodo-biphenyl-4-carbonitrile (2.043 g, 6.696 mmol) dispersed in anhydrous tetrahydrofuran (5 mL) was added. The reaction mixture was warmed to 50℃ for 23 hours to yield a precipitate. This precipitate was filtered-off and washed with 50 mL tetrahydrofuran, 50 mL water, 10 mL 10% hydrochloric acid, 50 mL acetone, and 250 mL hot 1,2,4-trichlorobenzene, and further purified by sublimation under a vacuum at 300℃. The solid remained in the heating zone was collected as the purified target compound, yielding 612 mg (1.02 mmol, 38 %).

Due to the low solubility in any solvents for obtained BP3T-OMe and BP3T-CN, identification by ^{1}H-NMR or ^{13}C-NMR were unavailable. However, both target compounds were identified by MALDI-TOF-MS, found [M] = 612 and 602, for BP3T-OMe and BP3T-CN respectively. Almost all of TPCO series were identified by mass spectroscopy instead of using NMR spectroscopy as in previous reports.[6]

Crystal growth and thin film preparation:

Single crystals for X-ray diffraction measurements were prepared via a modified sublimation process. Purified powder of BP3T-OMe or BP3T-CN was put in a quartz crucible, and the molecules were sublimed and collected into another quartz crucible facing each other in a vacuum chamber ($2\times10^{-4} \sim 4\times10^{-4}$ Pa). Thin films of BP3T-OMe and BP3T-CN for optical and photoelectron spectroscopy measurements were prepared by vapor deposition onto glass substrates. Purified powder of BP3T-OMe or BP3T-CN was evaporated from a resistively heated quartz crucible under a vacuum condition ($2\times10^{-4} \sim 4\times10^{-4}$ Pa). Their deposition rate and film thickness were monitored by a quartz crystal microbalance.

Optical characterization:

Absorption and PL spectra were measured for the vapor-deposited thin films of BP3T-OMe and BP3T-CN using an ultraviolet-visible (UV-Vis) spectrometer (JASCO V-530). The work functions of BP3T-OMe and BP3T-CN were measured by photo-electron spectroscopy in air (PESA, Riken Keiki AC-3) for the vapor-deposited thin films on ITO/glass substrates. Fluorescence images as well as PL spectra of single-crystal samples were measured using a

fluorescence microscope (Olympus BX-51) equipped with a digital camera (Olympus DP21) and a charge coupled device (CCD) spectrometer (Hamamatsu PMA-50), respectively, through a 10× objective lens.

2.3 Results and discussions

XRD measurements revealed crystal structures for both single crystals of BP3T-OMe (CCDC-1991924) and BP3T-CN (CCDC-1991925). BP3T-OMe crystallized in an orthorhombic form (a = 65.19 Å, b = 7.43 Å, c = 5.80 Å, space group: $Cmc2_1$, Z value: 4, cell volume: 2808 $Å^3$).

Same as the cases of BP3T and other TPCO series, the π-electronic transition dipole moment orients parallel to the molecular long axis. As shown in Figure 2.1(a-c), BP3T-OMe takes perfectly perpendicular molecular orientation to the crystal basal plane (*bc*-plane), which is ideal to confine the cavity photons inside a single crystal along in-plane direction. The orientation of the molecular long axis of BP3T is also perpendicular to the crystal basal plane (*ab*-plane), however, it's a little inclined with a tilting angle of 2.6°.[10,11] Therefore, the orientation of BP3T-OMe seems more favorable to confine photons in a self-cavity formed by the single crystal, comparing to the cases of BP3T and other TPCO series with slightly tilted molecular orientation.[10-17]

The origin of the perpendicularly aligned molecular orientation in the BP3T-OMe single crystal can be attributed to the H-bonding interaction between methoxy-groups of adjacent molecules as shown in Figure 2.1(d). In a previous report about other methoxy-substituted TPCO compounds, 2,5-bis(4'-methoxybiphenyl-4-yl)thiophene (BP1T-OMe) showed the same perpendicular orientation as a consequence of the hydrogen bonding between the

methoxy groups.[13]

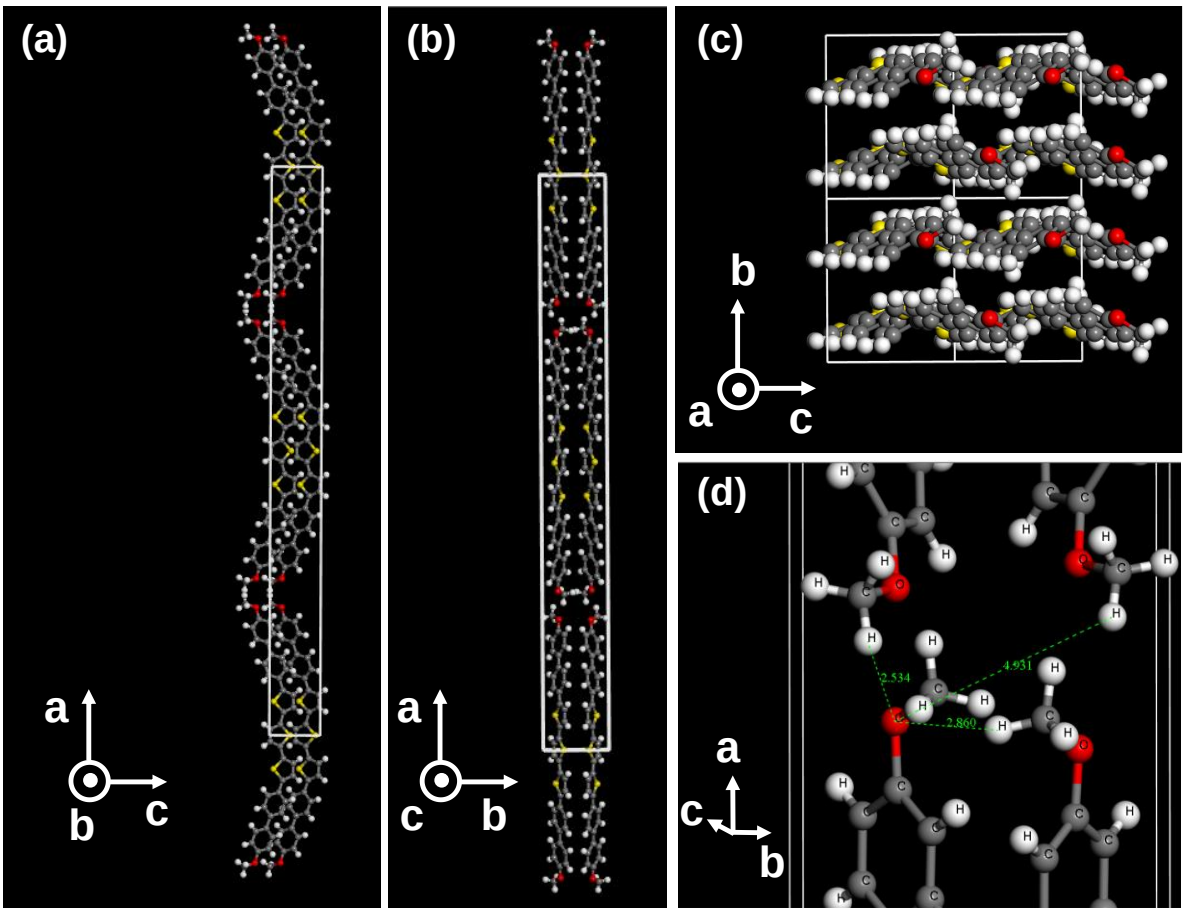

Figure 2.1 (a-c) Crystal structure of BP3T-OMe with a projection on ac-plane, ab-plane, and bc-plane, respectively. (d) Enlarged structure showing interatomic distances between oxygen and neighboring hydrogen atoms in the methoxy groups.

On the other hand, BP3T-CN crystallized in a triclinic form (a = 9.49 Å, b = 14.92 Å, c = 19.58 Å, α = 82.73°, β = 87.51°, γ = 89.92°, space group: P-1, Z value: 4, cell volume: 2746 Å^3). The molecular long axis of BP3T-CN is tilted by about 45° against the basal plane (*ab*-plane) as shown in Figure 2.2 (a,b).

An origin of this obliquely lying orientation is attributed to the electrostatic interaction between cyano substituents of neighboring molecules, as revealed in a previous report for 2,5-bis(4'-cyanobiphenyl-4-yl)thiophene (BP1T-CN).[16] The cyano-groups are oppositely oriented at the intermolecular interface, therefore, the C(δ^+)-N(δ^-) interaction is formed between the adjacent molecular terminals as shown in Figure 2.2(d). This lying molecular orientation is suitable for the formation of EPs or/and achieving of lasing from vertical cavity surface emitting lasers (VCSELs) using distributed Bragg reflector (DBR) mirrors since the tilted transition dipole moments allow sufficient emission components to the crystal surface direction. Actually, nonlinearly amplified emissions from VCSEL structures were observed using cyano-substituted TPCOs as active media in VCSELs.[17-22]

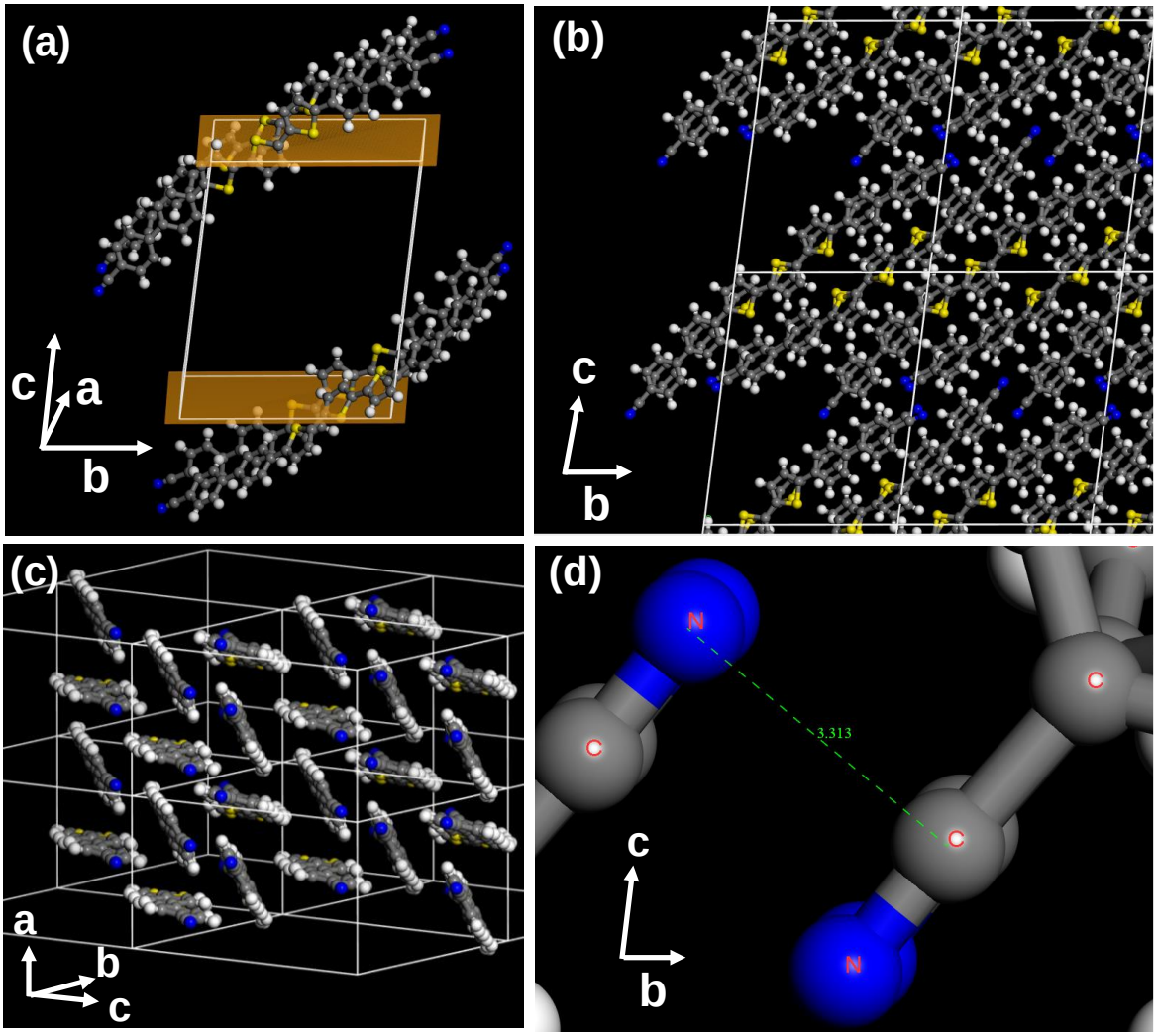

Figure 2.2 (a) Crystal structure of BP3T-CN showing tilted orientation of the long molecular axes relative to the crystal basal plane. (b and c) Crystal structure of BP3T-CN showing molecular packing in multiple unit cells. (d) Enlarged structure showing interatomic interaction between adjacent cyano-groups.

Next, we measured absorption and PL spectra using vapour deposited thin films as shown in Figure 2.3 (a, b). Figure 2.3 (c, d) show plots of $(\alpha hv)^2$ as a function of photon energy where α and h and v represent the absorption coefficient, Planck constant and the frequency, respectively. The values of α were obtained from the respective absorbance divided by the sample thickness. The frontier orbital gap value (E_g) was obtained by extrapolating the linear slope of $(\alpha hv)^2$ to the zero absorption coefficient ($\alpha = 0$). The obtained E_g values were 2.22 eV and 2.32 eV for BP3T-OMe and BP3T-CN, respectively.

Figure 2.3 (e, f) show plots of (photon yield)$^{0.5}$ as a function of incident photon energy in the measurements of PESA. The highest occupied molecular orbital (HOMO) levels estimated from the threshold photon energy in Figure 2.3 (e, f) were -5.31 and -5.91 eV for BP3T-OMe and BP3T-CN, respectively. The lowest unoccupied molecular orbital (LUMO) levels calculated by the HOMO levels and aforementioned E_g values were -3.09 and -3.59 eV for BP3T-OMe and BP3T-CN, respectively. The HOMO and LUMO levels of BP3T estimated by the same procedures were -5.78 eV and -3.40 eV, respectively.

As these results show that the methoxy and cyano-groups act as electron donating and electron withdrawing substituents, respectively, p-type and n-type semiconducting characteristics can be expected for BP3T-OMe and BP3T-CN, respectively.

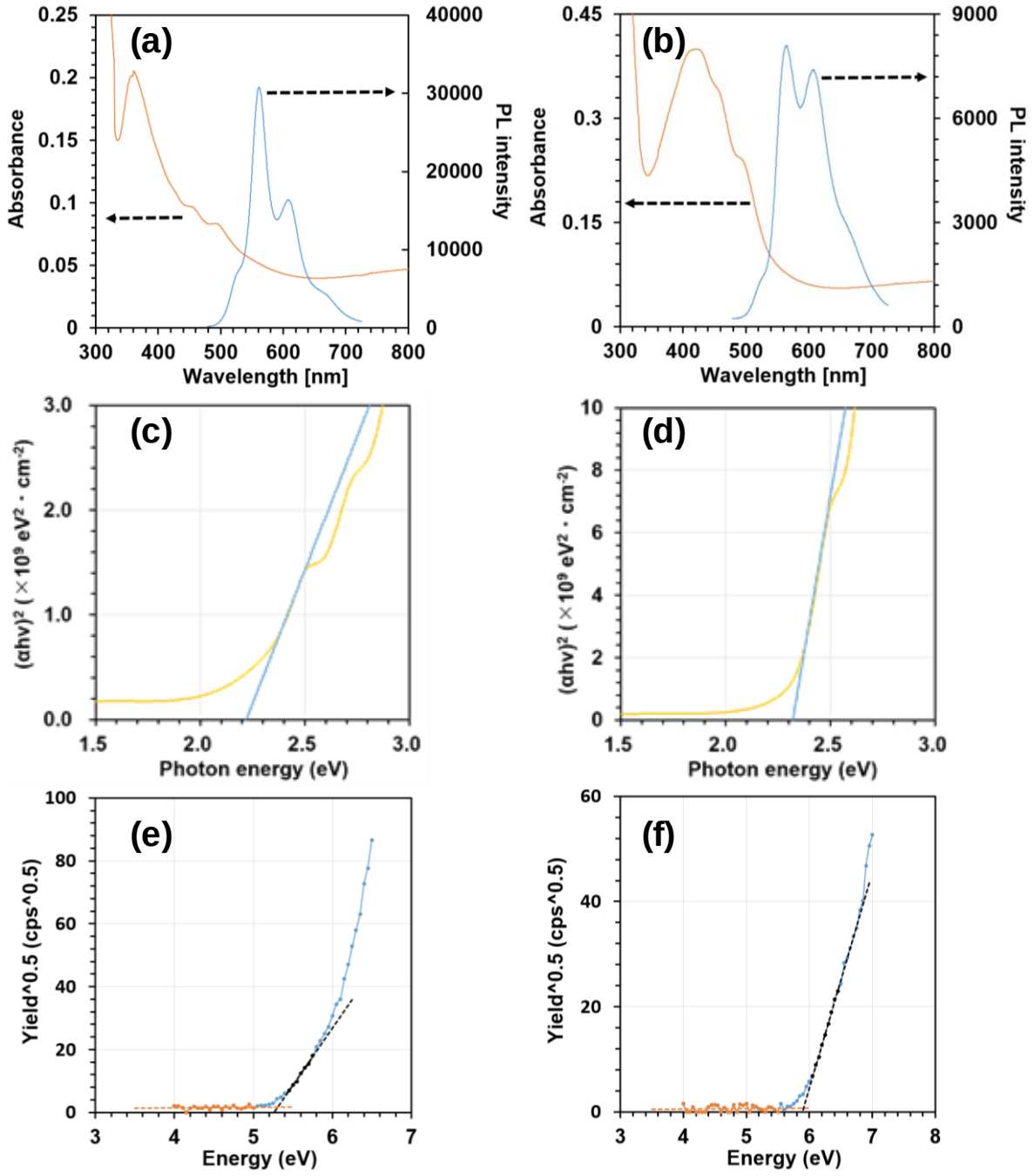

Figure 2.3 Absorption and PL spectra for BP3T-OMe (a) and BP3T-CN (b), $(ahv)^2$ vs. energy plots for estimation of E_g values of BP3T-OMe (c) and BP3T-CN (d), $(photon\ yield)^{0.5}$ vs. energy plots for estimation of HOMO values of BP3T-OMe (e) and BP3T-CN (f).

2.4 Conclusions

BP3T-OMe and BP3T-CN were successfully synthesized and their crystal structures were identified. BP3T-OMe and BP3T-CN crystallized in orthorhombic and triclinic forms, respectively. The molecular orientation of BP3T-OMe is perfectly perpendicular to the crystal basal plane, suggesting more efficient light confinement in the single-crystal cavity in a TM mode compared to that of BP3T single crystals with slightly inclined orientation. On the other hand, the molecular orientation of BP3T-CN was oblique to the crystal basal plane, seeming suitable for surface-emitting devices.

The HOMO and LUMO levels of BP3T-OMe and BP3T-CN estimated by absorption and photoelectron spectroscopies revealed that the methoxy- and cyano-groups act as electron-donating and electron withdrawing groups, leading to expected p- and n-type semiconduction, respectively. Those end-substituted BP3T derivatives are expectable as active media to pursue the fabrication of OLED structures for electrically pumped lasers.

References:

[1] S. Hotta, S. A. Lee and T. Tamaki, *J. Heterocycl. Chem.*, **2000**, 37, 25.

[2] S. Hotta, H. Kimura, S. A. Lee and T. Tamaki, *J. Heterocycl. Chem.*, **2000**, 37, 281.

[3] S. Hotta, *J. Heterocycl. Chem.*, **2000**, 38, 923.

[3] S. Hotta and T. Katagiri, *J. Heterocyclic Chem.*, **2003**, 40, 845.

[4] T. Katagiri S. Ota T. Ohira T. Yamao and S. Hotta, *J. Heterocyclic Chem.*, **2007**, 44, 853.

[5] R. Hirase, M. Ishihara, T. Katagiri, Y. Tanaka, H. Yanagi and S. Hotta, *Org. Electron.*, **2014**, 15, 1481.

[6] Y. Inada, M. Koda, Y. Urabe, T. Katagiri, T. Yamao, Y. Yoshida and S. Hotta, *Sci. Rep.*, **2019**, 9, 9739.

[7] J. Gierschner, S. Varghese and S. Y. Park, *Adv. Opt. Mater.*, **2016**, 4, 348.

[8] K. Wang, H. Zhang, S. Chen, G. Yang, J. Zhang, W. Tian, Z. Su and Y. Wang, *Adv. Mater.*, **2014**, 26, 6168.

[9] Z. Zuo, C. Ou, Y. Ding, H. Zhang, S. Sun, L. Xie, R. Xia and W. Huang, *J. Mater. Chem. C*, **2018**, 6, 4501.

[10] S. Hotta, M. Goto, R. Azumi, M. Inoue, M. Ichikawa and Y. Taniguchi, *Chem. Mater.*, **2004**, 16, 237.

[11] K. Bando, T. Nakamura, S. Fujiwara and Y. Masumoto, *Phy. Rev. B*, **2008**, 77, 045205.

[12] S. Hotta and M. Goto, *Adv. Mater.*, **2002**, 14, 498.

[13] S. Hotta, M. Goto and R. Azumi, *Chem. Lett.*, **2007**, 36, 270.

[14] H. Mizuno, U. Haku, Y. Marutani, A. Ishizumi, H. Yanagi, F. Sasaki and S. Hotta, *Adv. Mater.*, **2012**, 24, 5744.

[15] H. Mizuno, Y. Mekata, F. Sasaki and H. Yanagi, *Jpn. J. Appl. Phys.*, **2020**, 59, SGGG02.

[16] H. Mizuno, T. Maeda, H. Yanagi, H. Katsuki, M. Aresti, F. Quochi, M. Saba, A. Mura, G. Bongiovanni, F. Sasaki and S. Hotta, *Adv. Opt. Mater.*, **2014**, 2, 529.

[17] K. Yamashita, T. Nakahara, T. Hayakawa, Y. Sakurai, T. Yamao, H. Yanagi and S. Hotta, *Appl. Phys. Lett.*, **2014**, 104, 253301.

[18] Y. Tanaka, K. Goto, K. Yamashita, T. Yamao, S. Hotta, F. Sasaki and H. Yanagi, *Appl. Phys. Lett.*, **2015**, 107, 163303.

[19] R. Hatano, K. Goto, K. Yamashita, F. Sasaki and H. Yanagi, *Jpn. J. Appl. Phys.*, **2017**, 56,

04CL02.

[20] K. Goto, K. Yamashita, H. Yanagi, T. Yamao and S. Hotta, *Appl. Phys. Lett.*, **2016**, 109, 061101.

[21] K. Yamashita, U. Huynh, J. Richter, L. Eyre, F. Deschler, A. Rao, K. Goto, T. Nishimura, T. Yamao, S. Hotta, H. Yanagi, M. Nakayama, R. H. Friend, *ACS Photonics*, **2018**, 5, 2182.

[22] T. Nishimura, K. Yamashita, S. Takahashi, T. Yamao, S. Hotta, H. Yanagi and M. Nakayama, *Opt. Lett.*, **2018**, 43, 1047.

Chapter 3

Optically pumped lasing characteristics of thiophene/phenylene co-oligomer derivatives

3.1 Introduction

To obtain large-sized and thin platelet single crystals suitable for lasing media, PVT methods have been frequently utilized for BP3T and other TPCO series,[1-10] however, growth conditions to provide single crystals with a pair of parallel crystal edges serving as a resonator have not been well-established. On the other hand, the solution phase methods are better than the vapor ones to obtain well-shaped single crystals in general, and a few reports have proposed improved crystal growth methods for TPCO series in solution phases. Ref. [11] has proposed a method to grow a single crystal onto a substrate directly using a seed crystal in a solution phase (Figure 3.1). Ref. [12] also has proposed an improved crystal growth method in a solution phase using a seed crystal by evaporating a TPCO solution. However, those methods demand complicated crystal growth processes and long growth time.

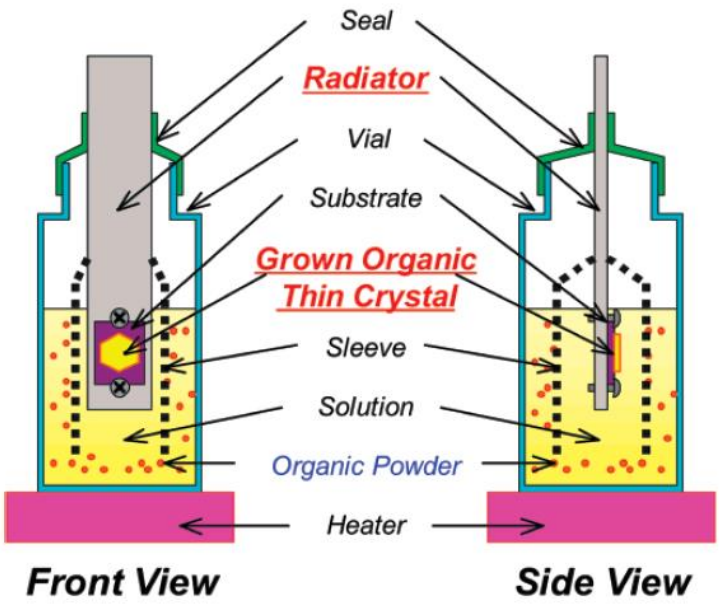

Figure 3.1 Schematic depiction of direct crystal formation on substrate by solution process. Reproduced with permission.[11] Copyright 2007, American Chemical Society.

In this Chapter, optically pumped lasing characteristics were investigated for single crystals of BP3T and its end-substituted derivatives, BP3T-OMe and BP3T-CN, shown in Figure 3.2 (a-c). To achieve optically pumped lasing in F-P oscillations, simplified and highly reproducible crystal growth methods for BP3T were proposed, and crystal growths to facilitate F-P lasing cavities were also carried out for BP3T-OMe and BP3T-CN. Then, optically-pumped lasing characteristics were described for single crystals of BP3T, BP3T-OMe and BP3T-CN, and their lasing characteristics were also discussed in terms of their structure dependences.

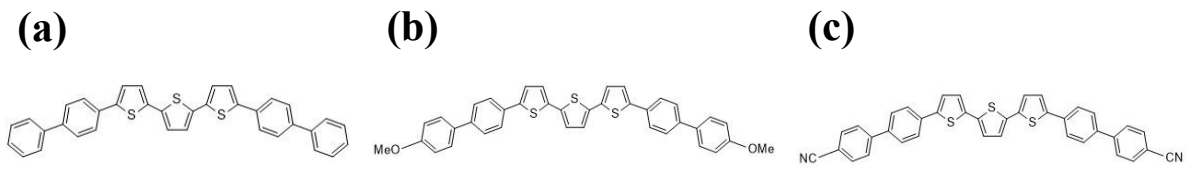

Figure 3.2 Molecular structures of (a) BP3T, (b) BP3T-OMe and (c) BP3T-CN.

3.2 Experimental section

Improved crystal growth in solution phase for BP3T

Same as the case of other TPCO series, BP3T can be hardly dissolved in any organic solvents, however, BP3T molecules can become somewhat soluble at higher temperature. Using this tendency, BP3T crystals with large sizes were grown with saturated BP3T solution at high temperature. Undissolved BP3T solids remaining even after heating should be removed from the growth solution, because they may cause unexpected growth seeds resulting in low crystal quality during the growth process. The protocol of BP3T crystal growth is as follows: As a source of BP3T crystals, commercially available BP3T powder (Sumitomo-Seika) was purified by sublimation. Using sublimed BP3T solids, a saturated 1,2,4-trichlorobenzene solution of BP3T was prepared at 190℃. The 10 mL solution was diluted by adding 2 mL 1,2,4-trichlorobenzene to remove possibly remaining undissolved BP3T solids. After that, the solution was heated to 190℃ again, and successively cooled down to 30-40℃ for 36 hours. Afterwards, the grown BP3T crystals dispersed in the solution were transferred onto glass substrates by handling with a metal needle.

Crystal growth of BP3T-OMe and BP3T-CN

To obtain single crystals with a pair of parallel crystal edges, the modified crystal growth were also applied for BP3T-OMe and BP3T-CN. For BP3T-OMe crystal growth, similar methodology of the case of BP3T was carried out. First, a saturated BP3T-OMe solution was prepared at 150℃ with 1,2,4-trichlorobenzene as a solvent. The solution was heated to 190 ℃, then, successively cooled down to 40 ℃ for 18 hours. For the case of BP3T-CN, crystals for optically pumped lasing measurements were obtained by the same crystal growth protocol described for X-ray analysis in Chapter 2.

Crystallographic characterization

To confirm the directions of crystal axes in the BP3T single crystal according to the reported crystal structure,[13] transmittance and fluorescence microscope observations were carried out. X-ray diffraction (XRD) measurement was also performed by θ/2θ scan (Cu-Kα, 50 kV, 300 mA). The thickness of crystals was confirmed by a surface profiler (Kosaka Laboratory).

Measurement of optically pumped lasing

As shown in Figure 3.3, PL measurements for the investigation of lasing characteristics were performed using a Nd:YAG pulsed laser (λ_{ex} = 355 nm, pulse frequency: 1.2 kHz, pulse duration: 1.1 ns) at room temperature under ambient condition. The excitation beam shaped into a stripe of 0.24 x 0.04 cm^2 through a cylindrical lens was focused on the single crystal surface with an incident angle of ca. 45°. Photoemission radiated from the edge of a single crystal was detected using a CCD spectrometer (Hamamatsu PMA-50) through an optical fiber.

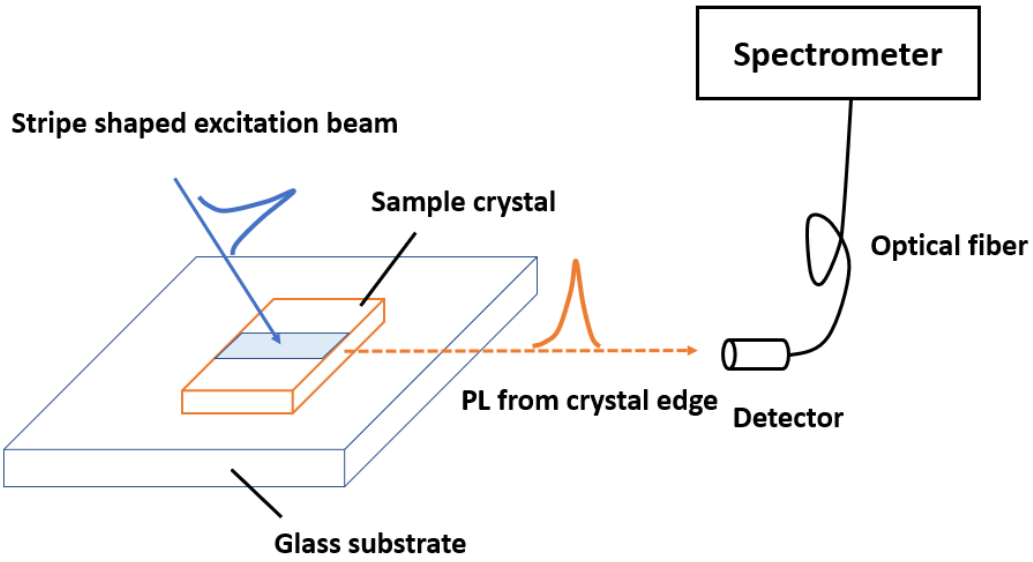

Figure 3.3 Schematic depiction of PL measurements for investigation of lasing characteristics.

3.3 Results and discussions

As shown in Figure 3.4 (a), a large number (> 100) of well-shaped BP3T single crystals were obtained. The obtained single crystals were large enough to confirm the crystal shape even by naked eyes, demonstrating that the growth protocol was highly reproducible. Moreover, the crystals were obtained with a pair of parallel edges suitable for F-P oscillation as shown in Figure 3.4 (b).

To confirm the versatility of this crystal growth method, single crystals of 5,5’’’-Bis(4-biphenylyl)-2,2’:5’,2’’:5’’,2’’’-quaterthiophene (BP4T) were also grown using similar process. Although BP4T seems less soluble than BP3T because of the larger molecular weight, the grown crystals were also large enough to confirm the shape by naked eyes and well-shaped. Furthermore, optically pumped lasing was achieved. Crystal growth and optically pumped lasing for BP4T was described in Appendix part.

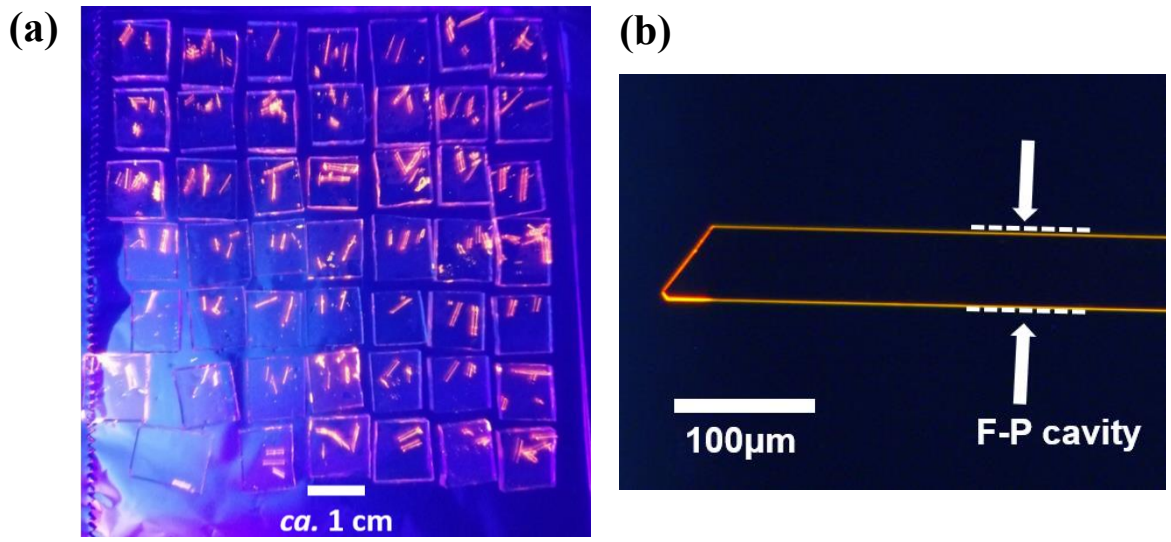

Figure3.4 (a) Fluorescence photograph under ultraviolet light irradiation of BP3T crystals on glass substrates (7x7 pieces, each ca. 1×1cm^2) transferred from one-batch growth solution, showing a large number of well-shaped crystals (orange color). (b) Fluorescence microscope image of a BP3T single crystal showing light emission from crystal edges.

To determine the crystal axe directions in the BP3T single crystals, the crystal structure was confirmed by observations using a fluorescence microscope and X-ray diffraction spectroscopy according to literature,[13] the crystal structure of BP3T has already been identified with assignment of mirror indices in the single crystal by estimating formed angle between the lines of crystal edges as shown in Figure 3.5 (a). The grown BP3T crystals were elongated to the *b*-axis direction, and the expectable direction of F-P oscillation by a pair of parallel crystal edges is along the *a*-axis. The XRD pattern shown in Figure 3.5 (b) was assigned by intense diffraction peaks of (0 0 *l*) planes (*l* = 2, 4, 6, 8, 10). According to the reported crystal structure of BP3T,[13] the molecular long axis is parallel to the *c*-axis which is almost perpendicular to the crystal basal plane. Since the π-electronic transition dipole moment was parallel to the

molecular long axis,[14] the emitted light propagated with the TM mode in the planar crystal cavity, and light emission appears at the edge of the crystal as shown in Figure 3.4 (b).

Crystal thickness confirmed by surface profiler was ca. 2 μm ~ 20 μm, thicker than that of PVT-grown crystal. The thicker thickness seems more favorable to confine cavity photons efficiently, which possibly enables lasing at lower excitation threshold.

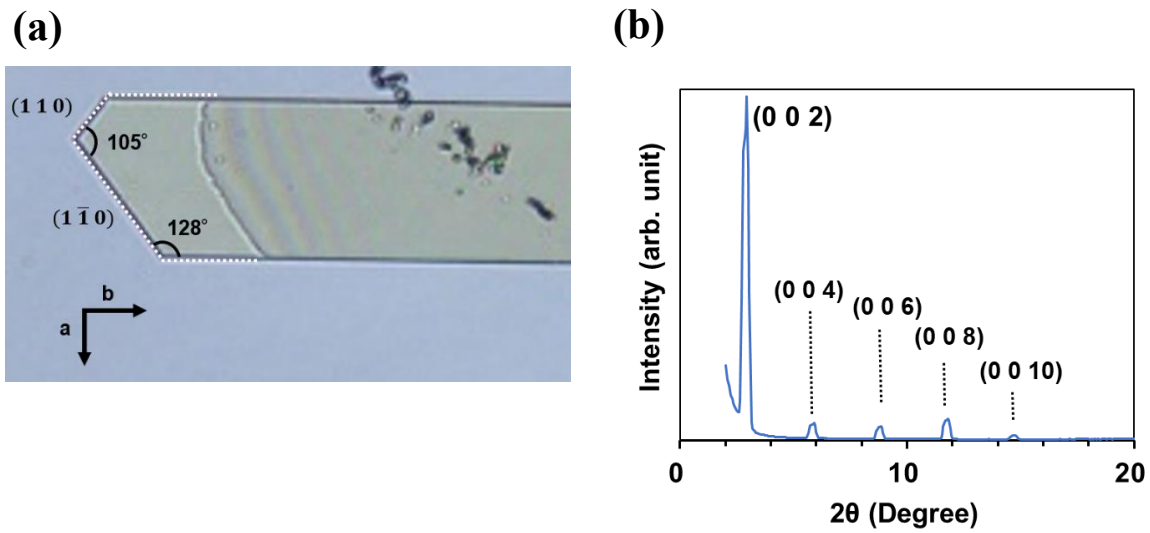

Figure 3.5 (a) Transmission microscope image of a representative BP3T single crystal and (b) XRD pattern obtained from BP3T single crystal.

Optically pumped lasing was measured for single crystals of BP3T and its derivatives. As shown in Figure 3.6 (a, b), either or both 0-1 and 0-2 emission bands were nonlinearly amplified with longitudinal multi-modes in PL spectra for BP3T single crystals. The threshold excitation density was estimated to be 398 μJ/cm^2 in the 0-1 band and 152 μJ/cm^2 in the 0-2 band, respectively. Figure 3.6 (c) depicts high resolution PL spectra showing longitudinal multi-modes oscillations at 658 μJ/cm^2 in the 0-1 band and (d) at 187 μJ/cm^2 in the 0-2 band, respectively. Almost constant mode intervals were clearly shown in Figure 3.6 (c, d), which is a direct evidence of F-P oscillation in the single-crystal self-cavity, resulting in the satisfaction

of criteria to claim lasing described in Chapter 1.

To evaluate the lasing characteristics, values of group refractive index (n_g) and quality (Q) factor were derived from the lasing spectra shown in Figure 3.6 (c, d) using following equations:

$$n_g = \frac{1}{2L\Delta\lambda^{-1}} \tag{3.1}$$

$$Q = \frac{Peak\ position\ (eV)}{FWHM(eV)} \tag{3.2}$$

where L is the cavity length estimated as the distance between a pair of parallel crystal edges, $\Delta\lambda^{-1}$ is the mode interval value in lasing spectra, and FWHM is the full width at half maximum of the multimode peaks. For lasing spectrum in the 0-1 band, n_g and Q factor values were 5.3 and 3.8×10^3, respectively while for the 0-2 band, n_g and Q factor values were 3.7 and 6.0×10^3, respectively. These values were large enough in comparison to the cases of optically pumped lasing from other organic single crystals, exhibiting the superiority of BP3T single crystals as laser media.[15-20]

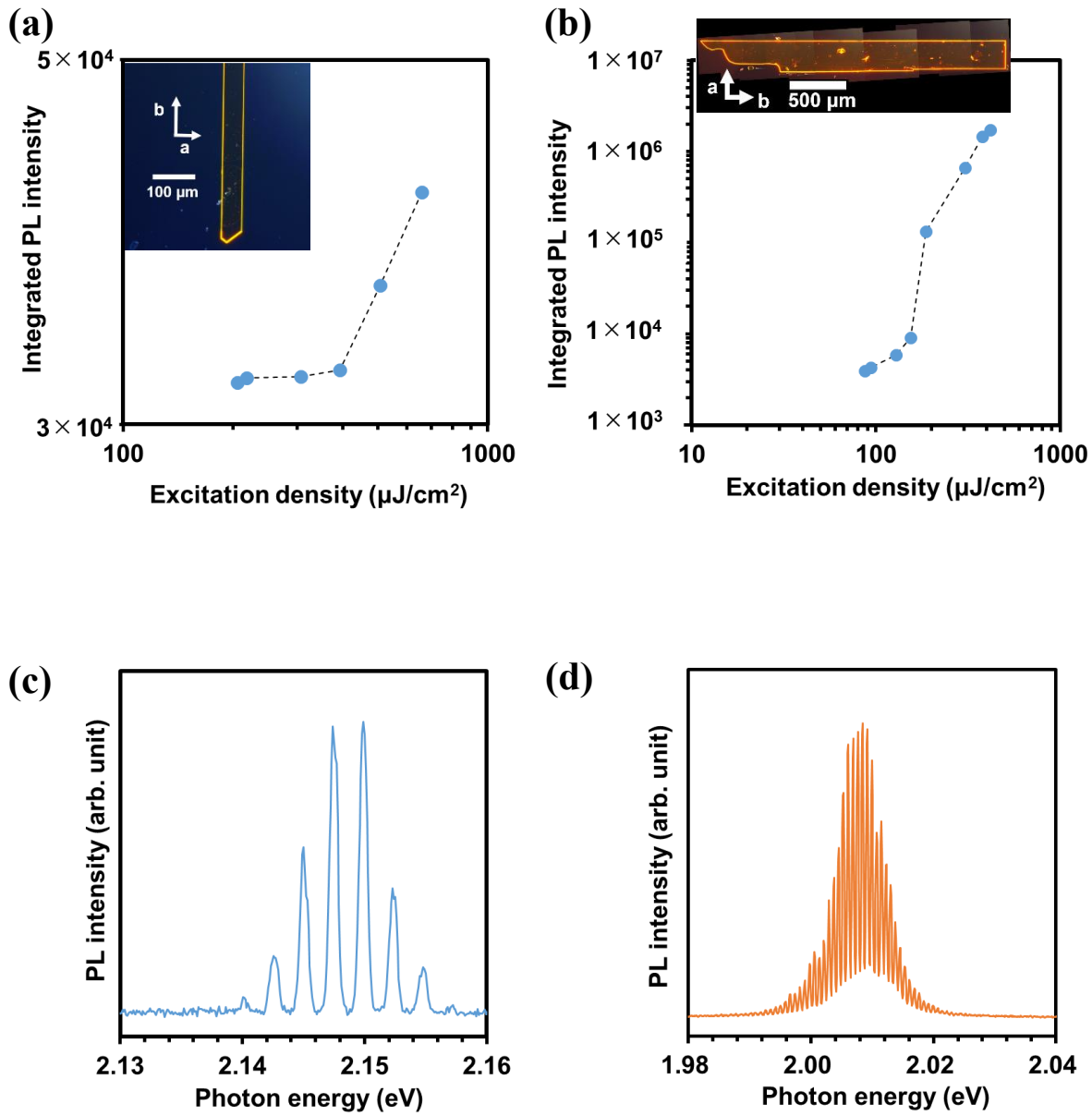

Figure 3.6 Excitation density dependence of integrated PL intensity obtained for BP3T single crystals in 0-1 band (a) and (b) 0-2 band with their fluorescence image in the insets. (c) High resolution PL spectra taken for BP3T single crystals at 658 μJ/cm² in 0-1 band and (d) at 187 μJ/cm² in 0-2 band, showing longitudinal multi-mode lasing.

Lasing characteristics were also investigated for single crystals of BP3T-OMe and BP3T-CN under optical pumping using a Nd:YAG pulsed laser as an excitation source. As the excitation density is elevated, the emission intensity was nonlinearly increased at a certain threshold in the 0-2 band both for BP3T-OMe and BP3T-CN crystals, as shown in Figure 3.7 (a) and (b).

The threshold excitation density was estimated to be 17 μJ/cm^2 for BP3T-OMe and 152 μJ/cm^2 for BP3T-CN, respectively. The threshold for the BP3T-OMe single crystal was lower than that of the BP3T-CN single crystal, which can be attributed to their different molecular orientation described in Chapter 2. The perpendicular orientation to the crystal basal plane in the BP3T-OMe single crystal is favorable for both efficient SE along the planar single-crystal cavity and EP formation by interaction between cavity photons propagating along the crystal basal plane and excitons compared to the inclining orientation in the BP3T-CN single crystal.[21-23]

As shown in Figure 3.7 (c) and (d), longitudinal multi-mode lasing spectra were observed both for the BP3T-OMe and BP3T-CN single crystals, owing to the self-cavity effect in the well-shaped single crystals. The calculated n_g value following equation 3.1 was 4.8 for BP3T-OMe while that was 3.7 - 5.3 for BP3T-CN, also showing large values as similar as the cases of other organic single crystals.[15-20]

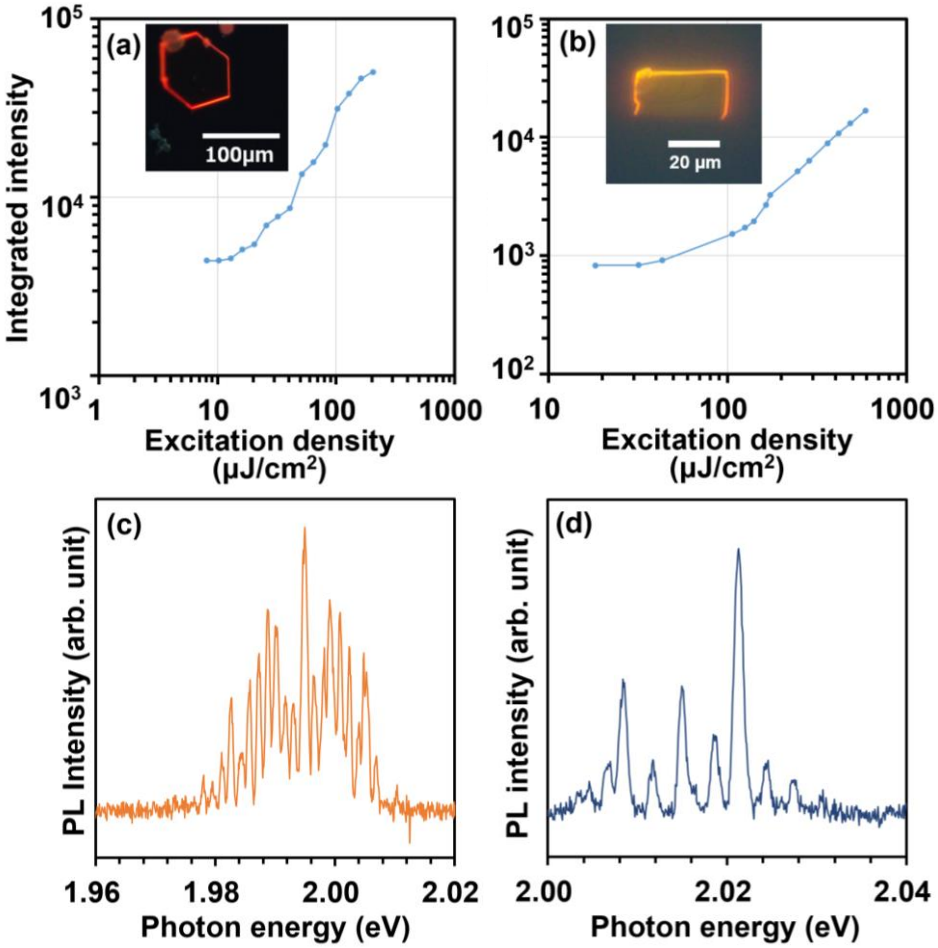

Figure 3.7 Excitation density dependence of integrated PL intensity in 0-2 band taken for single crystals of BP3T-OMe (a) and BP3T-CN (b) with their fluorescence image in the insets. PL spectra taken from single crystals of BP3T-OMe at 162 μJ/cm² (c) and BP3T-CN at 602 μJ/cm² (d) showing longitudinal multi-mode lasing.

3.4 Conclusions

Optically pumped lasing was achieved for single crystals of BP3T and its methoxy- and cyano-substituted derivatives. For measuring optically pumped lasing with F-P oscillation by a pair of parallel crystal edges, well-shaped single crystals were prepared using improved crystal growth methods in solution phase for BP3T and its derivatives. By this method, a large

number of well-shaped and large BP3T crystals were obtained with high reproducibility, and it was applicable for other TPCO series. Large n_g and Q values were obtained for the single crystals of BP3T series, indicating the superiority as active media for lasing. Furthermore, the lasing threshold in the single crystal of BP3T-OMe with perfectly perpendicular orientation was lower than that of BP3T-CN with the inclined orientation, demonstrating the significant dependence of lasing characteristics on molecular orientation, i.e. π-electronic transition dipole moments in the single-crystal cavity.

References:

[1] M. Ichikawa, K. Nakamura, M. Inoue, H. Mishima, T. Haritani, R. Hibino, T. Koyama and Y. Taniguchi, *Appl. Phys. Lett.*, **2005**, 87, 221113.

[2] Y. Inada, Y. Kawata, T. Kawai, S. Hotta and T. Yamao, *J. Appl. Phys.*, **2020**, 127, 053102.

[3] N. Matsuoka, T. Hiramatsu, H. Yanagi, F. Sasaki and S. Hotta, *Jpn. J. Appl. Phys.*, **2010**, 49, 01AD05.

[4] N. Matsuoka, T. Hiramatsu, H. Yanagi, F. Sasaki and S. Hotta, *Jpn. J. Appl. Phys.*, **2010**, 49, 052401.

[5] Y. Ono, F. Sasaki and H. Yanagi, *Mol. Cryst. Lliq.Cryst.*, **2016**, 629, 229.

[6] T. Hiramatsu, N. Matsuoka, H. Yanagi, F. Sasaki and S. Hotta, *Phys. Status solidi C*, **2009**, 6, 338.

[7] T. Hiramatsu, N. Matsuoka, H. Yanagi, F. Sasaki and S. Hotta, *Phys. Status solidi C*, **2009**, 6, 338.

[8] H. Mizuno, H. Yanagi, F. Sasaki and S. Hotta, *Phys. Status Solidi A*, **2012**, 209, 2437.

[9] H. Shang, H. Shimotani, S. Ikeda, T. Kanagasekaran, K. Oniwa, T. Jin, N. Asao, Y. Yamamoto, H. Tamura, K. Abe, M. Kannno, M. Toshizawa and K. Tanigaki, *J. Phys. Chem. C*, **2017**, 121, 2364.

[10] T. Kanagasekaran, H. Shimotani, K. Kasai, S. Onuki, R. D. Kavthe, R. Kumashiro and K. Tanigaki, arXiv:1903.08869, **2019**.

[11] T. Yamao, T. Miki, H. Akagami, Y. Nishimoto, S. Ota and Shu Hotta, *Chem. Mater.*, **2007**, 19, 3748.

[12] Y. Inada, T. Yamao, M. Inada, T. Itami, S. Hotta, *Synth. Met.*, **2011**, 161, 1869.

[13] S. Hotta, M. Goto, R. Azumi, M. Inoue, M. Ichikawa and Y. Taniguchi, *Chem. Mater.*, **2004**, 16, 237.

[14] K. Bando, T. Nakamura, S. Fujiwara and Y. Masumoto, *Phy. Rev. B*, **2008**, 77, 045205.

[15] H. Mizuno, T. Maeda, H. Yanagi, H. Katsuki, M. Aresti, F. Quochi, M. Saba, A. Mura, G. Bongiovanni, F. Sasaki and S. Hotta, *Adv. Opt. Mater.*, **2014**, 2, 529.

[16] H. Mizuno, U. Haku, Y. Marutani, A. Ishizumi, H. Yanagi, F. Sasaki and S. Hotta, *Adv. Mater.*, **2012**, 24, 5744.

[17] H. Mizuno, Y. Mekata, F. Sasaki and H. Yanagi, *Jpn. J. Appl. Phys.*, **2020**, 59, SGGG02.

[18] T. Yamao, K. Yamamoto, T. Inoue, Y. Okuda, Y. Taniguchi and S. Hotta, *Jpn. J. Appl. Phys.*, **2009**, 48, 04C174.

[19] Y. Ono, F. Sasaki and H. Yanagi, *Mol. Cryst. Lliq.Cryst.*, **2016**, 629, 229.

[20] H. Yanagi, K. Tamura, Y. Tanaka and F. Sasaki, *Adv. Nat. Sci-Nanosci.*, **2014**, 5, 045013.

[21] J. Gierschner, S. Varghese and S. Y. Park, *Adv. Opt. Mater.*, **2016**, 4, 348.

[22] K. Wang, H. Zhang, S. Chen, G. Yang, J. Zhang, W. Tian, Z. Su and Y. Wang, *Adv. Mater.*,

2014, 26, 6168.

[23] Z. Zuo, C. Ou, Y. Ding, H. Zhang, S. Sun, L. Xie, R. Xia and W. Huang, *J. Mater. Chem. C*, **2018**, 6, 4501.

Chapter 4

Cooperative behaviors in optically pumped lasing of thiophene/phenylene co-oligomer single crystals

---

4.1 Introduction

Although the origin of amplified light emissions from organic single crystals have been conventionally attributed to the SE process, that of TPCO single crystals including BP3T, could be attributed to cooperative phenomena.[1-3] Moreover, the existence of EPs have been suggested for one-dimensional organic single crystal cavities in spontaneous emission regime, recently.[4-7] Although single crystals of BP3T and its end-substituted derivatives showed optically pumped lasing as described in Chapter 3, BP3T has already been widely recognized as a superior laser medium owing to its high quantum yield and ambipolar carrier transport characteristics with high mobilities, resulting in the demonstration of electrically pumped lasing in OLEFET structures.[8-10]

In this Chapter, the lasing characteristics in BP3T single crystals are characterized in more detail in views of polaritonic and superfluorescent behaviors at room temperature. Cooperative behaviors in BP3T single crystals are investigated from the standpoints of SF by investigating excitation-beam area dependences of light amplification threshold as reported in ref. [2,11], and time-resolved PL measurements are also carried out as reported in ref. [1]. Moreover, the characteristics of optically pumped lasing in BP3T single crystals are investigated in terms of

EPs based on energy vs. wavenumber (*E-k*) dispersions obtained from lasing spectra with longitudinal multi-modes.

4.2 Experimental section

Crystal growth

BP3T crystals were prepared either solution process described in Chapter 3 or PVT process described in Figure 4.1. In the PVT process, 2 - 11 mg of BP3T powder was placed inside a glass tube, and heated at 320 ℃ for 20 - 56 hours under N_2 gas flow at 0.01 L/min.

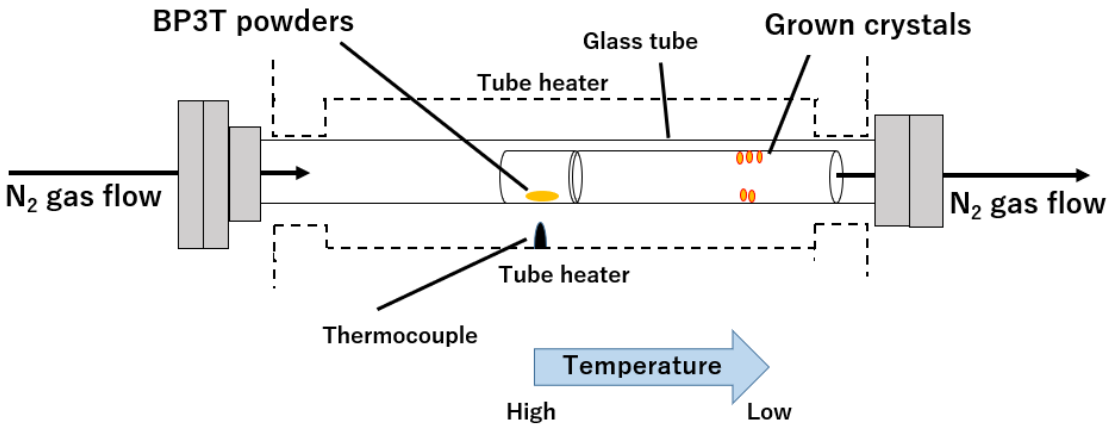

Figure 4.1 Schematic depiction for PVT process to grow platelet BP3T single crystals.

Optical measurements

Absorption spectra were measured using the same set-up described in Chapter 2. Fluorescence images as well as PL spectra of single crystal samples were measured using a fluorescence microscope (Olympus BX-51) equipped with a digital camera (Olympus DP21) and a charge coupled device (CCD) spectrometer (Hamamatsu PMA-50) through a 10× objective lens.

Optically pumped lasing was measured using the same set-up described in Chapter 3. Time-resolved PL measurements were performed using a streak camera (Hamamatsu Photonics C5680) and a Ti:S pulsed laser ($\lambda_{2\omega}$ = 397 nm, 150 fs pulse duration, 1 kHz repetition) as an excitation source. Corresponding PL spectra were measured using a CCD spectrometer (CCD; Roper Scientific ST-133 series).

4.3 Results and discussions

4.3.1 Evaluation of superfluorescent characteristics

Since cooperative amplified light emitting behaviors have been suggested for BP3T single crystals at low temperatures so far,[2] those characteristics were also investigated at room temperature in this work. Same as the cases of previous works described in Chapter 1, optical excitation-beam area dependences on the excitation threshold of light amplification were investigated using PVT grown single crystals. Although the crystal edges cannot serve as F-P cavities for BP3T single crystals grown via PVT processes, SF and SE can occur even without cavity structures. Moreover, BP3T single crystals are grown in two dimensional directions by PVT process while those tend to be grown unidirectionally in solution phase. BP3T single crystals grown via PVT processes seem to be ideal to perform PL measurements under varied excitation beam area because the effect of cavity reflection for light amplification can be removed due to their curved crystal edges. The size of prepared single crystals was more than 2.0 mm, and the thickness confirmed by a surface profiler was 0.51 μm.

The excitation beam was focused into a stripe shape and its stripe-beam shape was varied at 1.0 - 2.3 mm in length with a constant width of 0.4 mm using a cylindrical lens and a variable

slit, i.e. the excitation-beam area was variously changed by the stripe length *L*. Figures 4.6 (a) and (b) show excitation density dependences of normalized PL spectra at excitation stripe lengths of 1.0 mm and 2.3 mm, respectively. In those spectra, two emission bands appeared at around λ = 575 and 620 nm which are assigned to the vibronic 0-1 and 0-2 transitions, respectively. For the excitation length of 1.0 mm, with increasing the excitation density, the 0-1 emission intensity was first nonlinearly amplified. In the case of 2.3 mm, on the other hand, the 0-2 emission line was amplified first.

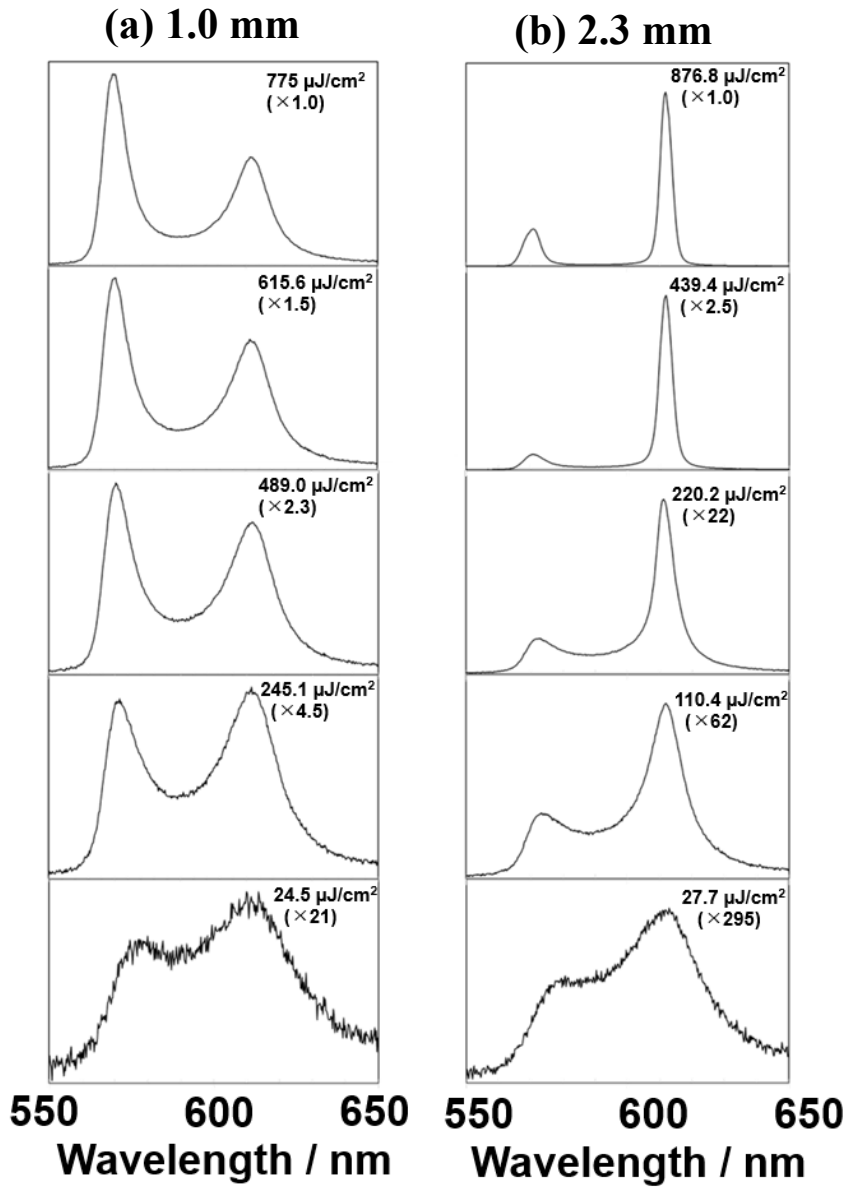

Figure 4.6. (a) Excitation density dependences of PL spectra taken at L = 1.0 mm and (b) 2.3mm.

In Figure 4.7 (a-c), the PL peak intensities of the 0-1 and 0-2 bands were plotted as a function of excitation density at each excitation length. In the case of the 0-1 emission line, the threshold for nonlinear amplification was almost constant independent of L. On the other hand, in the case of the 0-2 peak intensity, the threshold was gradually decreased with increasing L. Thus,

only the 0-2 emission line showed unusual excitation beam length dependence of the threshold for amplified emission, which was the same result as the previous report measured for BP3T at 12 K.[2]

According to a literature, the excitation density threshold for nonlinear amplification in PL peak intensity should be constant independent of excitation beam area in the case of the amplification by the SE process. Therefore, the observed 0-1 emission line followed the usual SE process in this measurement while the 0-2 emission line involves a different process that we should consider a contribution of cooperative phenomena such as SF.

As an origin of the wavelength selectivity for appearance of superfluorescent behaviors, the differences of Franck-Condon factors were considered. Spontaneous PL intensity in 0-2 band region was higher than that of 0-1 band, resulting in the indication of larger Franck-Condon factor in 0-2 band. Moreover, the existence of cooperative molecular vibrations has been suggested by the observation of SRRS for BP3T single crystals.[3] As a result of coupling between cooperative molecular vibrations and electronic transitions, cooperative emitting phenomena, i.e. superfluorescent behaviors can be indicated in vibronic transition in 0-2 band region.

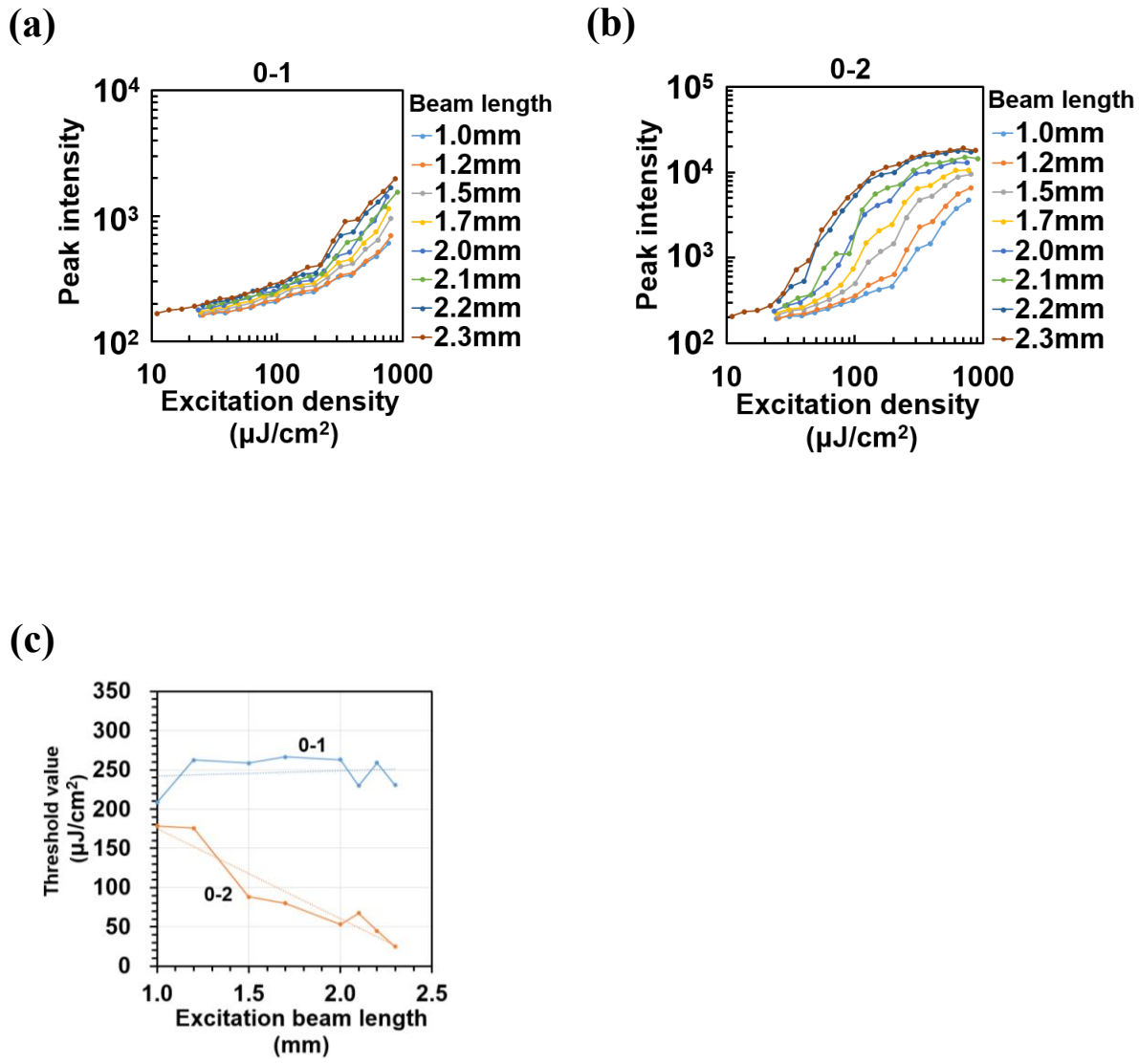

Figure 4.7 Excitation density dependences of (a) 0-1 and (b) 0-2 peak intensities at various excitation beam lengths. (c) Plots of excitation density threshold for nonlinear amplification of the 0-1 and 0-2 emissions as a function of excitation beam length.

4.3.2 Time-resolved PL measurements

For further investigation to understand the characteristics of cooperative behaviors described in sections 4.3.1, time-resolved PL measurements were performed using another BP3T single crystal with thickness of 0.78 μm placed on a glass substrate. As an optical excitation source, a Ti: Sapphire laser ($\lambda_{2\omega}$ = 397 nm, 150 fs pulse duration, 1 kHz repetition) was used and its stripe-beam shape was varied at 0.3 and 0.9 mm in length with a constant width of 0.2 mm. Figure 4.8 (a, b) show the results of time-resolved PL profiles around the threshold of amplified emissions at the excitation length L of 0.3 and 0.9 mm, respectively.

At L = 0.3 mm (Figure 4.8 (a)), the decay time was gradually shortened and the profiles converge to the time origin with increasing excitation density which is similar to typical characteristics of the SE process. By contrast, the profiles at L = 0.9 mm (Figure 4.8 (b)) are pulse-shaped with distinct time delay which is indicative of a cooperative emission process. In Figure 4.8 (b), the maximum delay time is 55 ps at the excitation density of 14.2 μJ/cm^2, and the delay time decreases with increasing excitation density.

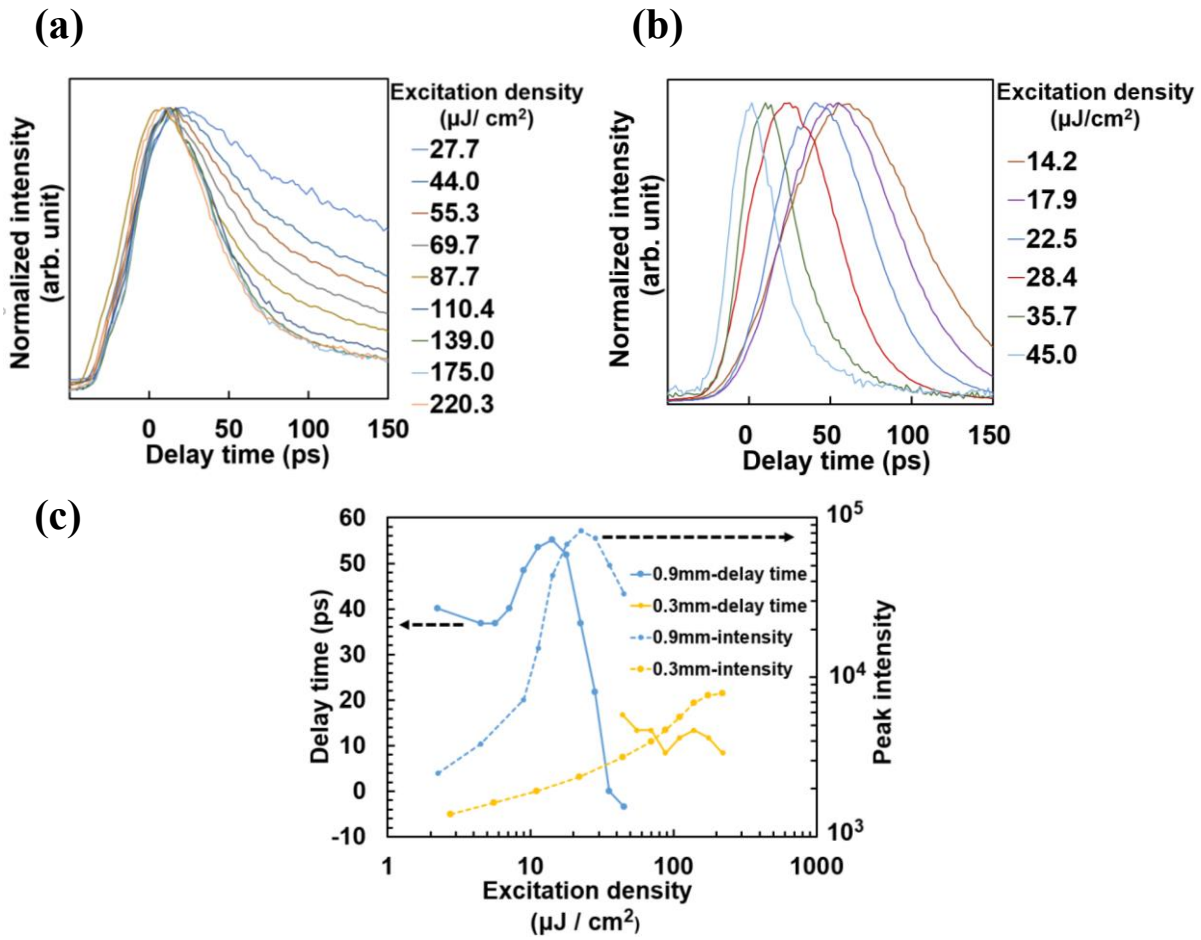

Figure 4.8 Time decay profiles of 0-2 emission at excitation beam length of (a) 0.3 and (b) 0.9 mm. (c) Delay time and PL peak intensity as a function of excitation density at beam length of 0.3 and 0.9 mm.

For further investigation of cooperative lasing characteristics, time-resolved PL measurements for solution-grown BP3T single crystals with F-P self-cavity structures on a glass substrate were performed. Figure 4.9 (a) shows time-decay profiles with intensity color maps obtained around the 0-2 band region at each excitation density, and Figure 4.9 (b) shows corresponding integrated intensity profiles. The maximum delay time of 77 ps is obtained at 182 μJ/cm^2, and the delay time gradually decreases with increasing excitation density. This excitation density dependence resembles that shown in Figure 4.8 (b). As shown in Figure 4.9

(c), corresponding PL spectra are unusually split above the threshold density around 182 μJ/cm^2, and the spectra are gradually converged into one band with increasing excitation density. These splitting behaviors can be attributed to polaritonic behaviors while the converged band appearance at higher excitation density is typical for the SE process, as same as the case of previous reports. Note that, large delay time was observed in 0-2 band for thicker BP3T single crystal, which showed the crystal size dependence for pulse shaped delayed emissions.

Therefore, the pulse shaped delayed emissions probably originate from cooperative process. The excited state coherence among BP3T molecules were indicated both in-plane and thickness directions.

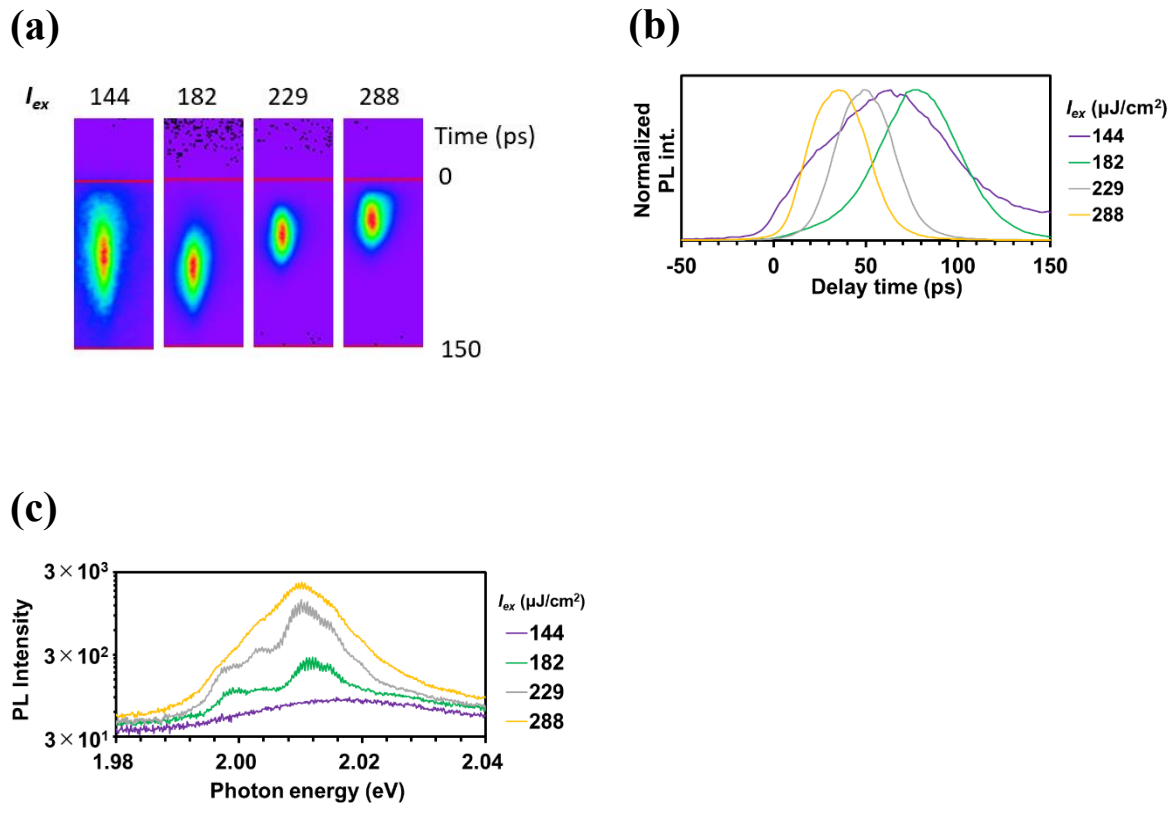

Figure 4.9 (a) Intensity color maps of time-resolved PL spectra obtained by streak camera at each excitation density around the 0-2 band, (b) corresponding time-decay profiles of normalized PL intensity and (c) PL spectra.

Figure 4.10 shows the results of time-resolved PL measurements around the 0-1 band. The maximum delay time is 30 ps, which is shorter than that of the 0-2 band. Moreover, the PL spectra were not apparently split. From those findings, cooperative behaviors are suggested for optically pumped lasing in BP3T single crystals significantly at the 0-2 band.

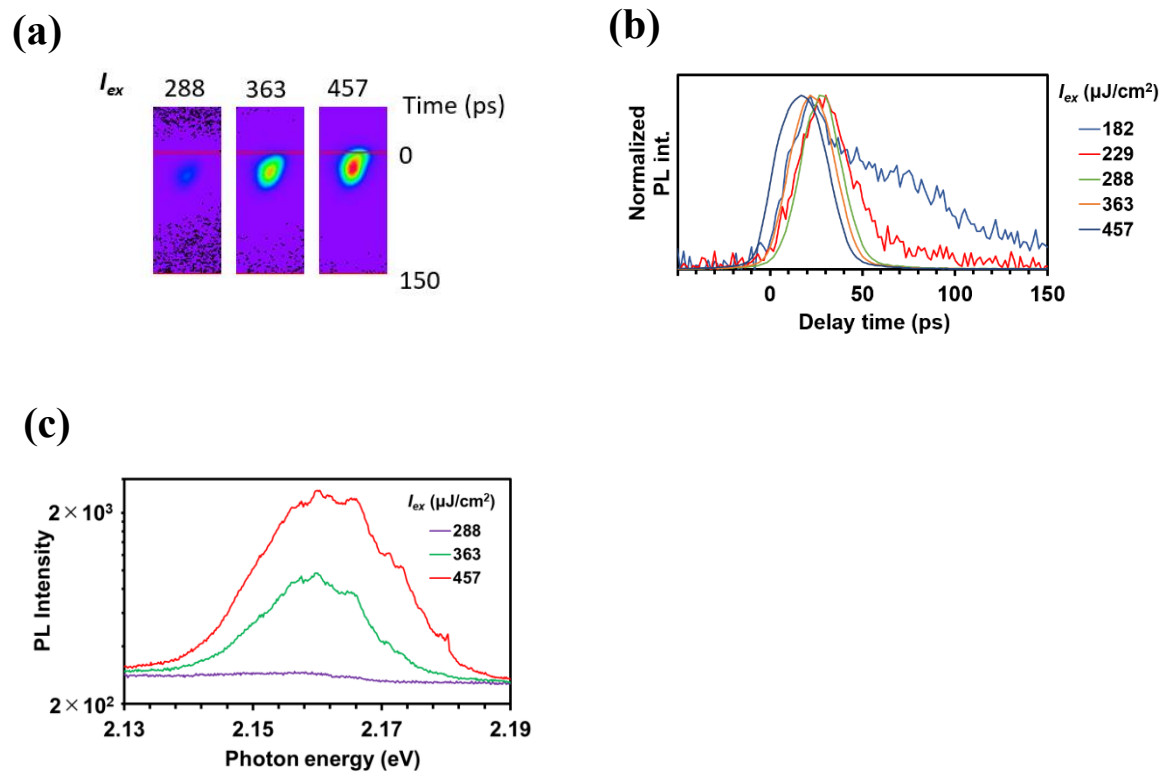

Figure 4.10 (a) Intensity color maps of time-resolved PL spectra obtained by streak camera at each excitation density around the 0-1 band, (b) corresponding time-decay profiles and (c) PL spectra.

4.3.3 Investigation of exciton-polariton (EP) characteristics

Lasing spectra observed from BP3T single crystals grown via improved crystal growth method described in Chapter 3 were sometimes split with longitudinal multi-modes as same as the cases of other TPCO single crystals.[12,13]

Since those behaviors in addition to pulse shaped delayed emissions have been attributed to polaritonic behaviors, characterization using *E-k* dispersion plots is adopted in this study. The dispersion plots were drawn using lasing spectra with longitudinal multi-modes shown in Figure 4.2 (a,b). Figure 4.2 (a,b) show optically pumped lasing spectra in the 0-1 and 0-2 bands, respectively, and the spectra were observed at the same time. Note that the values of *k* used here is the wavenumber in the direction of F-P oscillation in a single crystal self-cavity, different from *k* values usually used in microcavity structures.[14] *E-k* plots for the present single crystal cavities can be derived from the following equations.

$$n_g = \frac{1}{2L\Delta\lambda^{-1}} \tag{4.1}$$

$$k = \frac{2\pi n_g}{\lambda} \tag{4.2}$$

where n_g, L, $\Delta\lambda$, λ are the group refractive index, cavity length, mode interval and peak position of each multi-mode peak, respectively. Using equation (4.1) and (4.2), the dispersion of *k* is described as follows.

$$k = \frac{\pi}{L} \times \frac{\Delta\lambda}{\lambda} \tag{4.3}$$

Therefore, the dispersion of *k* plots can be obtained using the values of mode intervals and each multi-mode peak position in lasing spectra. This calculation has been utilized to evaluate EP characteristics for spontaneous emissions from one-dimensional organic single crystal

cavities[4-7] because of the difficulty to perform angle resolved optical measurements due to their unidirectional light emitting characteristics. In the present cases, those angle resolved optical measurements were also impossible because of the highly unidirectional light emitting characteristics in lasing.

To evaluate EP characteristics, the energy dispersions for excitons and photons must be determined. To determine the accurate exciton level (E_{ex}) for BP3T single crystals, absorption and PL spectra were measured as shown in Figure 4.2 (c). The value E_{ex} was estimated to be 2.376 eV, which was evaluated the mid position between the 0-1 absorption peak and the 0-1 emission peak shown in Figure 4.3 (c). The energy dispersion of cavity photons (E_{ph}) is obtained from the following equation,

$$E_{ph} = \frac{\hbar c}{n_p} \times k \tag{4.4}$$

where $\hbar$, c and n_p are the Dirac's constant, speed of light and phase refractive index of BP3T single crystals, respectively.

Consequently, the energy dispersions of UPB and LPB (E_{UPB} and E_{LPB}, respectively) can be derived as a result of strong coupling between excitons and cavity photons, which is defined as the Rabi-splitting energy ($2\hbar\Omega$), using E_{ex}, E_{ph} as expressed as the following equation.

$$E_{UPB,LPB,} = \frac{1}{2}\left(E_{ex} + E_{ph}\right) \pm \frac{1}{2}\sqrt{\left(E_{ex} - E_{ph}\right)^2 + (2\hbar\Omega)^2} \tag{4.5}$$

The dispersion plots obtained from lasing spectra were attributable to LPB because the population in UPB is relaxed to the exciton reservoir at a fast rate, resulting in the disappearance of light emissions from UPB. Following the equations (4.4) and (4.5), *E-k* dispersion plots obtained from the lasing spectra were well-fitted as the dispersion curve of E_{LPB} as shown in Figure 4.2 (d). The obtained fitting parameters were $n_p = 2.11$ and $2\hbar\Omega = 1.74$

eV, respectively. Moreover, the values of $2\hbar\Omega$ estimated for four samples were ranged in 1.54 ~ 1.74 indicating a quite small deviation in the $2\hbar\Omega$ values. The estimated values of $2\hbar\Omega$ were larger than band width of excitons which was roughly estimated by 0-0 transitions of PL or absorption spectra shown in Figure 4.2 (c) to be ca. 100 meV. Therefore, the estimated values of $2\hbar\Omega$ were satisfied the conditions of strong coupling.

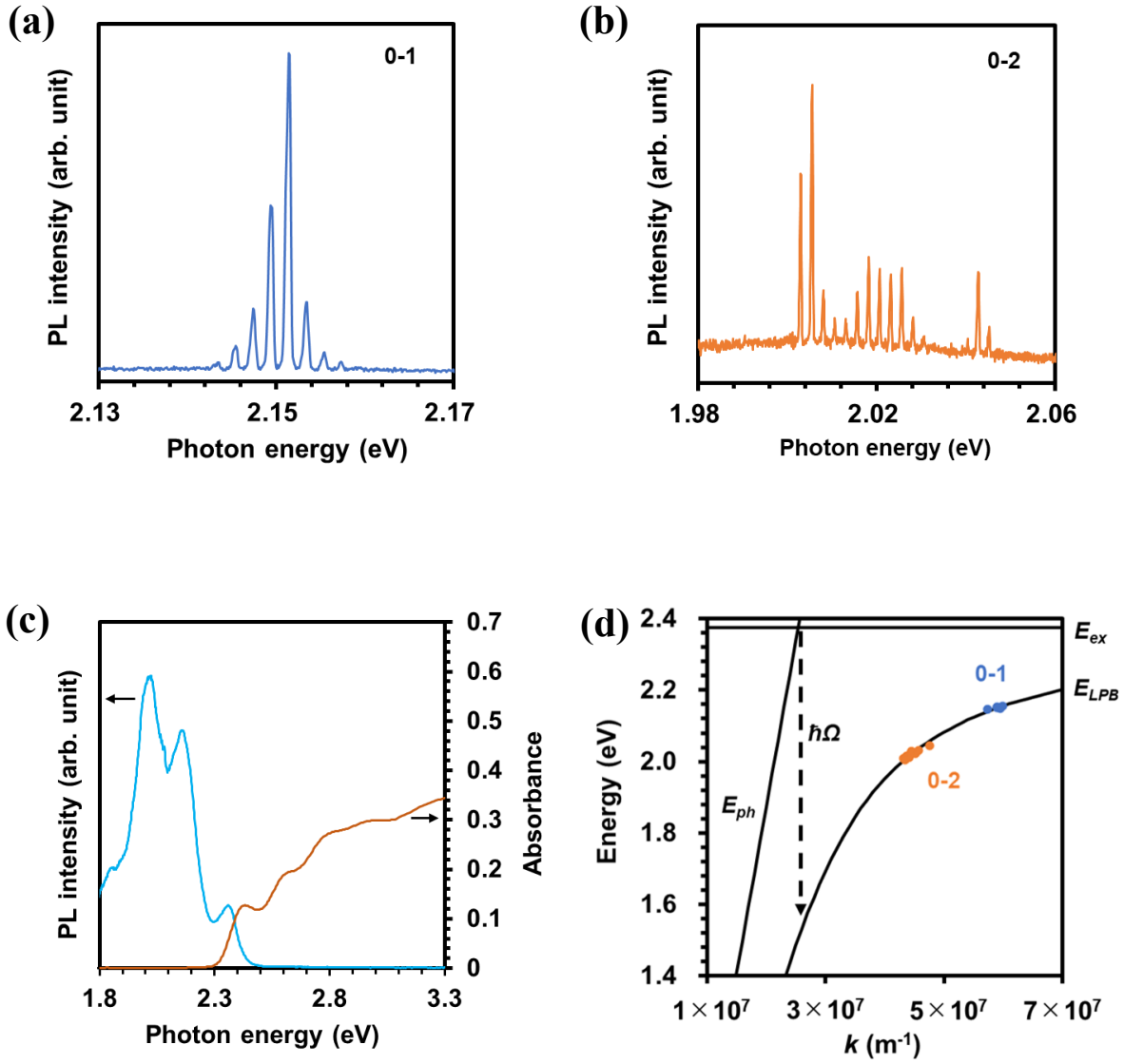

Figure 4.2 (a) Optically pumped lasing spectra obtained from a BP3T single crystal in the 0-1 band and (b) the 0-2 band. (c) PL and absorption spectra for BP3T single crystal. (d) Energy vs. wavenumber (k) dispersion plots obtained from lasing spectra shown in (a) and (b) with a fitting curve of LPB branch indicating strong coupling between excitons and cavity photons.

According to the following equation known as the Jaynes-cummings model, the Rabi-splitting energy is described as,[15,16]

$$\hbar\Omega = \sqrt{\frac{2|\mu|^2\hbar\omega(N/V_0)}{\varepsilon}} \tag{4.6}$$

where μ, ω, ε are the transition dipole moment, angular frequency of cavity photons and dielectric constant, respectively. (N/V_0) expresses the density of excited state molecules. According to a literature,[17] $|\mu|$ for the crystal-state of BP3T has been calculated to be 13.8 Debye. The unit cell volume of BP3T crystal including 4 molecules is 2609.3 Å^3,[18] leading to the estimation of the maximum (N/V_0) number to be 1.53×10^{-3} Å^{-3}. The exciton energy $\hbar\omega$ is 2.376 eV. ε was estimated as square of n_p to be 4.45 where the used n_p is 2.11, which was obtained by fitting described in Figure 4.2 (d). After all, the calculated value of $2\hbar\Omega$ was estimated to be 1.12 eV, which is not much different from that obtained from the above-mentioned fitting.

The values of Rabi-splitting energies in microcavity structures are generally a few hundred meV,[16,19,20] however, the values obtained for the present BP3T single crystals are significantly one order of magnitude larger.

A presumable reason is attributed to the difference of $|\mu|$ values comparing to the cases of microcavities. When the excitons interact with cavity photons in single crystal self-cavities, macroscopically correlated excitons with coherence among excited state molecules over the scale of microcavity structures are formed as similar as the formation mechanism of superfluorescence, resulting in considerably large $|\mu|$ values in equation (4.6). Therefore, the Rabi-splitting energy obtained for the present BP3T single crystal cavities could be drastically larger than that in usual microcavity structures. This mechanism seems reasonable because cooperative behaviors such as SF have been observed for BP3T and another organic single crystal.[2,11] The formation of macroscopically correlated excitons also strongly supported for

the BP3T single crystals owing to the densely packed and linearly ordered transition dipole moments with large $|\mu|$.

As another reason of the large Rabi-splitting energy estimated for BP3T single crystals, the effect of sample morphology could be deduced. Molecules in a single crystal without external cavity structures seem to be easily excited by optical pumping while molecules in microcavity are less excited due to high reflectivity of DBR mirrors. According to the equation of Jaynes-cummings model shown as equation (4.6), with increasing the population of excited state molecules, the value of Rabi-splitting energy also become larger, resulting in the larger Rabi-splitting energy values for single crystal cavities in comparison to the those of microcavity structures.

Furthermore, *E-k* dispersion plots obtained from unusually split lasing spectra were sometimes not simply well-fitted as a dispersion curve of E_{LPB}. In those cases, molecular vibrations should be assumed as additional interaction parameters, resulting in the formation of vibrationally dressed exciton polaritons (VDEPs).

Figure 4.3 (a,b) shows a representative example of unusually split lasing spectra in the 0-1 band and 0-2 band, respectively, attributed to VDEPs. For unusually split lasing spectrum in the 0-1 band shown in Figure 4.3 (a), *E-k* plots were well-fitted by coupling among E_{ex}, E_{ph} and $E_{ex(0\text{-}1)}$ as shown in Figure 4.3 (c) where $E_{ex(0\text{-}1)}$ is the energy of a vibrationally dressed exciton at the 0-1 emission band. The corresponding phenomenological Hamiltonian can be described as the following 3×3 matrix,

$$\begin{pmatrix} E_{ph} & \hbar\Omega & \hbar\omega_{0-1} \\ \hbar\Omega & E_{ex} & 0 \\ \hbar\omega_{0-1} & 0 & E_{ex(0-1)} \end{pmatrix} \tag{4.7}$$

where $\hbar\omega_{0\text{-}1}$ is the coupling energy with $E_{ex(0\text{-}1)}$. As a result of fitting using E_{ex} = 2.376 eV,

$E_{ex(0\text{-}1)}$ = 2.164, n_p = 2.11, the interaction energies were obtained as $\hbar\Omega$ = 0.88 eV and $\hbar\omega_{0\text{-}1}$ = 3.5 meV, respectively. To determine the dispersion of E_{ph}, the value of n_p obtained in Figure 4.2 (d) was used.

For fitting of the lasing spectrum shown in Figure 4.3 (b), *E-k* plots were fitted by assuming coupling among E_{ex}, E_{ph} and $E_{ex\text{-}2A1}$, $E_{ex\text{-}(A1+B1)}$, $E_{ex\text{-}2B1}$. A_1 and B_1 are the symmetric and asymmetric stretching vibration modes, respectively, along the linear π-conjugated framework of the BP3T molecule. $E_{ex\text{-}2A1}$, $E_{ex\text{-}(A1+B1)}$, $E_{ex\text{-}2B1}$ are the energies of vibrationally dressed excitons at the 0-2 emission band corresponding to the doubled frequency of A_1, the sum-frequency of A_1 and B_1, and the doubled frequency of B_1, respectively. Using these energies, the phenomenological Hamiltonian is described as follows.

$$\begin{pmatrix} E_{ph} & \Omega & \omega_{2A_1} & \omega_{(A_1+B_1)} & \omega_{2B_1} \\ \Omega & E_{ex} & 0 & 0 & 0 \\ \omega_{2A_1} & 0 & E_{ex-2A_1} & 0 & 0 \\ \omega_{(A_1+B_1)} & 0 & 0 & E_{ex-(A_1+B_1)} & 0 \\ \omega_{2B_1} & 0 & 0 & 0 & E_{ex-2B_1} \end{pmatrix} \tag{4.8}$$

Energy levels of vibronic transitions were determined through PL measurement as described in Appendix part. In the 0-2 PL band for BP3T single crystals, three energy levels originating from A_1 and B_1 modes, $E_{ex\text{-}2A1}$, $E_{ex\text{-}(A1+B1)}$, $E_{ex\text{-}2B1}$, are involved in the fitting shown in Figure 4.3 (d). These energy levels were determined to be 2.021, 2.012 and 2.000, respectively. As same as the case shown in Figure 4.3 (c), n_p = 2.11 was used. As a result of fitting, the coupling energy corresponding to $E_{ex\text{-}2A1}$, $E_{ex\text{-}(A1+B1)}$, and $E_{ex\text{-}2B1}$ were estimated to be all ~3 meV, respectively, and $\hbar\Omega$ was estimated to be 0.75 eV.

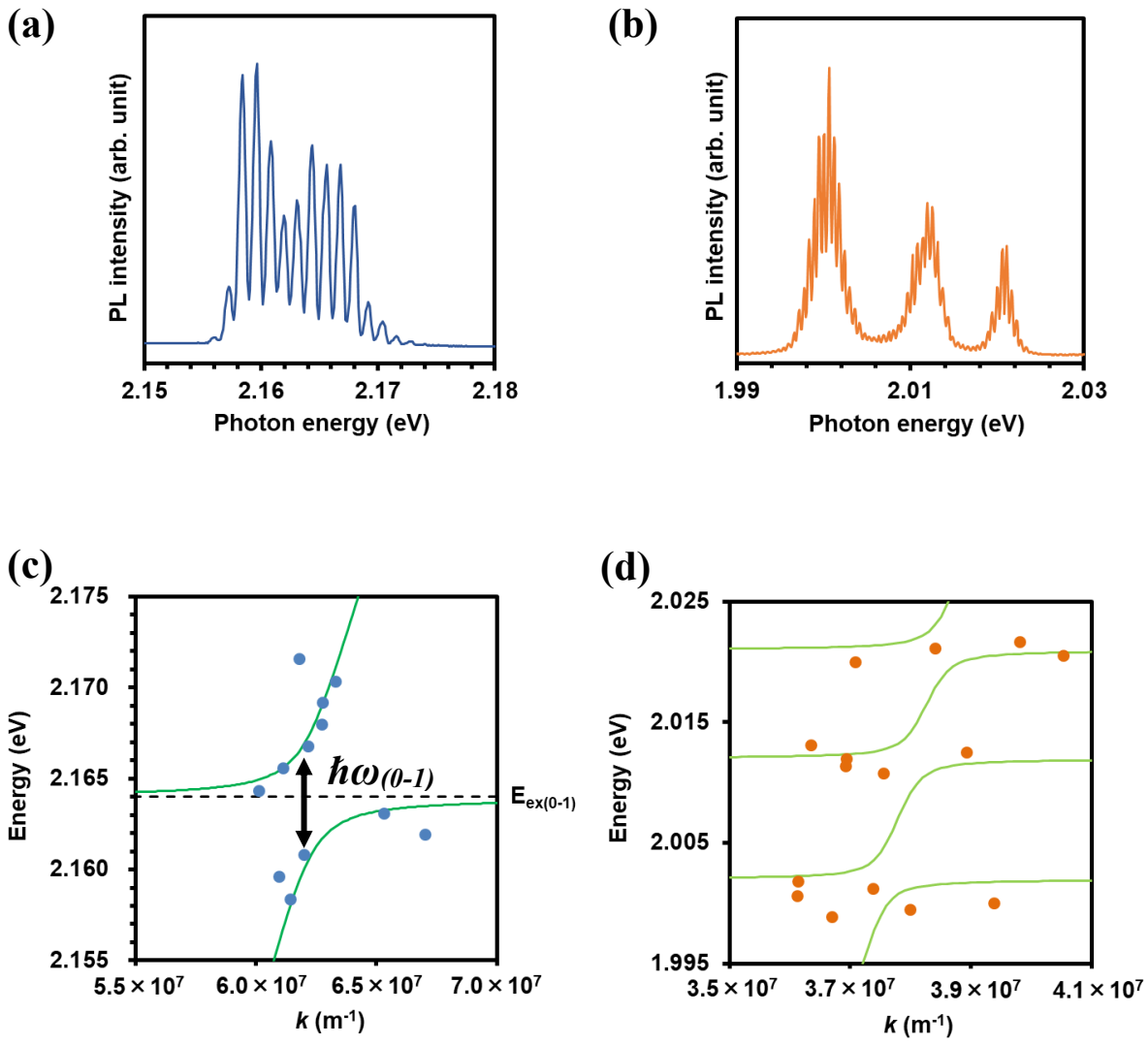

Figure 4.3 Optically pumped lasing spectra obtained for BP3T single crystal in the 0-1 band (a) and the 0-2 band (b). Corresponding E-k dispersion plots with fitting curves for the 0-1 band (c) and the 0-2 band (d).

The molecular symmetry of BP3T belongs to the point group of C_{2V}, which has two Raman active A_1 and B_1 modes. According to a literature,[21] the Raman shift of A_1 and B_1 are assigned

to in-plane symmetric stretching mode at 1458 cm^{-1} and in-plane asymmetric stretching mode at 1600 cm^{-1}, respectively. Moreover, ASE spectra observed for the BP3T single crystals at 12K have been assigned to vibronic transitions coupled with the A_1, B_1 and their sum frequency in the 0-1 and 0-2 bands.[3] In the present study, however, the Raman spectrum observed from the BP3T single crystal under off-resonant excitation showed other small peaks except for the A_1 and B_1 modes as shown in Figure 4.4 (a). The lasing spectra shown in Figure 4.3 were well-fitted as the VDEP models, however, they sometimes complicatedly split into several bands with longitudinal multi-modes as shown in Figure 4.4 (b,c), which are not simply attributed to the VDEP models probably due to the existence of other exciton levels with unassigned vibronic transitions.

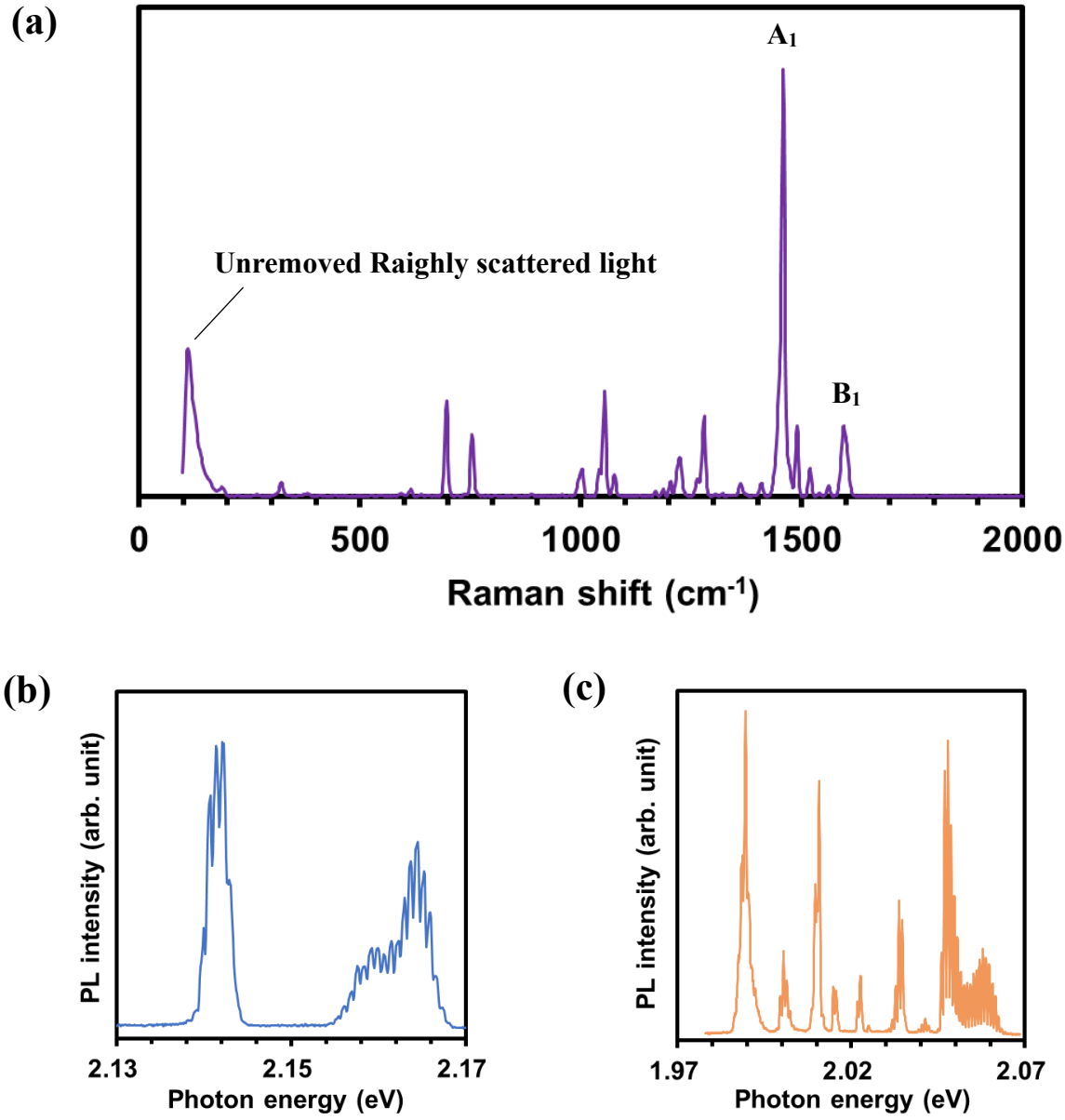

Figure 4.4 (a) Raman spectrum obtained from a BP3T single crystal showing Raman peaks including A_1 and B_1 modes, and optically pumped lasing spectra obtained from a BP3T single crystal in the 0-1 band (b) and the 0-2 band (c) showing complicatedly split lasing bands with longitudinal multi-modes.

A presumable mechanism of optically pumped lasing based on polaritonic states in BP3T single crystals is depicted in Figure 4.5. The schematic diagram of lasing usually attributed to LPB is described as shown in Figure 4.5 (a). The population of LPB is developed by relaxation

of excitons through coupling with cavity photons, and the energy of LPB is dispersed depending on the values of k, as pointed out for microcavity structures using organic materials as active media.[22] Along with the accumulation of population in LPB, vibronic progressions ($E_{ex\text{-}vib.}$) may coherently couple to generate vibrationally dressed excitons (E_{VDEP}) as shown in Figure 4.5 (b). After the resonant coupling between LPB and vibrationally dressed excitons is established, the light emissions occur from the thus split LPB levels. As a result, the lasing based on VDEP states can be attributed to the resonant interaction between E_{LPB} and $E_{ex\text{-}vib.}$.

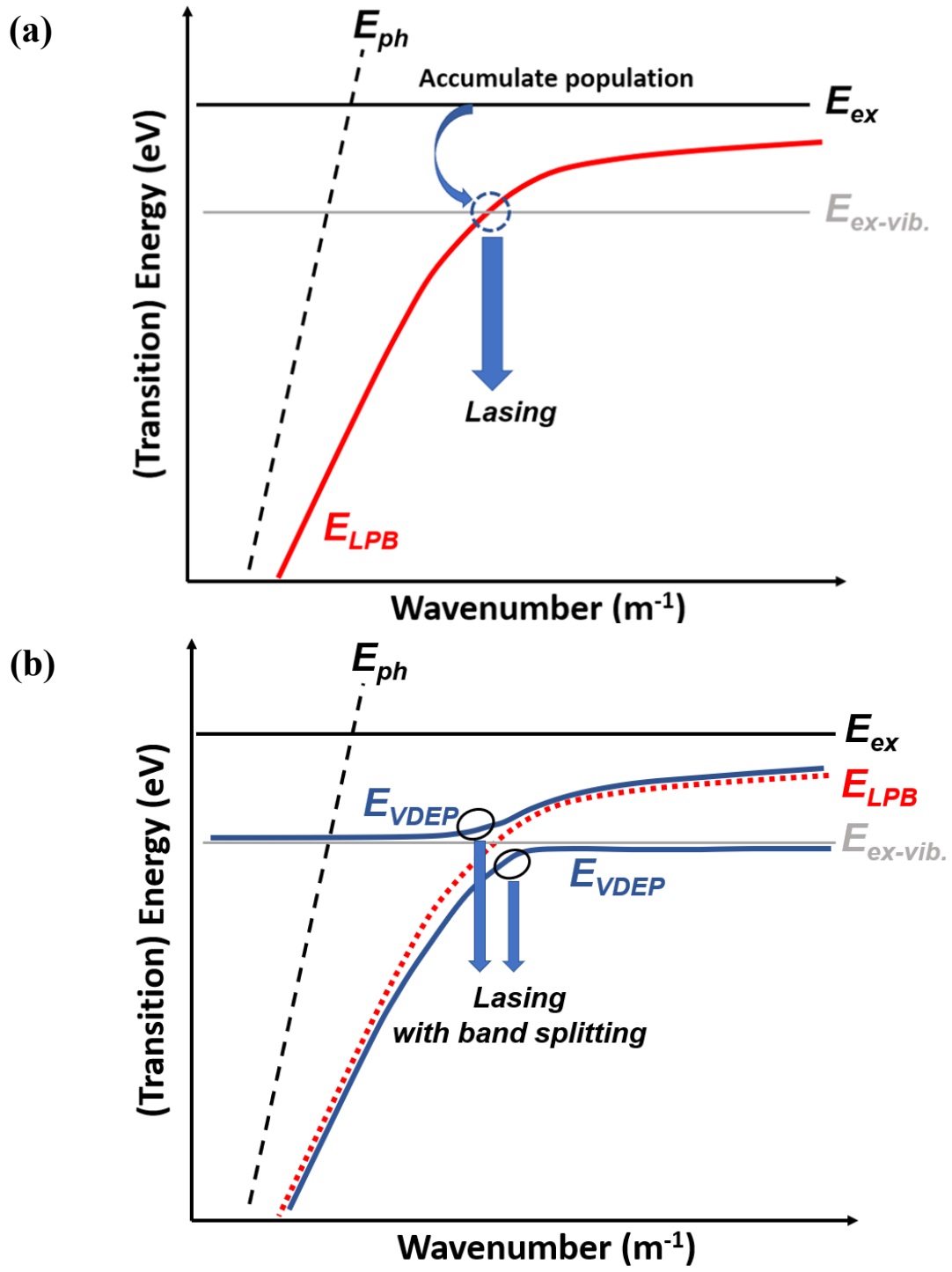

Figure 4.5 Schematic depiction of population accumulation in LPB (a) and formation of VDEPs as a result of coupling with vibronic progressions (b).

4.4 Conclusions

Cooperative behaviors resembling SF are typically observed in amplified light emissions at the 0-2 band while the SE process is often obtained in light amplification at the 0-1 band in the measurements of excitation-beam length dependences of light amplification threshold. Pulse-shaped emissions with time delay also appear typically at the 0-2 band, and the maximum delay time depends on the excitation beam area, suggesting cooperative behaviors interpreted as SF. The wavelength-selective delayed emissions were also observed for solution grown BP3T single crystals. With increasing excitation density, the delay time gradually decreased and spectra shape of lasing approached to the SE-like behaviors.

Furthermore, the origin of optically pumped lasing from BP3T single crystals was firstly attributed to light emissions form LPB. Moreover, the origin of unusually split lasing spectra was also attributable to VDEPs.

In summary, both superfluorescent behaviors and polaritonic behaviors were suggested for BP3T single crystals. The origin of F-P lasing under optical pumping was interpreted as polaritonic behaviors, and the existence of macroscopic coherence was also suggested for light amplification characteristics in BP3T single crystals resulting in the suggestion of macroscopic coherence among EPs or VDEPs. Although SE process was suggested for 0-1 band in PL measurements under varied beam length, fitting curves for *E-k* dispersion plots suggested that both 0-1 and 0-2 PL bands originated from EPs or VDEPs. In conclusion, polaritonic behaviors were suggested in both 0-1 and 0-2 bands, however, macroscopic coherence was selectively suggested for 0-2 band.

References:

[1] N. Matsuoka, T. Hiramatsu, H. Yanagi, F. Sasaki and S. Hotta, *Jpn. J. Appl. Phys.*, **2010**, 49, 052401.

[2] T. Hiramatsu, N. Matsuoka, H. Yanagi, F. Sasaki and S. Hotta, *Phys. Status solidi C*, **2009**, 6, 338.

[3] H. Yanagi, Y. Marutani, N. Matsuoka, T. Hiramatsu, A. Ishizumi, F. Sasaki and S. Hotta, *Appl. Phys. Lett.*, **2013**, 103, 243301.

[4] K. Takazawa, J. Inoue, K. Mitsuishi and T. Takamasu, *Phys. Rev. Lett.*, **2010**, 105, 067401.

[5] K. Takazawa, K. Mitsuishi and J. Inoue, *Appl. Phys. Lett.*, **2011**, 99, 253302.

[6] C. Zhang, C. L. Zou, Y. Yan, R. Hao, F. W. Sun, Z. F. Han, Y. S. Zhao and J. Yao, *J. Am. Chem. Soc.*, **2011**, 133, 7276.

[7] Q. Liao, Z. Xu, X. Zhong, W. Dang, Q. Shi, C. Zhang, Y. Weng, Z. Lid and H. Fu, *J. Mater. Chem. C*, **2014**, 2, 2773.

[8] S. Kanazawa, M. Ichikawa, T. Koyama, Y. Taniguchi, *Chem. Phys. Chem.*, **2006**, 7, 1881.

[9] S. Z. Bisri, T. Takenobu, Y. Yomogida, H. Shimotani, T. Yamao, S. Hotta and Y. Iwasa, *Adv. Funct. Mater.*, **2009**, 19, 1728.

[10] T. Kanagasekaran, H. Shimotani, K. Kasai, S. Onuki, R. D. Kavthe, R. Kumashiro and K. Tanigaki, arXiv:1903.08869, **2019**.

[11] H. Shang, H. Shimotani, S. Ikeda, T. Kanagasekaran, K. Oniwa, T. Jin, N. Asao, Y. Yamamoto, H. Tamura, K. Abe, M. Kannno, M. Toshizawa and K. Tanigaki, *J. Phys. Chem. C*, **2017**, 121, 2364.

[12] T. Yamao, K. Yamamoto, T. Inoue, Y. Okuda, Y. Taniguchi and S. Hotta, *Jpn. J. Appl. Phys.*,

2009, 48, 04C174.

[13] H. Yanagi, Y. Marutani, F. Sasaki, Y. Makino, T. Yamao and S. Hotta, *Appl. Phys. Express*, **2011**, 4, 062601.

[14] T. Byrnes, N. Y. Kim and Y. Yamamoto, *Nat. Phys.*, **2014**, 10, 803.

[15] M. Fox, Quantum Optics (Oxford University Press, Oxford, 2006), p. 191.

[16] K. Goto, K. Yamashita, H. Yanagi, T. Yamao and S. Hotta, *Appl. Phys. Lett.*, **2016**, 109, 061101.

[17] K. Bando, T. Nakamura, S. Fujiwara and Y. Masumoto, *Phy. Rev. B*, **2008**, 77, 045205.

[18] S. Hotta, M. Goto, R. Azumi, M. Inoue, M. Ichikawa and Y. Taniguchi, *Chem. Mater.*, **2004**, 16, 237.

[19] D. G. Lidzey, D. D. C. Bradley, M. S. Skolnick, T. Virgili, S. Walker and D. M. Whittaker, *Nature*, **1998**, 395, 53.

[20] S. K. Cohen and S. R. Forrest, *Nat. Photonics.*, **2010**, 4, 371.

[21] H. Yanagi, A. Yoshiki, S. Hotta and S. Kobayashi, *J. Appl. Phys.*, **2004**, 96, 4240.

[22] D. M. Coles, P. Michetti, C. Clark, W. C. Tsoi, A. M. Adawi, J. S. Kim and D. G. Lidzey, *Adv. Funct. Mater.*, **2011**, 21, 3691.

Chapter 5

Summary and future prospect

5.1 Summary

In Chapter 1, fundamental research backgrounds for organic lasers were described. Among them, optoelectronic characteristics for TPCO series as laser media were explained in detail. Moreover, indication of cooperative behaviors in optically pumped lasing from TPCO single crystals were described. After that, cooperative behaviors suggested in organic materials were stated as contrasts to conventional photon lasing based on SE processes. Then, cooperative behaviors were described in terms of both polaritonic behaviors and SF.

In Chapter 2, BP3T-OMe and BP3T-CN were successively synthesized by referring a previously published literature.[1] Their crystal structures were identified as orthorhombic and triclinic forms, respectively, which were different from the monoclinic form of BP3T and other TPCO series,[2-4] resulting in the different orientation of π-electronic transition dipole moments with respect to the crystal basal planes. Those varied orientations lead to various types of laser devices such as edge emitting F-P lasers and VCSELs.

In Chapter 3, optically pumped lasing from single crystals of BP3T, BP3T-OMe and BP3T-CN was described. To achieve optically pumped lasing in F-P oscillation, an improved crystal growth method in solution phase was proposed. A large number of well-shaped BP3T single crystals with a pair of parallel crystal edges were obtained. Moreover, large and well-shaped single crystals were also obtained for other TPCO series, which showed the versatility of this

method. Optically pumped lasing was achieved for BP3T, BP3T-OMe and BP3T-CN in F-P oscillating conditions using a pair of parallel crystal edges. High n_g and Q values were estimated for those single crystals of derivatives under lasing conditions, indicating their suitability as lasing media. Moreover, the lasing threshold for the BP3T-OMe was smaller than that of the BP3T-CN single crystal, which was attributed to the perpendicular orientation of π-electronic transition dipole moments in the former while the inclined one in latter, as described in Chapter 2.

In Chapter 4, following cooperative behaviors reported for amplified light emissions in the BP3T single crystals,[5-7] their characteristics were further characterized at room temperature. Polaritonic behaviors in optically pumped lasing from the BP3T single crystals were further characterized using *E-k* dispersion plots derived from lasing spectra with longitudinal multi-modes. The obtained *E-k* plots were attributed to LPB formed by strong coupling between excitons and cavity photons. Moreover, the *E-k* dispersion plots obtained from the unusually split lasing spectra were attributed to VDEPs. Although the origin of lasing from organic single crystals have been conventionally attributed to the SE process, it was attributed to EPs or VDEPs for the first time in BP3T single crystals in this study.

5.2 Future Prospect

Improvement of polaritonic characteristics in optically pumped lasing

Although the existence of EPs was suggested in lasing from BP3T single crystals through this research, the reflectivity at their side facets acting as self-organized FP resonators is low in comparison to that of external microcavity structures with DBR mirrors. The reflectivity between the BP3T crystal and air (R) was estimated to be only 13%, using n_p = 2.11 obtained in Chapter 4 according to the following Fresnel equation.

$$R = \left(\frac{1 - n_p}{1 + n_p}\right)^2 \tag{5.1}$$

To enhance the interaction between cavity photons and excitons, introduction of external cavity structures seems critical. For this purpose, coupling between plasmonic modes and excitons have been demonstrated by placing one-dimensional perovskite single crystals onto Ag/insulator coated glass substrates.[8] Moreover, towards the demonstration of BEC in organic single crystal cavities, DFB structures have been introduced. Although polariton lasing has not been demonstrated by those structures, the reflectivity at a certain wavelength has been successively enhanced ($\simeq$ 70%).[9]

To enhance the reflectivity of photons, Au coating onto the surface of BP3T single crystals and following PL measurements were preliminary performed in this research as shown in Figure 5.1. Improvement of Q values of cavity photons can be expected owing to the increased reflectivity of cavities. Although lasing based on F-P oscillation have not been observed, observation of gain-narrowed emissions was achieved in these structures. To achieve lasing in F-P condition, further optimization of sample morphology is probably inevitable.

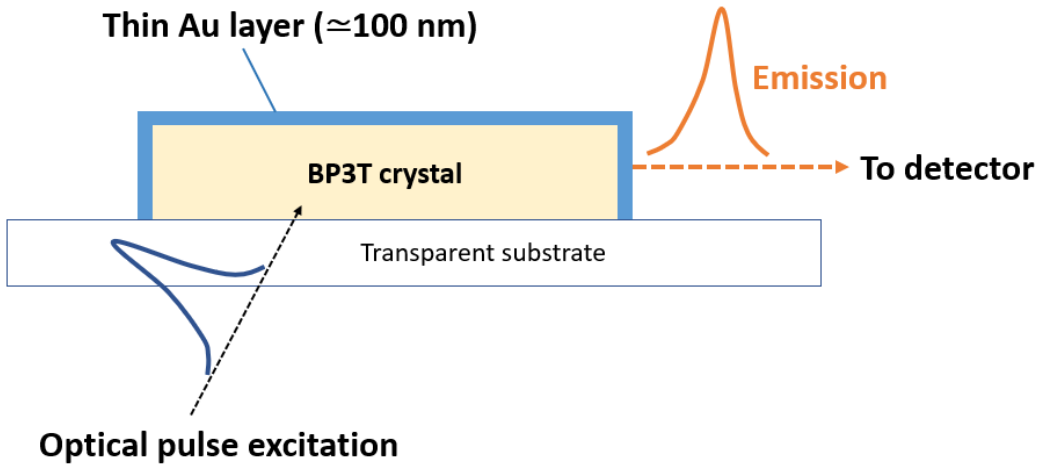

Figure 5.1 Schematic depiction of set-up of PL measurements for an Au-coated BP3T single crystal.

Characterization of cooperative behaviors by time-resolved optical measurements

For further characterization of polaritonic states in the BP3T single crystals, pump-probe measurements can be a critical method. The existence of polaritonic energy levels has been confirmed by observing transient absorption from polaritonic states, and their excited state dynamics have also been confirmed in organic microcavity structures.[10,11]

As another characterization, measurements of second order coherence are also critical. In microcavity structures, lasing from polaritonic states and that based on SE process have been clearly distinguished.[12] Not only for polaritonic behaviors, SF has also been characterized through this measurement.[13]

Possibility of electrically pumped lasing based on cooperative behaviors

Although electrically pumped EP formations and electrically pumped conventional photon lasing have been demonstrated for organic materials,[14-18] electrically pumped lasing based on

EP states has not been demonstrated yet. Since electrically pumped photon lasing has been demonstrated for BP3T single crystals, aside from the cooperative behaviors under optically pumped conditions at room temperature presented in this work, the single crystal of BP3T seems to be a promising candidate to demonstrate electrically pumped lasing based on cooperative behaviors, which can be achieved even without introducing cavity structures owing to the existence of well-shaped self-cavity structures.

However, the crystal morphology should be optimized toward device fabrication. As shown in Figure 5.2 (a,b), in the cases of OLEFET devices using thick organic single crystals, carriers are transported to recombination zone in long distance, which conditions easily dissipate carriers through transportation while thinner organic single crystals are ideal to achieve efficient carrier transportations. Thickness of solution grown BP3T single crystals (> 2 μm) was larger than that of PVT grown BP3T single crystals (≃ hundreds of nm), which suggested that solution grown BP3T crystals were disadvantageous in terms of the efficiency of carrier transportations.

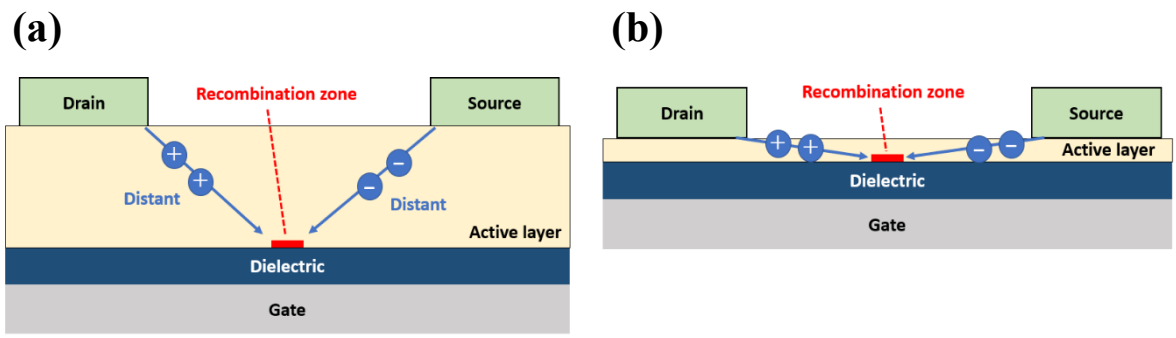

Figure 5.2 Schematic depiction of carrier transportation in OLEFET devices for both holes and electrons in case of using a thicker organic single crystal active medium (a) and a thinner one (b).

Investigation and comparison of cooperative behaviors among BP3T, BP3T-OMe and BP3T-CN

As described in Chapter 4, both polaritonic and superfluorescent behaviors were suggested for lasing from single crystals of BP3T. Moreover, orientation dependence appeared in threshold of light amplification between single crystals of BP3T-OMe and BP3T-CN. Since BP3T-OMe and BP3T-CN showed high n_g values under lasing conditions, their optically pumped lasing was possibly based on polaritonic states as elucidated for optically pumped lasing in BP3T single crystals. According to an equation of Jaynes-cummings model in equation (4.6), Rabi-splitting energy can be tuned by controlling molecular orientations since it's proportional to the values of $|\mu|$. By comparing the values of Rabi-splitting energy among BP3T and its derivatives, the existence of polaritonic states can be elucidated in more detail, and it will be first time to prove molecular orientation dependences for the lasing characteristics based on EPs.

Not only the polaritonic characteristics, superfluorescent behaviors can be also modulated by controlling molecular orientations. Single crystals of BP3T-OMe are expectable to show excitation beam area dependences since their perfectly standing transition dipole moments seem to be ideal to form macroscopically correlated excited states while single crystals of BP3T-CN seem to be less ideal to show superfluorescent behaviors since their π-electronic orbitals could be less delocalized in-plane direction inside a platelet single crystal.

References:

[1] T. Katagiri S. Ota T. Ohira T. Yamao and S. Hotta, *J. Heterocyclic Chem.*, **2007**, 44, 853.

[2] S. Hotta and M. Goto, *Adv. Mater.*, **2002**, 14, 498.

[3] S. Hotta, M. Goto and R. Azumi, *Chem. Lett.*, **2007**, 36, 270.

[4] S. Hotta, M. Goto, R. Azumi, M. Inoue, M. Ichikawa and Y. Taniguchi, *Chem. Mater.*, **2004**, 16, 237.

[5] N. Matsuoka, T. Hiramatsu, H. Yanagi, F. Sasaki and S. Hotta, *Jpn. J. Appl. Phys.*, **2010**, 49, 052401.

[6] T. Hiramatsu, N. Matsuoka, H. Yanagi, F. Sasaki and S. Hotta, *Phys. Status solidi C*, **2009**, 6, 338.

[7] H. Yanagi, Y. Marutani, N. Matsuoka, T. Hiramatsu, A. Ishizumi, F. Sasaki and S. Hotta, *Appl. Phys. Lett.*, **2013**, 103, 243301.

[8] Q. Shang, S. Zhang, Z. Liu, J. Chen, P. Yang, C. Li, W. Li, Y. Zhang, Q. Xiong, X. Liu and Q. Zhang, *Nano Lett.*, **2018**, 18, 3335.

[9] K. Takazawa, K. Mitsuishi and J. Inoue, *Appl. Phys. Lett.*, **2011**, 99, 253302.

[10] T. Virgili, D. Coles, A. M. Adawi, C. Clark, P. Michetti, S. K. Rajendran, D. Brida, D. Polli, G. Cerullo and D. G. Lidzey, *Phys. Rev. B*, **2011**, 83, 245309.

[11] K. Yamashita, U. Huynh, J. Richter, L. Eyre, F. Deschler, A. Rao, K. Goto, T. Nishimura, T. Yamao, S. Hotta, H. Yanagi, M. Nakayama, R. H. Friend, *ACS Photonics*, **2018**, 5, 2182.

[12] H. Deng, H. Haug and Y. Yamamoto, *Rev. Mod. Phys.*, **2010**, 82, 1489.

[13] G. Rainò, M. A. Becker, M. I. Bodnarchuk, R. F. Mahrt, M. V. Kovalenko and T. Stöferle, *Nature*, **2018**, 563, 671.

[14] A. Graf1, M. Held, Y. Zakharko, L. Tropf, M. C. Gather and J. Zaumseil, *Nat. Mater.*, **2017**, 16, 911.

[15] M. Held, A. Graf, Y. Zakharko, P. Chao, L. Tropf, M. C. Gather and J. Zaumseil, *Adv. Opt. Mater.*, **2018**, 6, 1700962.

[16] S. Dokiya, H. Mizuno, H. Mizuno, H. Katsuki, K. Yamashita, F. Sasaki and H. Yanagi, *Appl. Phys. Express*, **2019**, 12, 111002.

[17] S. Sandanayaka, T. Matsushima, F. Bencheikh, S. Terakawa, W. J. Potscavage Jr, C. Qin, T. Fujihara, K. Goushi, J. Ribierre and C. Adachi, *Appl. Phys. Express*, **2019**, 12, 061010.

[18] T. Kanagasekaran, H. Shimotani, K. Kasai, S. Onuki, R. D. Kavthe, R. Kumashiro and K. Tanigaki, arXiv:1903.08869, **2019**.

Appendices

Appendix 1. Optically pumped lasing in solution grown 5,5'''-Bis(4-biphenylyl)-2,2':5',2'':5'',2'''-quaterthiophene (BP4T) single crystals

Brief introduction

Here, as described in Chapter 3, improved crystal growth for one of TPCO series, BP4T, and its optically pumped lasing characteristics were described. PL measurements were performed using same set-up shown in Chapter 3.

Experimental section

BP4T powders were sublimed once for purification through the PVT process as described in Figure 4.1. Using sublimed BP4T solids, a saturated 1,2,4-trichlorobenzene solution of BP4T was prepared at 190℃. The 8 mL solution was diluted by adding 2 mL 1,2,4-trichlorobenzene to remove possibly remaining undissolved BP4T solids. After that, the solution was heated to 190℃ again, and successively cooled down to 30℃ for 15 - 36 hours. Afterwards, the grown BP4T crystals dispersed in the solution were transferred onto glass substrates by immersing glass substrates into the solution.

Results and discussions

As a result of crystal growth in solution phase, well-shaped BP4T single crystals were obtained. BP4T crystallized in parallelogram or rhombus shape as shown in Figure S1 (a) while

BP3T crystallized in elongated hexagonal shape. The crystal size was successively controlled by modifying cooling time in the crystal growth process in solution phase; smaller crystals were obtained in shorter cooling time while larger ones were produced in longer cooling time. As same as the case of BP3T, the grown BP4T single crystals were edge-emissive which is suitabile for efficient confinement of cavity photons, as described in Chapter 1.

As shown in Figure S1 (b), both 0-1 and 0-2 emission bands were nonlinearly amplified with longitudinal multi-modes in PL spectra. The threshold excitation density was estimated to be 81 μJ/cm^2 in the 0-1 band and 30 μJ/cm^2 in the 0-2 band. Figure S1 (c,d) depicts high resolution PL spectra showing longitudinal multi-modes oscillations at 259 μJ/cm^2 in the 0-1 band (c) and at 644 μJ/cm^2 in the 0-2 band (d).

As well as the cases for BP3T and its derivatives, n_g and Q factor values for the BP4T single crystals were evaluated using equations (3.1) and (3.2). For lasing spectrum in the 0-1 band, n_g and Q factor values were estimated to be 4.7 and 6.0×10^3, respectively while those in the 0-2 band were 3.5 and 6.0×10^3, respectively. The cavity length of the BP4T single crystal shown in Figure S1 (a) was estimated to be 152 μm in the diagonal direction, because bright light emissions under lasing conditions appeared from corners of the crystal. These n_g and Q factor values were large enough as same as the cases of other TPCO series. These results also suggest the versatility of the crystal growth method proposed in Chapter 3, even for other organic semiconducting species.

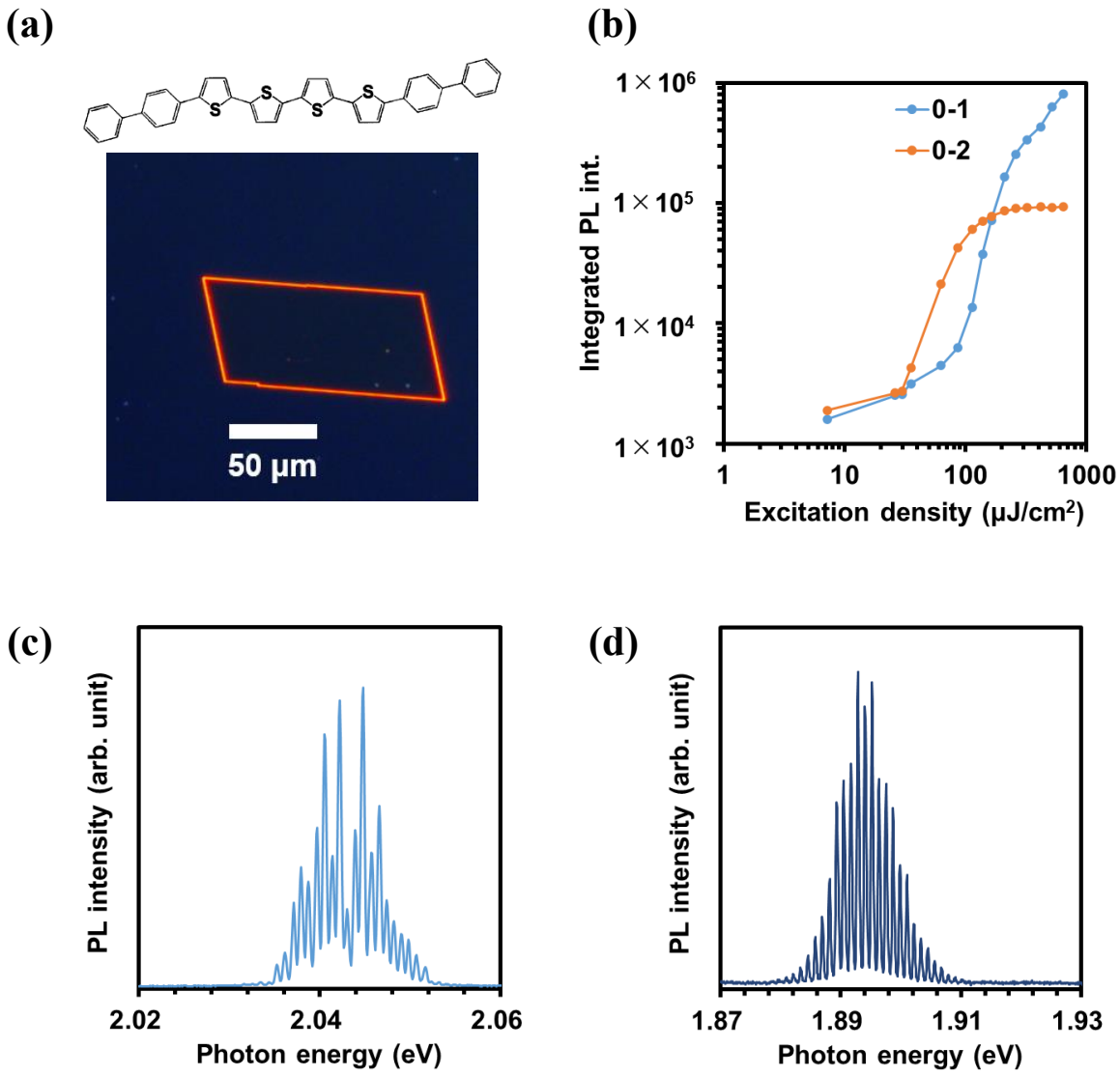

Figure S1. (a) Molecular structure and a fluorescence microscope image of BP4T crystal grown via modified solution growth process. (b) Excitation density dependences of integrated PL intensity in the 0-1 and 0-2 bands. Lasing spectra in the 0-1 band (c) and 0-2 band (d).

Appendix 2. Exact estimation of energy levels of vibronic progressions for BP3T single crystals.

As stated in Chapter 4, the energy levels of $E_{ex\text{-}2A1}$, $E_{ex\text{-}(A1+B1)}$ and $E_{ex\text{-}2B1}$ were determined through PL measurements. Although amplified light emissions from the PVT-grown BP3T single crystals without self-organized F-P cavities have usually shown a Gaussian-shaped spectral band, unordinary splitting has been sometimes observed in the 0-2 band region. Supposing that these splitting was attributable to vibronic transitions, energy gaps between $E_{ex\text{-}2A1}$ and $E_{ex\text{-}(A1+B1)}$, or $E_{ex\text{-}(A1+B1)}$ and $E_{ex\text{-}2B1}$ was assumed from those splitting band. The splitting energy in the 0-2 band region shown in Figure S2 was estimated to be 10 meV, which was almost equal to the energy gaps among three splitting bands shown in Figure 4.3 (b). The accurate values of $E_{ex\text{-}2A1}$, $E_{ex\text{-}(A1+B1)}$ and $E_{ex\text{-}2B1}$ were estimated from peak positions of each three of lasing band.

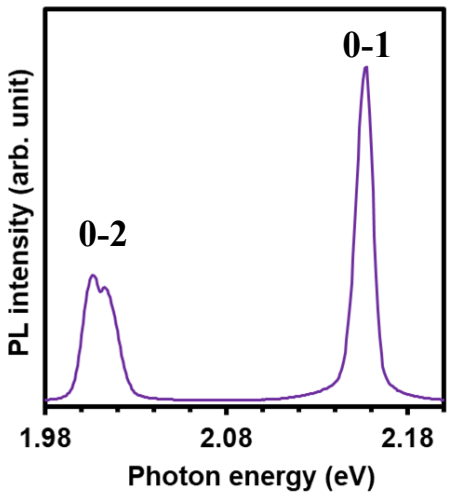

Figure S2. Amplified PL spectrum observed from a PVT-grown BP3T single crystal showing two peaks in the 0-2 band region.

List of publications

[1] T. Matsuo, H. Mizuno, F. Sasaki and H. Yanagi, "Indication of cooperative light amplification in 5,5″-bis(4-biphenylyl)-2,2′:5,2″-terthiophene single crystals at room temperature," *Jpn. J. Appl. Phys.*, **2019**, 59, SDDB02.

[2] T. Matsuo, C. Rössiger, J. Herr, R. Göttlich, D. Schlettwein, H. Mizuno, F. Sasaki and H. Yanagi, "Synthesis and characterization of methoxy- or cyano-substituted thiophene/phenylene co-oligomers for lasing application," *RSC adv.*, **2020**, 10, 24057.

[3] T. Matsuo *et al.*, "Organic laser based on vibrationally-dressed exciton polaritons in single-crystal cavity of thiophene/phenylene co-oligomer at room temperature," in preparation.

Awards

[1] Student Presentation Award: 10th International Conference on Molecular Electronics and Bioelectronics (M&BE10), Nara, Japan, T. Matsuo, H. Mizuno, F. Sasaki and H. Yanagi, "Amplified Light Emission Based on Cooperative Process in Single Crystals of Thiophene/Phenylene Co-Oligomer," 27 June, 2019.

[2] The Best Poster Presentation Award: Organic Crystal Symposium, Kagawa, Japan, T. Matsuo, C. Rössiger, J. Herr, R. Göttlich, D. Schlettwein, H. Mizuno, F. Sasaki and H. Yanagi, "Synthesis and Characterization of Methoxy or Cyano-substituted Thiophene Phenylene Co-Oligomer," 10 November, 2020.

[3] CrystEngComm Poster Award: Organic Crystal Symposium, Kagawa, Japan, T. Matsuo, C. Rössiger, J. Herr, R. Göttlich, D. Schlettwein, H. Mizuno, F. Sasaki and H. Yanagi, "Synthesis and Characterization of Methoxy or Cyano-substituted Thiophene Phenylene Co-oligomer," 10 November, 2020.

Acknowledgements

The author would like to express great appreciation to my supervisor Prof. Hisao Yanagi at Quantum Materials Science Laboratory, Graduate School of Materials Science, Nara Institute of Science and Technology (NAIST) for grateful supports in my Ph.D research. His supports helped me to carry out research work smoothly, and I learned a lot from his sincere and positive attitude to science.

The author also expresses sincere appreciation to Associate Prof. Hiroyuki Katsuki at Quantum Materials Science Laboratory, Graduate School of Materials Science, Nara Institute of Science and Technology (NAIST) for his experimental supports, useful advices in meeting and personal discussion.

The author expresses appreciation to Assistant Prof. Hitoshi Mizuno at Quantum Materials Science Laboratory, Nara Institute of Science and Technology (NAIST) for his helpful discussion and advice through doctoral research.

The author would like to express sincere appreciation to Prof. Yukiharu Uraoka at Information Device Science Laboratory and Associate Prof. Hiroaki Benten at Laboratory for Organic Electronics, NAIST, for helpful advice through doctoral course research.

The author thanks to Dr. Fumio Sasaki at Electronics and Photonics Research Institute, National Institute of Advanced Industrial Science and Technology (AIST) for his experimental guidance and helpful discussions.

The author appreciates to Professor Kenichi Yamashita at Faculty of Electrical Engineering and Electronics, Kyoto Institute of Technology (KIT) for his helpful discussion and advise to interpretation of my experimental results.

The author wishes to thank Prof. Richard Göttlich, Mrs. Carina Rössiger and Ms. Jasmin Martha Herr at Institute of Organic Chemistry, Justus-Liebig-University Giessen and Prof. Derck Schlettwein at Institute of Applied Physics, Justus-Liebig-University Giessen for their kind guidance and helpful discussion during my stay in Giessen as an internship student. Also, the author wishes to thank other members in their laboratory members for a lot of helps during my stay in Giessen.

The author would like to make acknowledgement to Yasuo Okajima, Noritaka Koike and Shohei Katao, NAIST, for their guidance and discussion through optical and X-ray measurements.

Finally, the author's sincere appreciation goes to all members in Quantum Materials Science Laboratory for continuous supporting through my research.